SPECIAL REPORT 90-5

X-Ray Photography Method for Experimental Studies of the Frozen Fringe Characteristics of Freezing Soil

Satoshi Akagawa

February 1990

Special Report 90-5

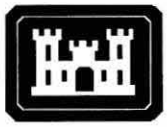

U.S. Army Corps of Engineers
Cold Regions Research & Engineering Laboratory

X-Ray Photography Method for Experimental Studies of the Frozen Fringe Characteristics of Freezing Soil

Satoshi Akagawa

February 1990

Prepared for
OFFICE OF THE CHIEF OF ENGINEERS

PREFACE

This report was prepared by Satoshi Akagawa, researcher for the Shimizu Corporation, Tokyo, Japan, while he was a visiting scientist with the Civil and Geotechnical Engineering Research Branch, Experimental Engineering Division, U.S. Army Cold Regions Research and Engineering Laboratory. The data shown in this report were observed by the author at the Research Institute of Shimizu Corporation in 1984 and 1985. Most of the figures in this report were acquired from the data analysis performed during the author's stay at CRREL from 1986 to 1988. During the analysis, the author had many worthwhile discussions with the CRREL staff, especially Dr. Richard Berg, Edwin Chamberlain, William Quinn, Dr. Yoshisuke Nakano and Dr. Patrick Black. The author also appreciates the assistance of David Cate in helping to revise this report.

CONTENTS

	Page
Preface	ii
Introduction	1
Experimental methods	3
Test apparatus	3
Soil specimens	5
Test conditions	5
Test procedure	6
X-ray photograph exposure procedure	6
Image processing for the X-ray photographs	6
Test results	10
Conventional heave test results	10
Positions of the lead spheres	12
Temperature profiles	12
Strain rate of each soil layer	23
Apparent temperature range of the frozen fringe	23
Apparent thickness of the frozen fringe	28
Thermal conductivity of the frozen fringe during stationary heaving	28
Problems in determining T_s and L_{ff}	32
Summary and conclusion	34
Literature cited	35
Appendix A: Coordinates and temperatures	37
Appendix B: Strain observed in the soil layers	43
Appendix C: Strain distribution in the freezing soil	45
Appendix D: Strain rate observed in the soil layers	55
Appendix E: Strain rate distribution in the soil layers	59
Appendix F: Listings of T_s, L_{ff} and location of the 0°C isotherm	69
Abstract	71
Appendix G: X-ray photographs	73

ILLUSTRATIONS

Figure	
1. Frost heave cell	2
2. Schematic drawing of the X-ray facilities	3
3. Geometrical relationship of the two X-ray photos	4
4. Lead spheres	4
5. Typical X-ray photograph and temperature profile	7
6. Image-processing filters for analyzing the sphere coordinates	8
7. General heave properties of the soil	9
8. Conventional results of frost heave tests	10
9. Pore water leakage after 13 hours in Test A	12
10. Analyzed Z coordinates of the lead spheres	13
11. Analyzed temperature profiles	14
12. Comparison of temperature profiles for the lead spheres and the surface of the samples	15

Page

13. Strain development in freezing soils 18
14. Consolidation properties of the test soil and nomographic pore water pressure of segregating ice 21
15. Expansion and shrinkage in the freezing soil 22
16. Heave properties in the early stage of freezing 24
17. Strain rate development in the freezing soil 25
18. Apparent segregation temperature 27
19. Comparison of T_s in Test A and Test B 28
20. Apparent thickness of the frozen fringe 29
21. Comparison of L_{ff} in Test A and Test B 30
22. Heat flow density in the unfrozen soil and thermal conductivity of the frozen fringe 31
23. Difference in frozen fringe location determined from the location of the warm side of the warmest ice lens and from the expansion rate profile converted from the intensity profile of the X-ray photo 32

TABLES

Table

1. Test conditions 3
2. Physical, mechanical and thermal properties of the soil 5
3. Hours when X-ray photographs were taken 6

X-Ray Photography Method for Experimental Studies of the Frozen Fringe Characteristics of Freezing Soil

SATOSHI AKAGAWA

INTRODUCTION

By the early 1980s, the study of frost heave appeared to be complete because several numerical frost heave models had been developed. Some of them (Gilpin 1980, O'Neill and Miller 1982) predict realistic ice-banding patterns. However, these models are based on assumptions that still remain to be proven by precise experiments. Most of the assumptions that affect the reliability of the models are related to the "frozen fringe," because phenomena that occur in this area seem to initiate the entire frost heaving process. Unfortunately, insufficient knowledge about the frozen fringe makes it difficult to verify the frost heave models.

The main objectives of this report are

- To describe the development of an X-ray photographic method for observing the frost-heaving properties of soil, especially the characteristics of the frozen fringe;
- To describe observations of the temperature and strain field change in the frozen fringe using the procedure developed; and
- To publish the test results as a data base that can be used in evaluating frost heave models.

The method used X-ray photography with thermocouples installed inside lead marking spheres to observe soil expansion, including expansion due to in-situ freezing and expansion due to segregation freezing. The method is an improvement over the methods of Penner (1975), Ishizaki (1985) and Svec (1986), who used X-ray radiography. The improvements include an image-processing technique for analyzing the coordinates of the lead spheres on the photos, a three-dimensional analysis of the lead spheres' coordinates to compensate for the geometrical distortion caused by the use of a point X-ray source, and direct measurements of the temperature at each lead sphere using thermocouples in the spheres. Therefore, both the deformation and the temperature field in a freezing soil can be observed directly.

The experiments produced results on the following characteristics:

- Temperature profiles in two freezing soil specimens;
- The expansion activity (strain and strain rate) distributions in two specimens;
- The apparent temperature range of the frozen fringe;
- The apparent thickness of the frozen fringe; and
- The thermal conductivity of the frozen fringe while the warmest ice lens is segregating.

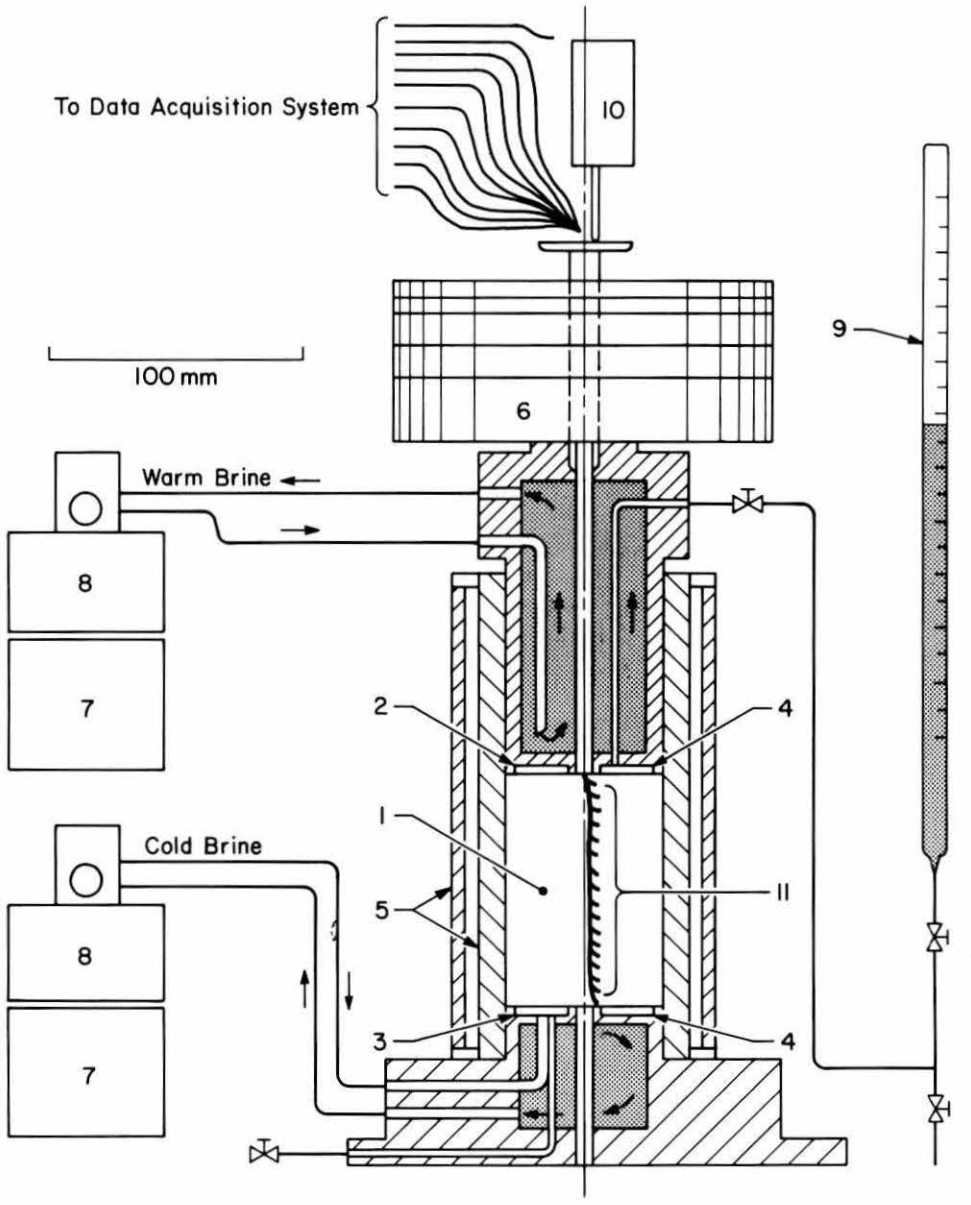

Figure 1. Frost heave cell.

1. *Specimen*
2. *Warm plate*
3. *Cold plate*
4. *Porous plate*
5. *Double acrylic cylinder*
6. *Dead weight*
7. *Cooling unit*
8. *Brine temperature controller*
9. *Burette for water table*
10. *Deformation transducer*
11. *Thermocouples*

These data can be applied to studies of the heaving activity distribution in conjunction with temperature field, the dominance of the heave mode (in-situ freezing and segregation freezing) (discussed in Akagawa 1988a), and water sources for segregating ice (discussed in Akagawa 1988a). The method could also be used to study the permeability of the frozen fringe. The present technology is not adequate for microscopic observations, such as the distribution of ice and unfrozen water around soil skeleton, the mechanical properties of absorbed water, and the ice segregation mechanism in freezing soil.

EXPERIMENTAL METHODS

Two step-temperature-change frost heave tests were conducted (Test A and Test B in Table 1). During the tests, 136 X-ray photos were taken. The X-ray photos were taken in pairs with different locations of the X-ray source so that the three-dimensional coordinates of the lead spheres could be analyzed.

Table 1. Test conditions.

	Test A	*Test B*
Overburden pressure (kPa)	60	110
Pore water pressure (kPa)	0	0
Cold-side temperature (°C)	–5.9	–5.5
Warm-side temperature (°C)	2.2	3.0

Test apparatus

The frost heave test apparatus is shown in Figure 1. It has one-dimensional heat flow through the cylindrical specimen, accomplished by reducing the heat flow normal to the specimen axis using an annular dead air space maintained at 0°C. The overburden pressure was kept constant by using a dead weight for loading. The apparatus has a ripple-free temperature control employing a large-volume (11 L) circulating coolant system. It uses drift-free deformation transducers for recording the total heave, accomplished by using a digital deformation measuring system without an amplifier. The rest of the features of this frost heave cell are given by Akagawa (1983, 1985).

The X-ray facilities (Fig. 2) have the appropriate X-ray radiation strength obtained by applying 100 kV and 5 mA to the X-ray tube. The X-ray source can move between two

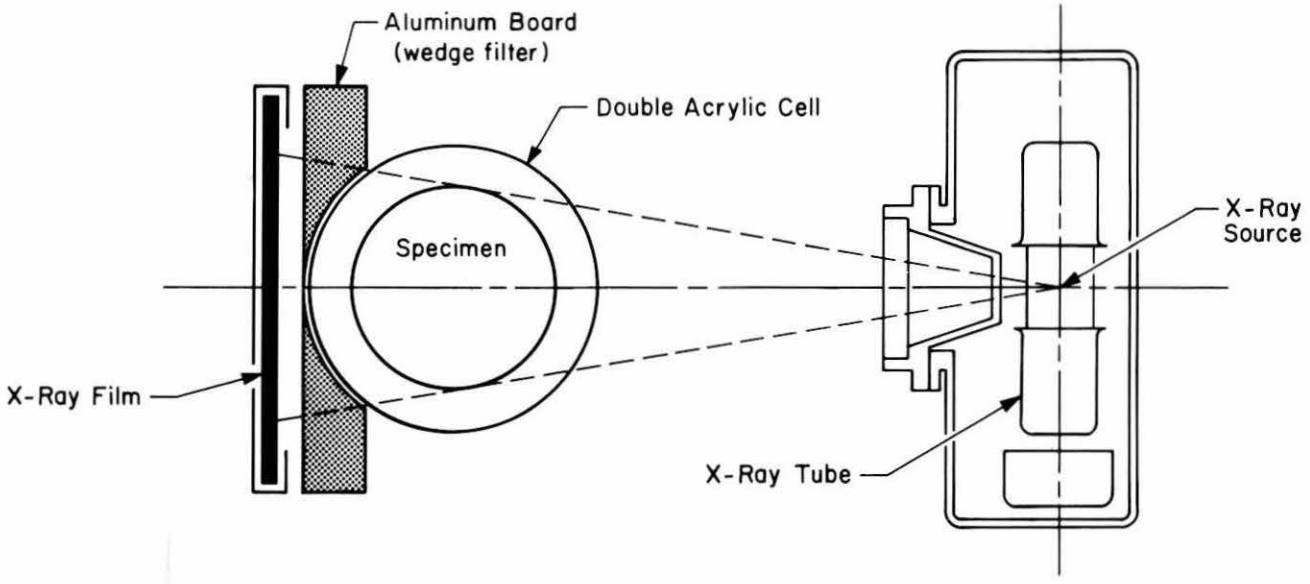

Figure 2. Schematic drawing of the X-ray facilities.

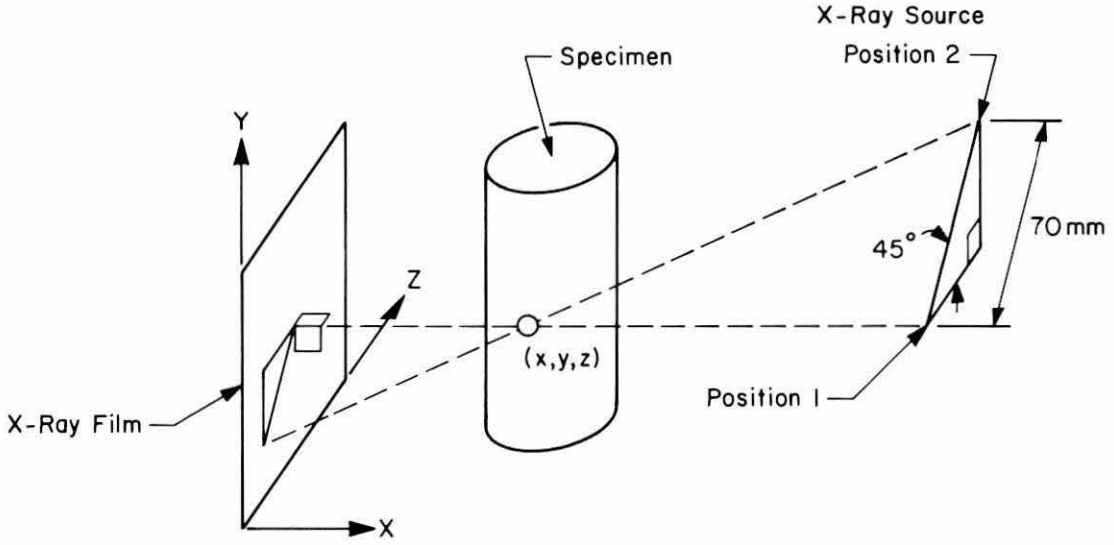

Figure 3. Geometrical relationship of the two X-ray photos.

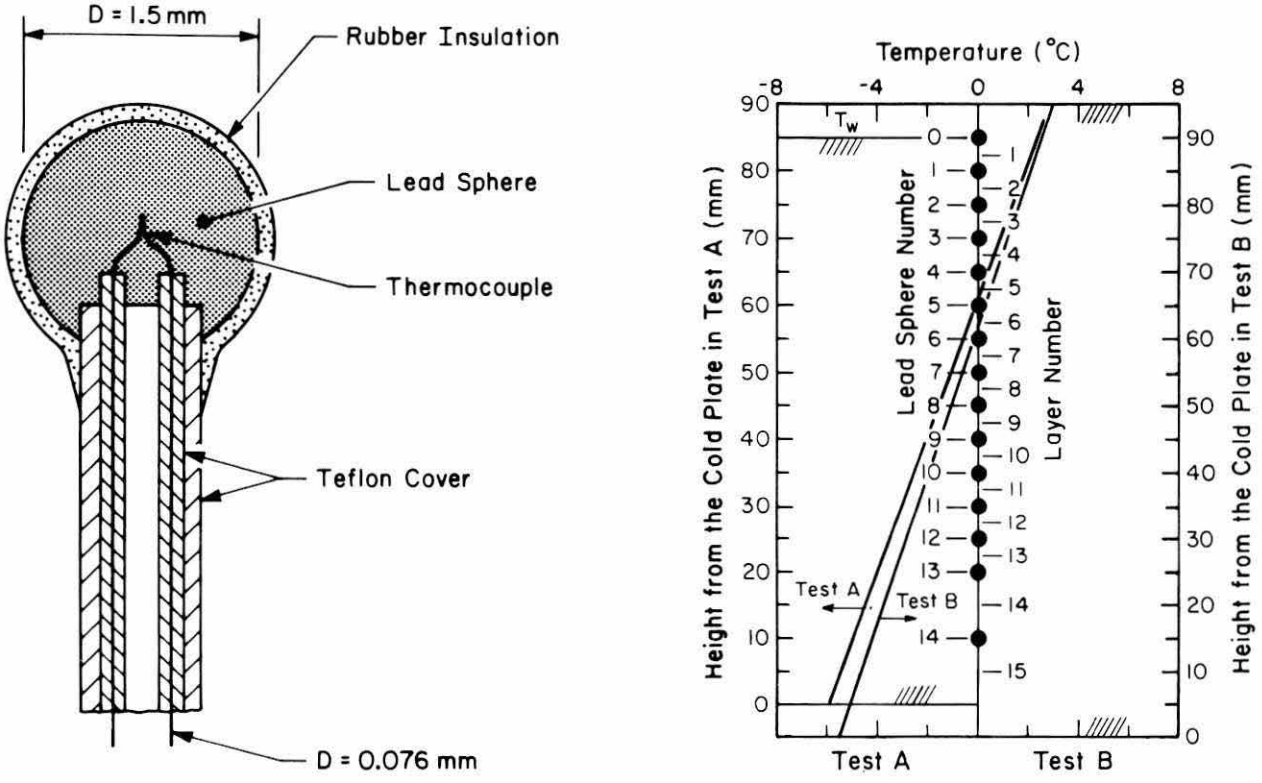

a. Structure. *b. Installed depths.*

Figure 4. Lead spheres.

positions in a plane parallel to the X-ray film, as shown in Figure 3. This enables X-ray photos to be taken from two consistent (but different) X-ray source positions, allowing a three-dimensional coordinate analysis. The difference in X-ray path length through the circular section of the specimen is compensated for by using the axisymmetrical aluminum wedge filter shown in Figure 2 (this technique was used only in Test B).

The lead spheres and thermocouples are shown in Figure 4. The timing and position of the coordinate and temperature measurements matched precisely because the thermo-

couples were installed within the lead spheres. The thermal disturbance created by the installation of the spheres and thermocouples was negligible because the spheres were very small (1.5 mm in diameter) and the sensors were thin (0.01 mm in diameter).

The thermocouples were calibrated by tying them into a bundle and putting them into a mixture of cooled water and crushed ice at a temperature of about –20°C. The bundle was left until the temperature of the mixture rose above the freezing point. Then the recorded temperatures of the thermocouples at which water and ice were in equilibrium were read, and the thermocouples that showed 0.0 C during the two-phase equilibrium were selected. The temperatures were measured with a digitally linearized data logger that had been calibrated at the factory to an accuracy of 0.1°C. All the thermocouples worked during the frost heave test except Numbers 7 and 8 in Test A. Thermocouple Number 7 stopped functioning after about 200 hours and Number 8 stopped after 500 hours.

Soil specimens

Some physical, mechanical and thermal properties of the soil studied are listed in Table 2. The soil was overconsolidated and contained a lot of unfrozen water. This test specimen was cored from a water-saturated alluvium bed and trimmed in the undisturbed state. A real undisturbed soil was used so that real frost heave phenomena would be observed. The result and applicability of proposed frost heave models can be verified by comparing them with the experimental data shown in this report.

Table 2. Physical, mechanical and thermal properties of the soil.

Size distribution		(% by weight)
Clay (<0.002 mm)		45.0
Silt (0.002–0.074 mm)		41.0
Sand (0.074–2.000 mm)		14.0
Gravel (>2.000 mm)		0
Atterberg limits		
LL		101.0 (%)
Ip		68.7
Specific gravity		2.48
Wet density		1.45 g/cm^3
Void ratio		2.6
Preconsolidation stress		0.248 MPa
Consolidation coefficient		5.78×10^{-2} cm^2/min
Compression index		1.233
Permeability		
By consolidation test		1.77×10^{-6} cm/min
By permeability test		4.61×10^{-6} cm/min
Volumetric unfrozen water content by TDR		
at	–0.2°C	60.7%
	–0.3	53.2
	–0.4	38.0
	–0.6	29.8
	–0.75	27.7
	–1.0	25.1
	–1.5	22.1
	–2.0	20.2
	–3.0	18.3
	–5.0	14.6
	–7.0	13.1
	–10.0	12.3
Thermal conductivity by thermal probe method		
at	24°C	6.0 cal/cm-hr-°C
	–5	12.0
	–10	16.1

Test conditions

The test conditions are listed in Table 1. The temperatures at both the top and the bottom surfaces were kept constant except between 360 and 377 hours and 930.5 and 1006 hours in Test A and between 111 and 167 hours in Test B. The overburden pressures were also kept constant up to 329 hours in Test A and 383 hours in Test B. During the growth of the final ice lens (stationary heaving), the warm-side temperature T_w, the cold-side temperature T_c and the overburden pressure P were changed several times to observe the effects on heave rate.

In this report the frost heave modes of the step-temperature-change frost heave test are identified as "transient heaving" and "stationary heaving" (Akagawa 1985). Transient heaving is characterized by soil freezing that causes a decrease in the unfrozen soil length, i.e. a penetrating 0°C isotherm. It results in what is called ice cement first and then ice

banding. Stationary heaving, on the other hand, is characterized by soil freezing that causes no decrease in the unfrozen soil length, i.e. a stationary 0°C isotherm. It is the result of the growth of what is called the last or final ice lens.

Test procedure

The frost heave test was conducted using the following procedure. The undisturbed specimen was placed in the water-filled, double-acrylic cylinder on top of the bottom cold plate. (The test sample was frozen from the bottom upward.) After the warm plate was placed on top of the specimen, the air bubbles were extracted from the space between the top of the soil and the warm plate through the upper pore-water supply line. An overburden pressure of 100 kPa was applied in addition to the test pressure to ensure good contact between the temperature control plate and the specimen surface. This pressure was maintained until consolidation was complete. During consolidation the warm-plate and cold-plate temperatures were maintained at +3°C. The overburden pressure was reduced to the value shown in Table 1 by unloading the extra 100-kPa surcharge and waiting until the rebound was complete. A cold brine with enough heat removal capacity to cool the cold plate and brine circulating system to the specified temperature was circulated to start the test, and then the surface temperature of the cold plate was adjusted to the test temperature when the temperature at the cold plate dropped slightly below the test temperature.

X-ray photograph exposure procedure

The X-ray photos were taken at the times listed in Table 3. For the first exposure the X-ray film was set behind the specimen at a right angle to the X-ray source through the center of the specimen, shown as Position 1 in Figure 3. The specimen was then exposed to X rays for 3–5 minutes depending upon the thickness of the ice lens. Another X-ray film was set in place, and the X-ray source was moved from Position 1 to Position 2, shown in Figure 3. A second exposure was taken using the same procedure as the first.

Table 3. Hours when X-ray photographs were taken.

Test A	*Test B*
–0.5 to 23.5*	–1 to 24*
44.5	28
141.5	46
304.5	70
524.5	118
664.5	166
832.5	172
1408.5	214
	286
	382
	388
	502
	646

* Every hour between these times.

A typical X-ray photo, taken at 118 hours during Test B, is shown in Figure 5 along with a temperature profile. All the X-ray photos are included in Appendix G. Since each lead sphere appears clearly in the photo, the coordinates of each sphere can be measured precisely. Since the lead spheres' temperatures have also been measured, a precise temperature profile associated with each photo is available. The ice lens distribution is also visible in this X-ray photo. Therefore, the temperature where the warmest ice lens is growing can be determined.

The X-ray photo in Figure 5 shows 20 lead spheres. Fifteen of them, numbered 0 to 14, represent the lead spheres that were installed within the soil specimen. The rest of the spheres, numbered from 21 to 25, were set between the soil specimen and the X-ray film; these five X-ray shadows were used as fixed control points for the coordinate analysis for Test B. For Test A, four immobile points numbered 21 to 24 were used.

Image processing for the X-ray photographs

An image processing procedure was used so that the coordinates of the lead spheres could be determined by computer. The X-ray photo image was converted to 640 × 400 pixels of digital data using a high-resolution CCD camera that has 8-bit (256) intensity grades (one pixel represents an area of 0.17 × 0.17 mm on the X-ray photograph).

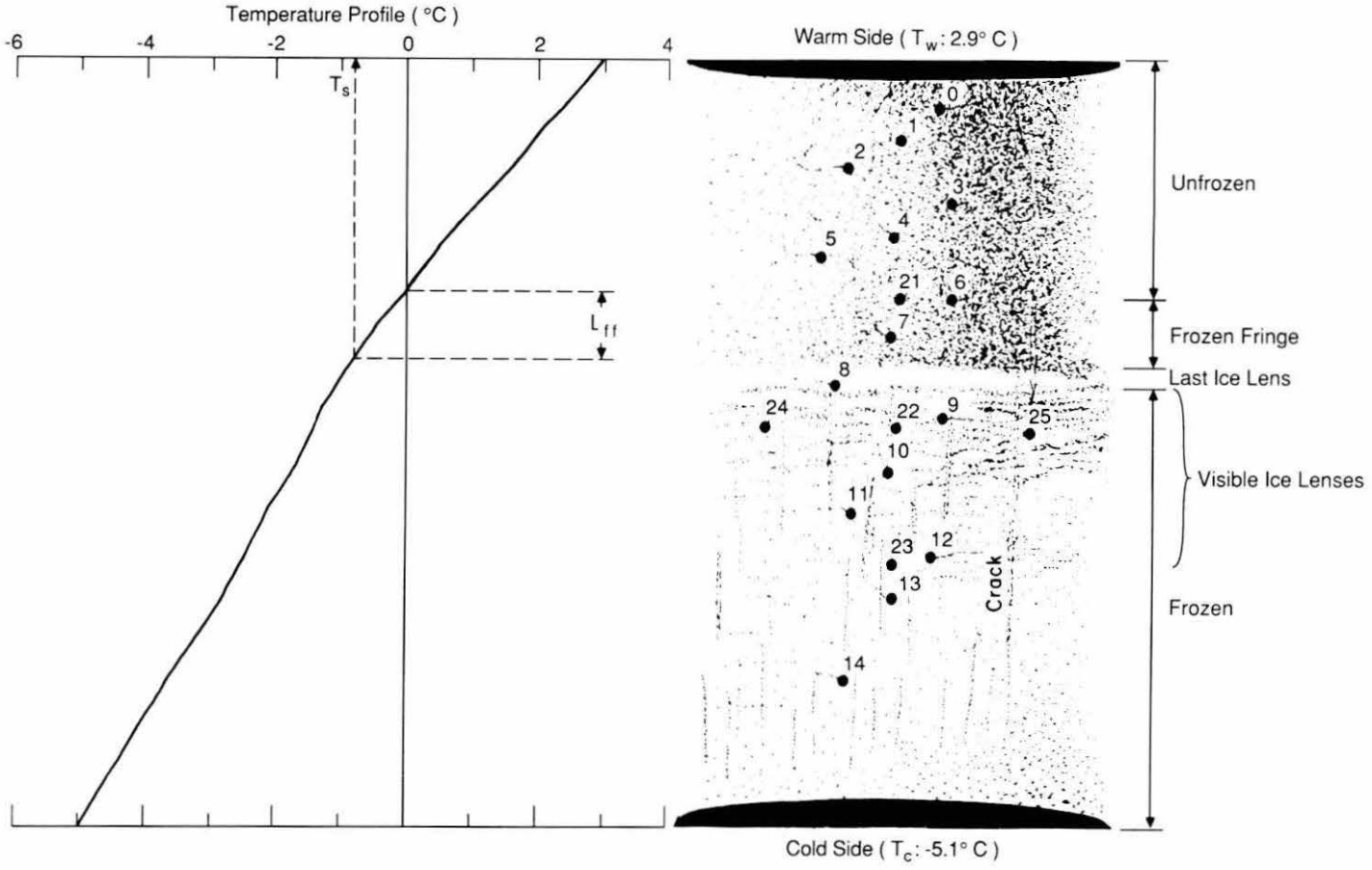

a. Temperature profile.

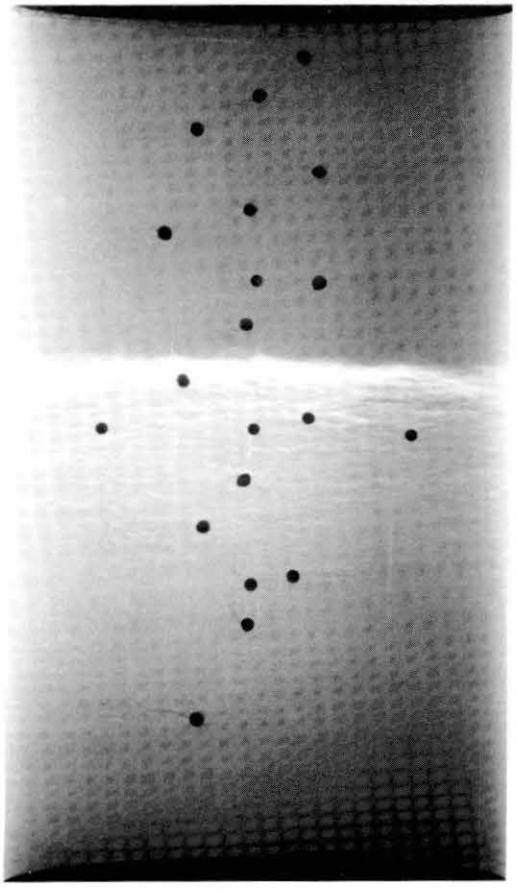

b. X-ray photograph.

Figure 5. Typical X-ray photograph and temperature profile.

The digitized data were processed by two kinds of window operators (spatial filtering). First, a 3 × 3 low-pass filter was applied to improve the signal-to-noise ratio, and then a 3×3 spatial differential filter was applied to enhance the edge of the lead spheres' images. By this process the image of a lead sphere was converted from a low-intensity black circular spot to the ring pattern shown in Figure 6a. A computer can distinguish this pattern from other patterns, such as vertical shrinkage cracks and lamina-shaped ice lenses.

The addresses or coordinates of the interior of the circle from which a centroid can be calculated were determined by applying two other filters (Fig. 6b,c). Because of the large number of pixels in a photo (256,000), rough filtering requiring rather short computation times was applied first. This filter (Fig. 6b) searches the area for the ring-shaped image surrounding the lead spheres by checking nine pixel intensities. If a pixel has low intensity and is surrounded by four outer or inner high-intensity pixels, this pixel is selected for further filtering. The subsequent filterings need much more computation time than the first. These are only applied to the pixels nominated by the first simple filter. These filters (Fig. 6c) determine the shape of the ring by checking the integrated intensity of the pixels in the high-intensity ring and the low-intensity circle in the center. Only about five pixels located in the interior of the ring pass all these filtering stages. The centroids of all the ring images were computed by calculating the mean value of every nominated pixel's coordinates.

Since these coordinates represent only relative locations, the absolute coordinates were computed by comparing them to a reference coordinate. In this conversion the coordinates of lead sphere 22 in X-ray photos taken from Position 1 were selected as the reference. The three-dimensional coordinates of the ring image were calculated using the geometry shown in Figure 3. The mean value of the coordinates' standard deviation for the immobile points (numbers 21, 23, 24 and 25) was found to be 0.053 mm.

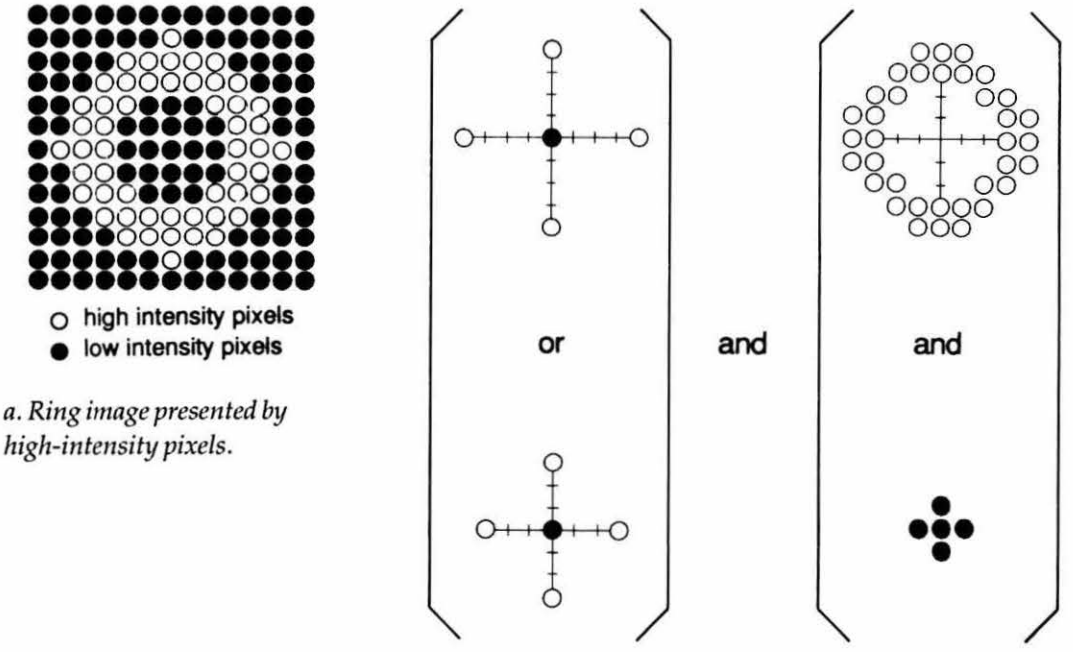

a. Ring image presented by high-intensity pixels.

b. First filter.

c. Second filter.

Figure 6. Image-processing filters for analyzing the sphere coordinates.

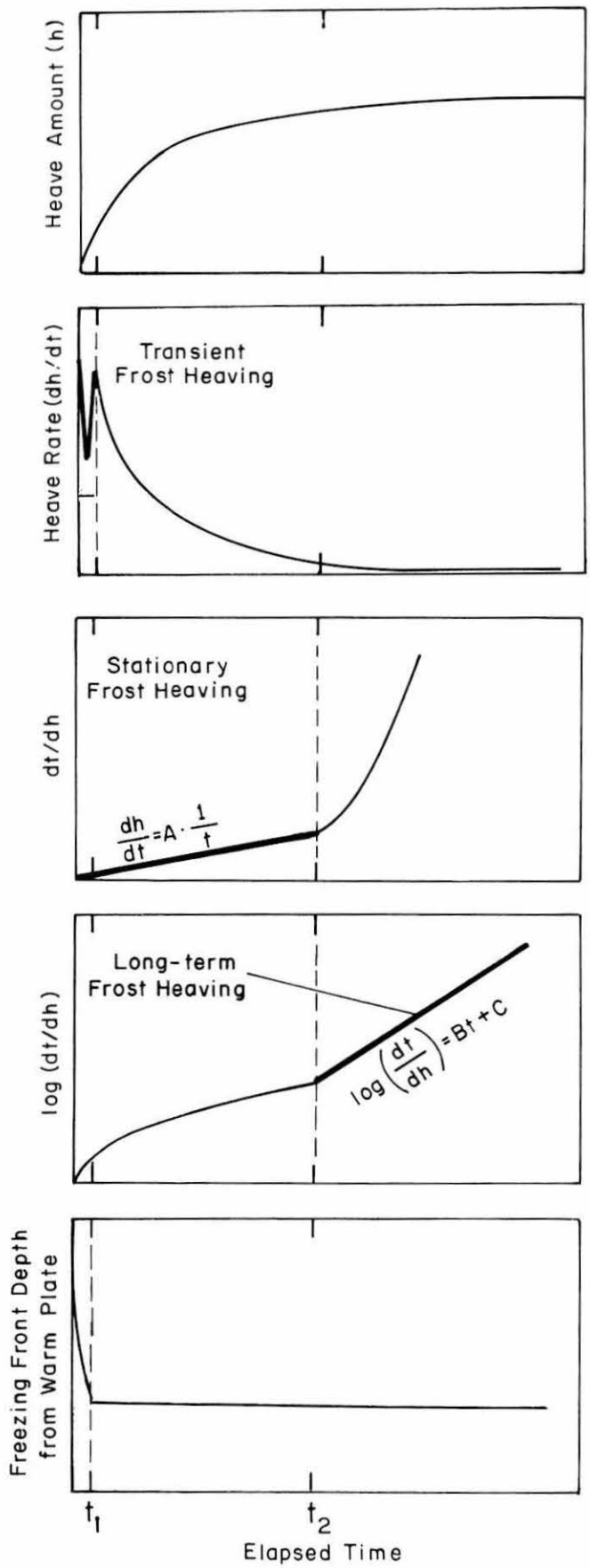

Figure 7. General heave properties of the soil. A, B *and* C *are constants, and* dh/dt *is the total heave rate. (After Akagawa 1985.)*

TEST RESULTS

Conventional heave test results

Total heave and total heave rate curves of this soil under step-temperature-change freezing, discussed by Akagawa (1983, 1985), are shown in Figure 7. As in other similar frost heave tests, this soil consistently heaves at a high rate during the early stages of freezing with one minimum point and at a gradually decreasing rate during the later stages.

Figure 8 shows that the same types of heaving properties were observed in both Test A and Test B. The figure also shows the durations of the overburden pressure and the

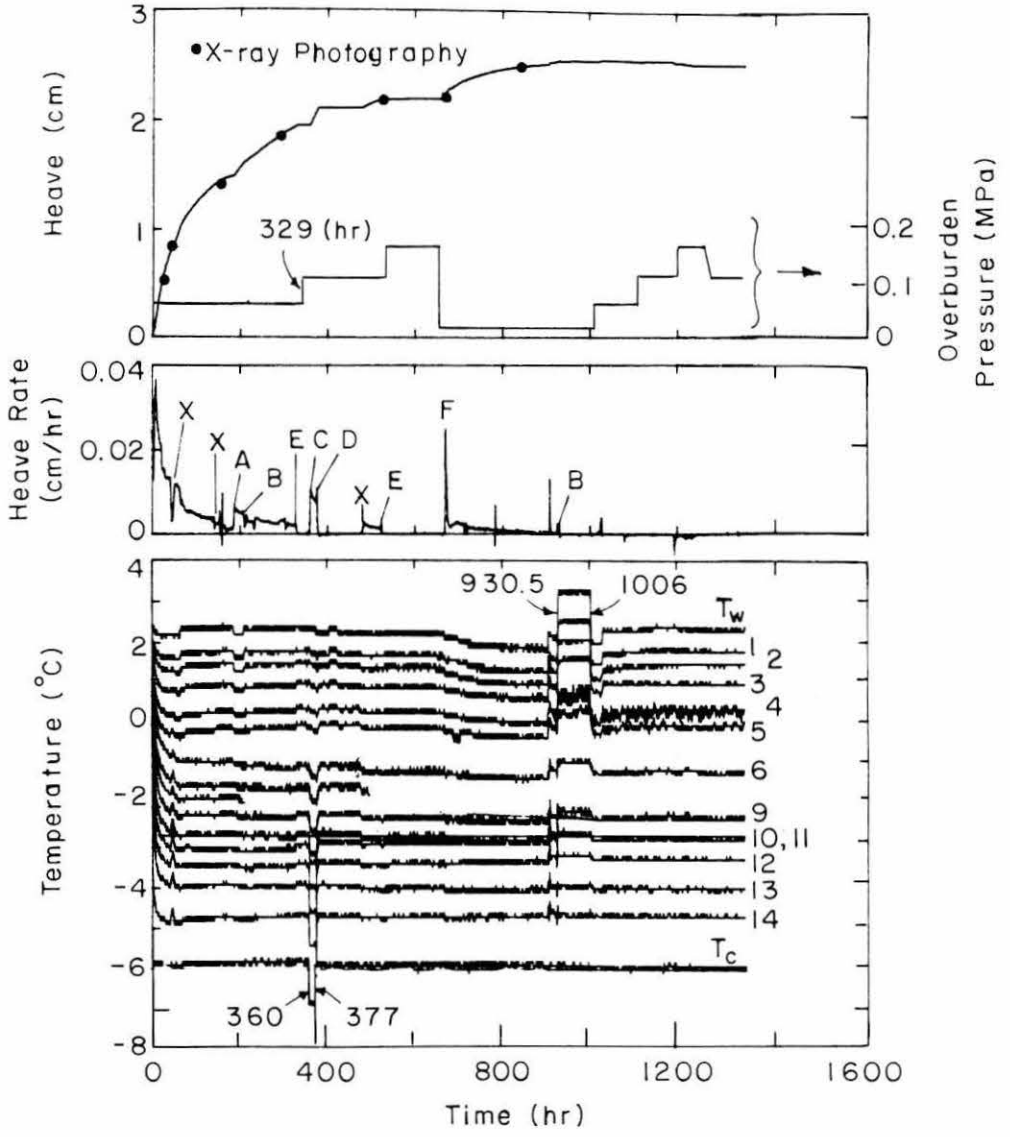

a. Test A.

X: Uncertain disturbance of the heave rate, possibly caused by disturbance of the coldroom temperature.
A: Heave rate increase due to lowering of the warm-side temperature.
B: Heave rate decrease due to raising of the warm-side temperature.
C: Heave rate increase due to lowering of the cold-side temperature.
D: Heave rate decrease due to raising of the cold-side temperature.
E: Heave rate decrease due to raising of the overburden pressure.
F: Heave rate increase due to lowering of the overburden pressure.

Figure 8. Conventional results of frost heave tests.

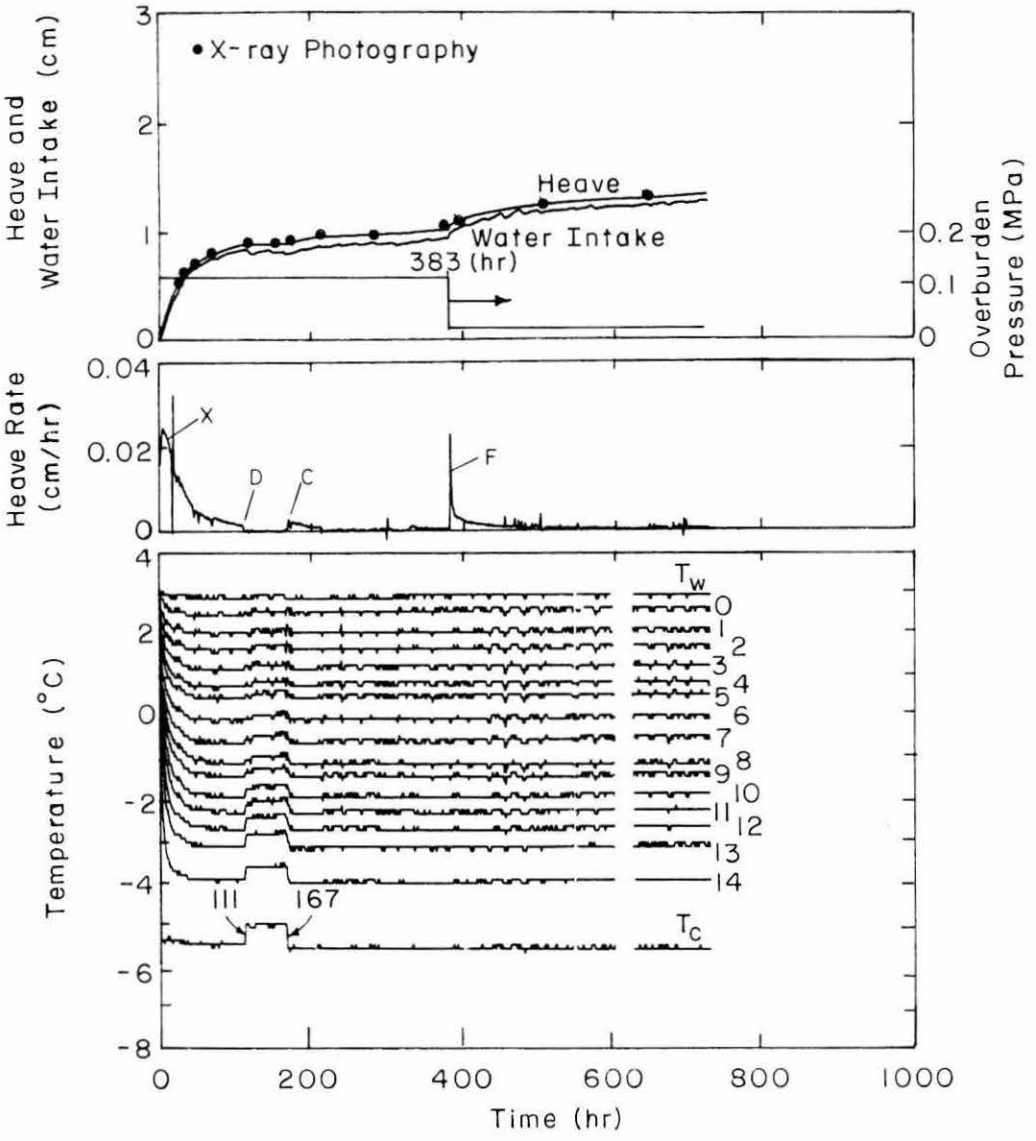

b. Test B.

Figure 8 (cont'd).

times when X-ray photos were taken. In Figure 8b (Test B) the water intake amount is shown as the height of water in the cell (the amount of intake water divided by the horizontal section area of the cell). Figure 9 shows the water intake amount for Test A. During the early stages of Test A (13–14 hours), pore water started to leak from a small hole in the upper part of the cell through which a thermocouple was installed. After that the water head of the pore water source was maintained just below the level of the hole to prevent leakage. Thus the water flow measurements for Test A were abandoned after 13 hours, when the leak began.

Figure 8 confirms the following experimental results:

- Under similar thermal conditions, the lower overburden pressures resulted in higher total heave amounts. (The total heave amount in Test A was greater than in Test B.) However, this trend is not clear during transient heaving.
- Raising the cold-plate temperature at 377 hours in Test A and 111 hours in Test B resulted in a decrease in heave rate, and lowering the cold-plate temperature at 360 hours in Test A and 167 hours in Test B increased the heave rate.

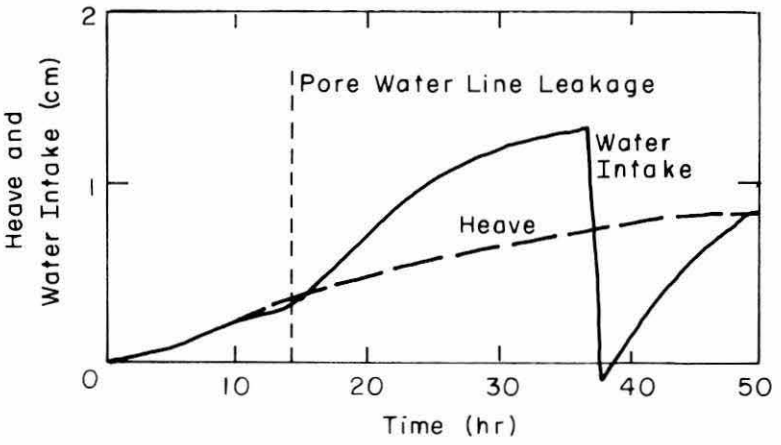

Figure 9. Pore water leakage after 13 hours in Test A.

- The heave rate varied during step-temperature freezing. Therefore, a simple description of the heave rate or heave amount seems meaningless.

These are the experimental results normally observed by conventional measurements during frost heave tests.

Positions of the lead spheres

The changes in the Z coordinates of all the lead spheres in Test A and Test B are shown in Figure 10 in comparison with 0°C isotherm. Each data point represents the Z coordinate or the distance from the cold plate at a specific time. Each distance between two adjacent data points at a specific time shows the thickness of the soil layer between them. This figure shows when and where the soil expands. As the 0°C isotherm penetrates, the soil layers below it expand. However, since it is difficult to make precise observations from these figures, the expansion properties of each soil layer will be shown later in detail.

Since the 0°C isotherm penetration into the unfrozen soil seems to become stationary at about 40–50 hours, stationary heaving had presumably started around this time.

Temperature profiles

From the Z coordinates and the temperatures of the lead spheres, temperature profiles can be drawn (Fig. 11). Appendix A lists the Z coordinates and temperatures at each observation time for both tests. All the temperature profiles are shown in Appendices C and E along with the strain or strain rate distributions.

Each temperature profile shows the location of the warmest ice lens if the lens was visible in the X-ray photo. Since past definitions of the term "frozen fringe" are not clear, the distance between the location of the visible warmest ice lens and the 0°C isotherm will be assumed to be the apparent thickness of the frozen fringe L_{ff}. The temperature at the warm side of the warmest ice lens is assumed to be the apparent ice segregation temperature T_s.

During Test A, temperatures at the side boundary between the frost heave cell and the test specimen were also measured every 5 mm. Figure 12 shows the temperature profiles for the side of the specimen and the center of the specimen. Even though care was taken to prevent it, lateral heat flow may have caused a slight temperature difference, especially at the lower end of the cell. This tendency is reasonable because the temperature difference at the cold end of the specimen is the largest; the room temperature was kept at about 0°C and the specimen temperature was kept at about +2°C at the warm side and –6°C at the

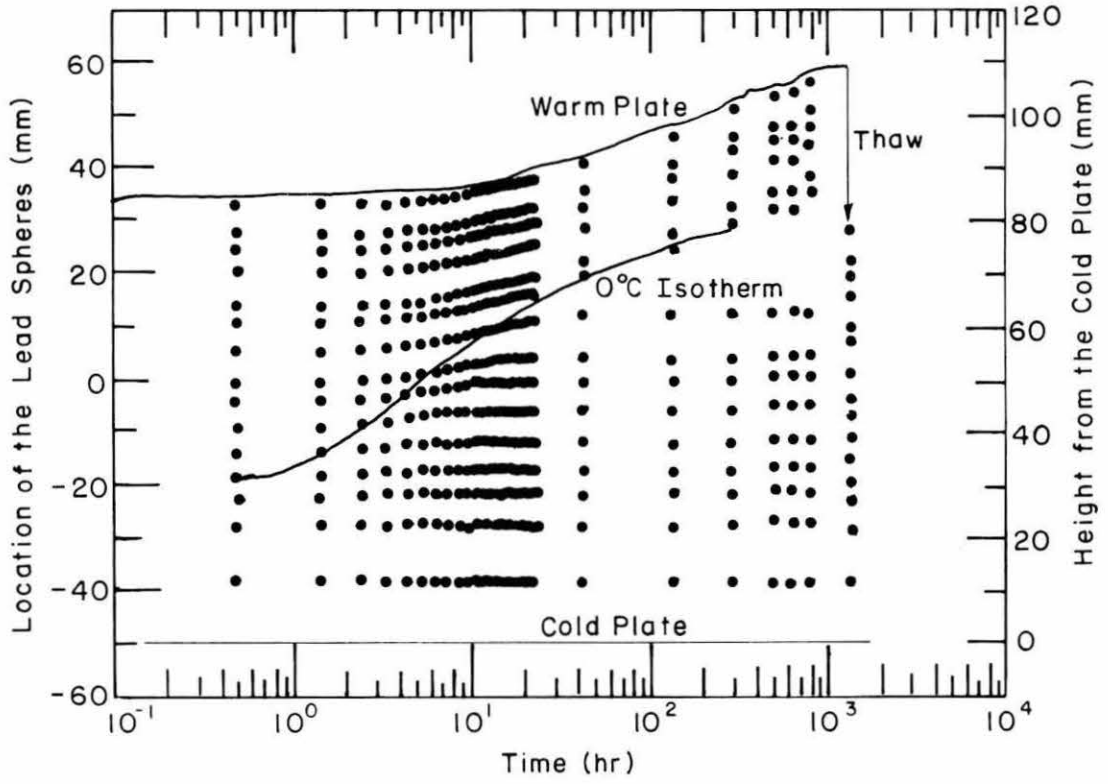

a. Test A.

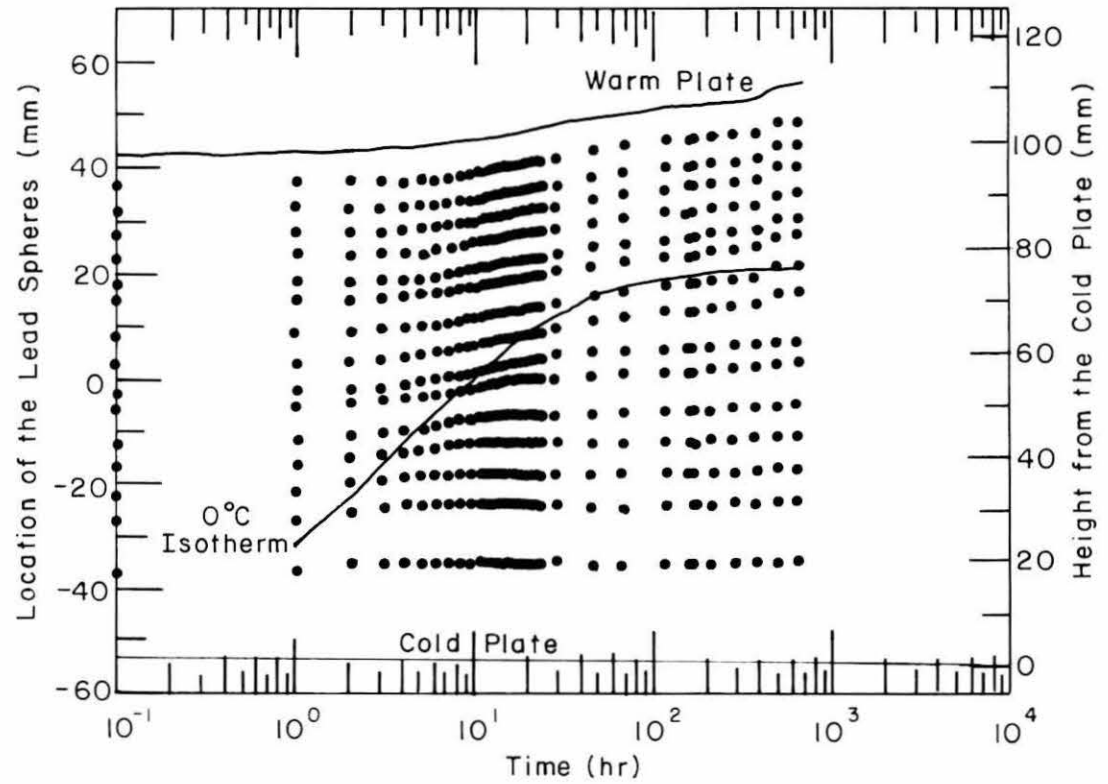

b. Test B.

Figure 10. Analyzed Z coordinates of the lead spheres.

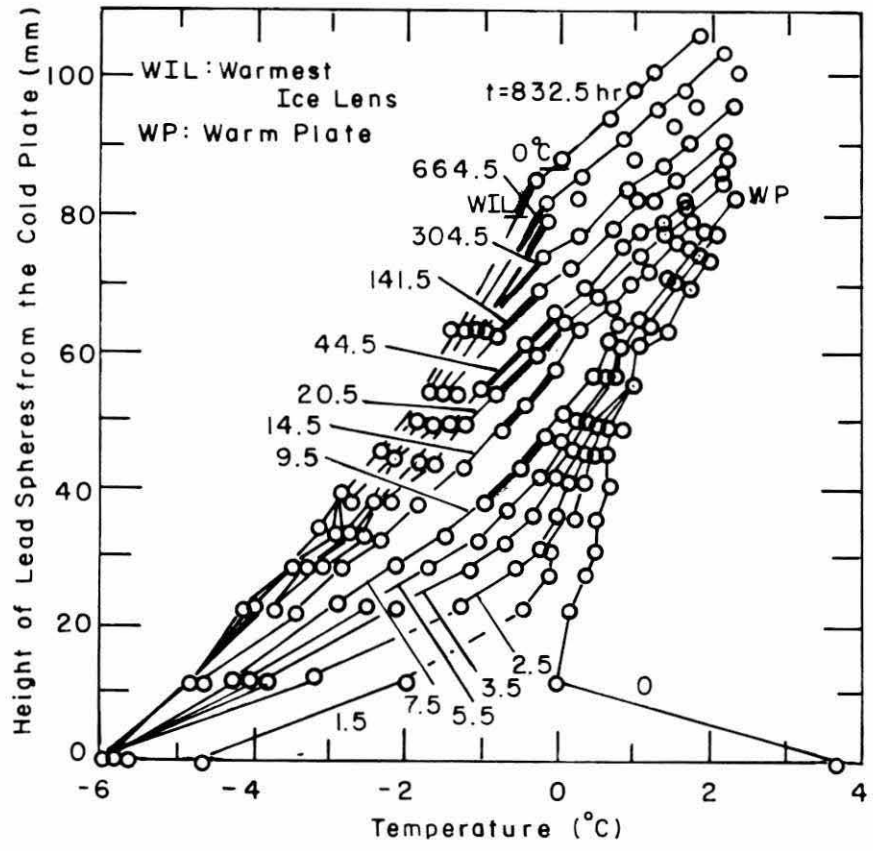

a. Test A.

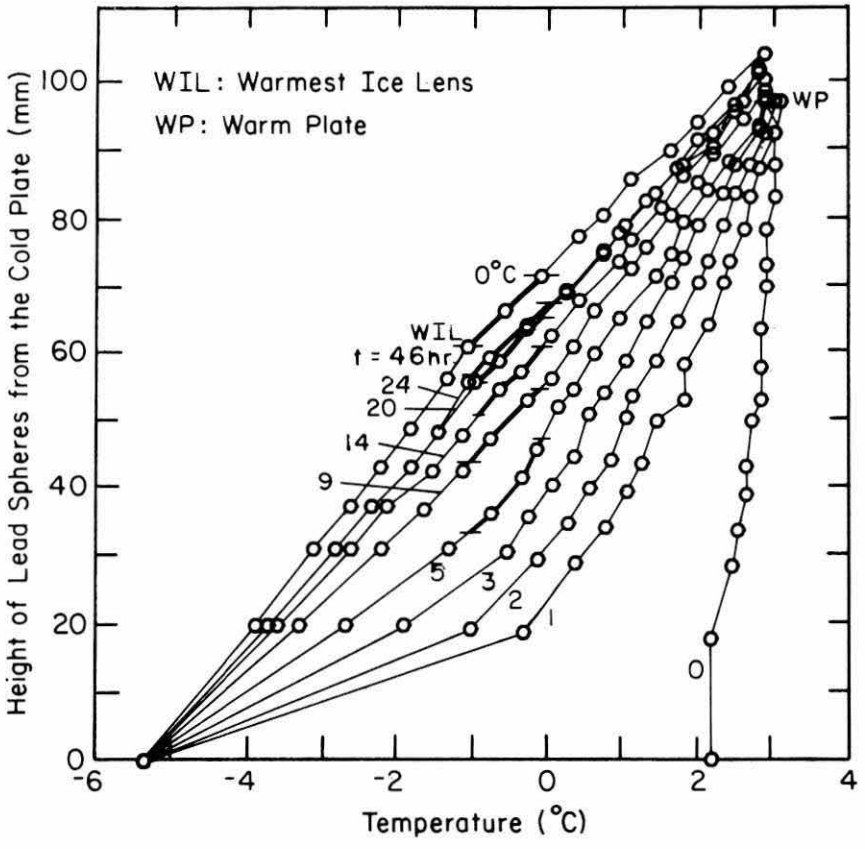

b. Test B.

Figure 11. Analyzed temperature profiles.

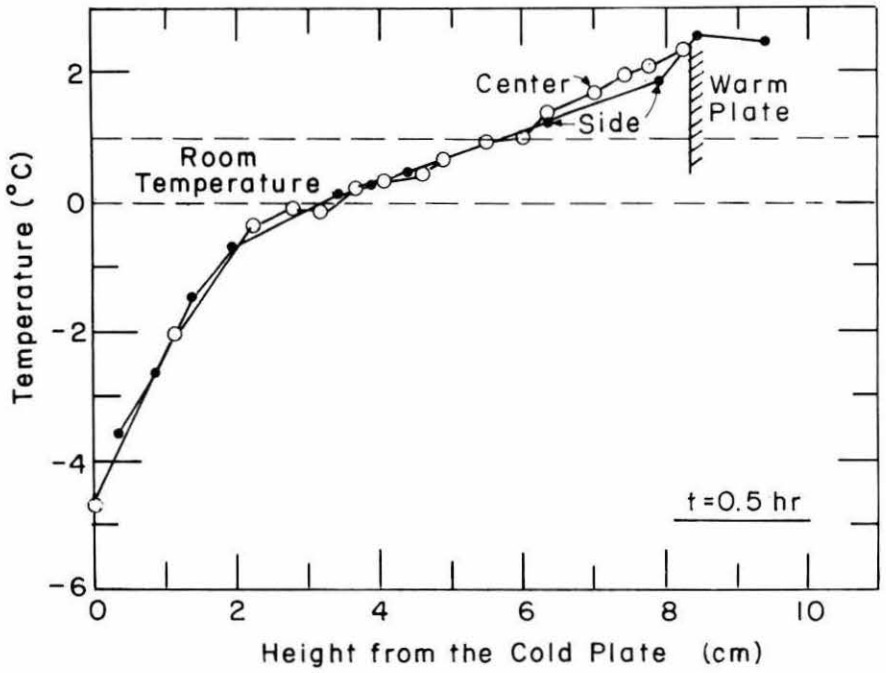

a. After 0.5 hours.

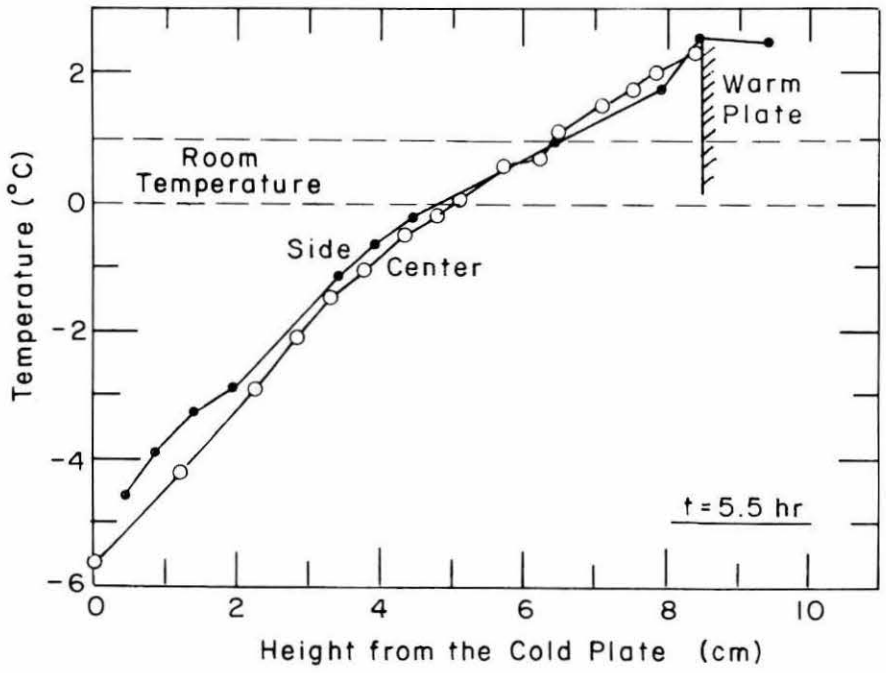

b. After 5.5 hours.

Figure 12. Comparison of temperature profiles for the lead spheres and the surface of the samples.

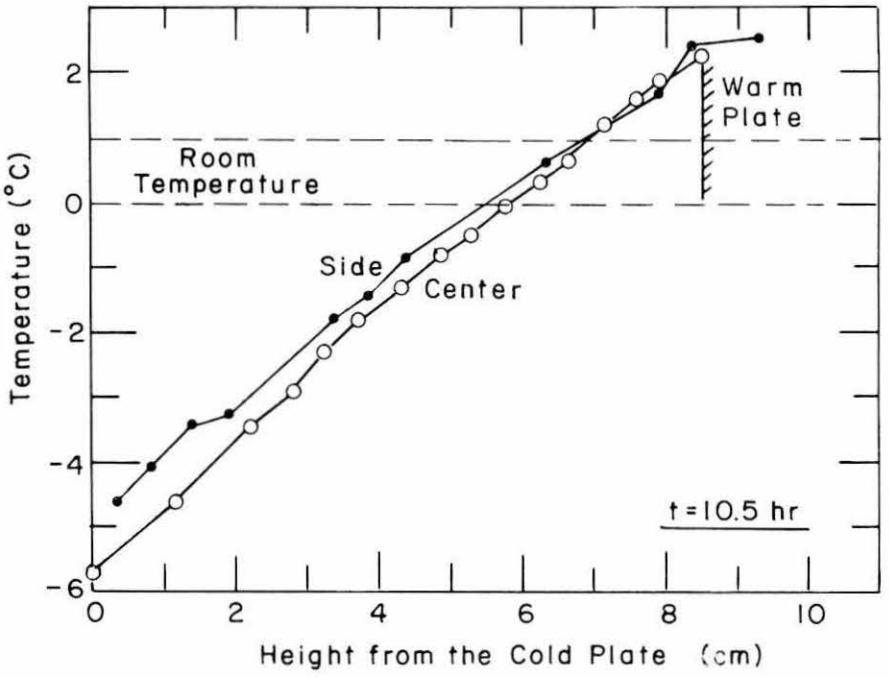

c. After 10.5 hours.

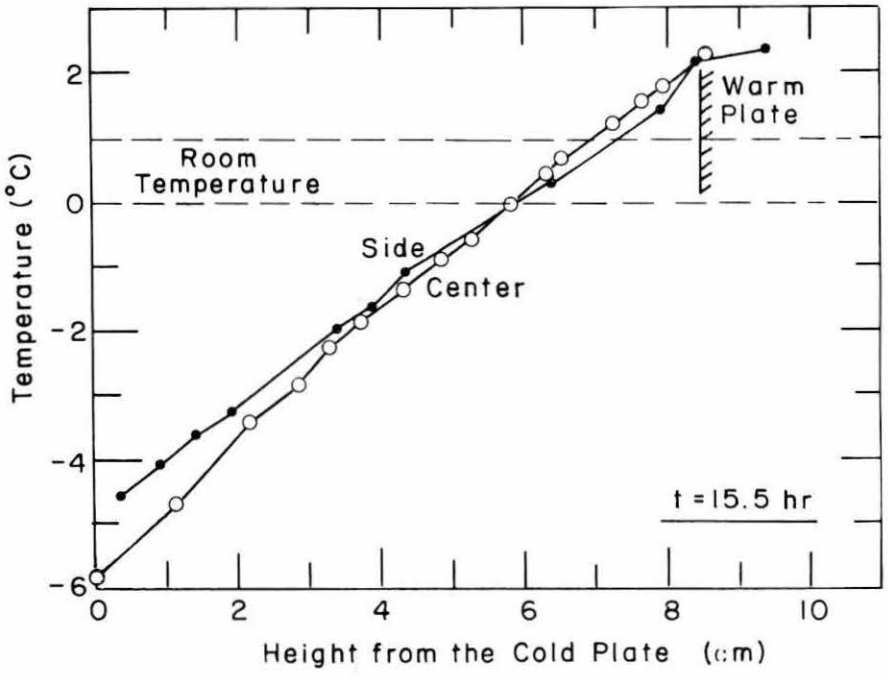

d. After 15.5 hours.

Figure 12 (cont'd). Comparison of temperature profiles for the lead spheres and the surface of the samples.

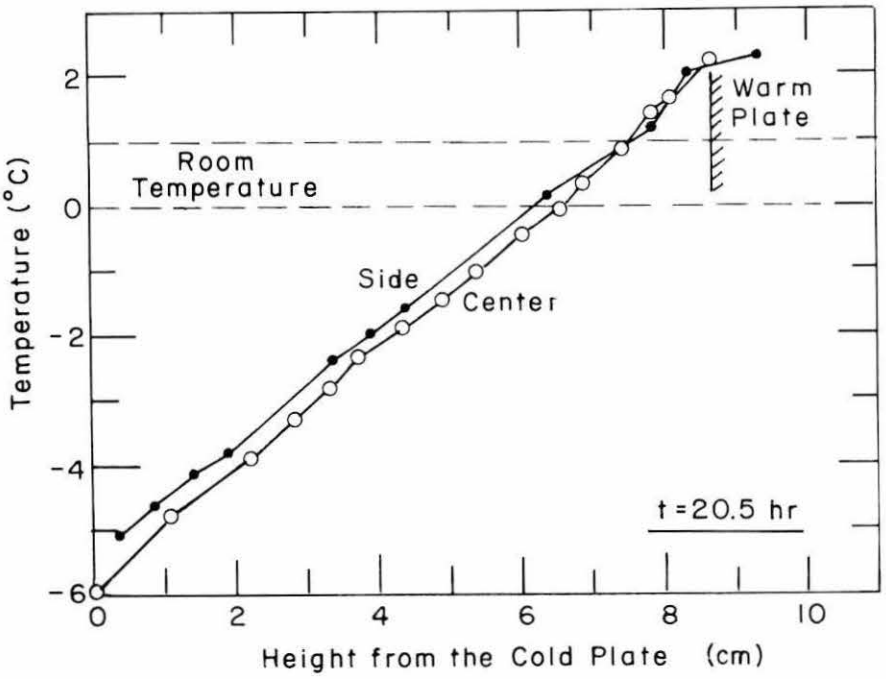

e. After 20.5 hours.

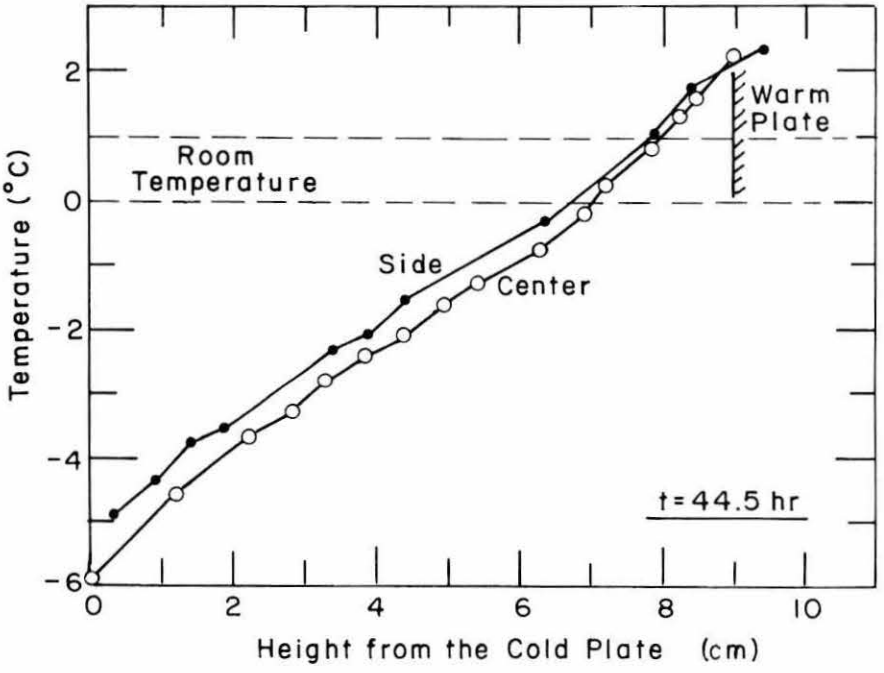

f. After 44.5 hours.

Figure 12 (cont'd).

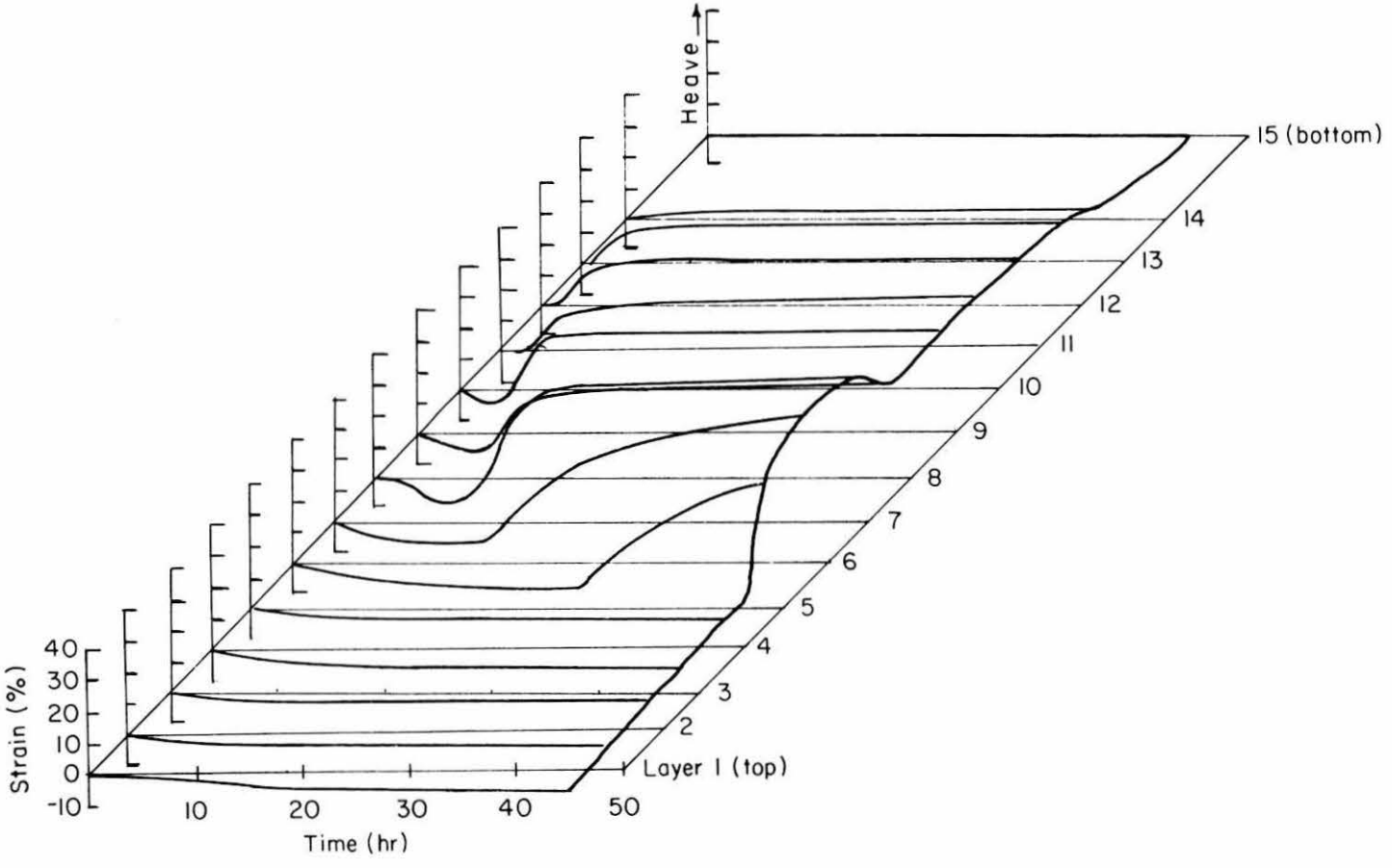

a. Test A.

Figure 13. Strain development in freezing soils. Heave is positive.

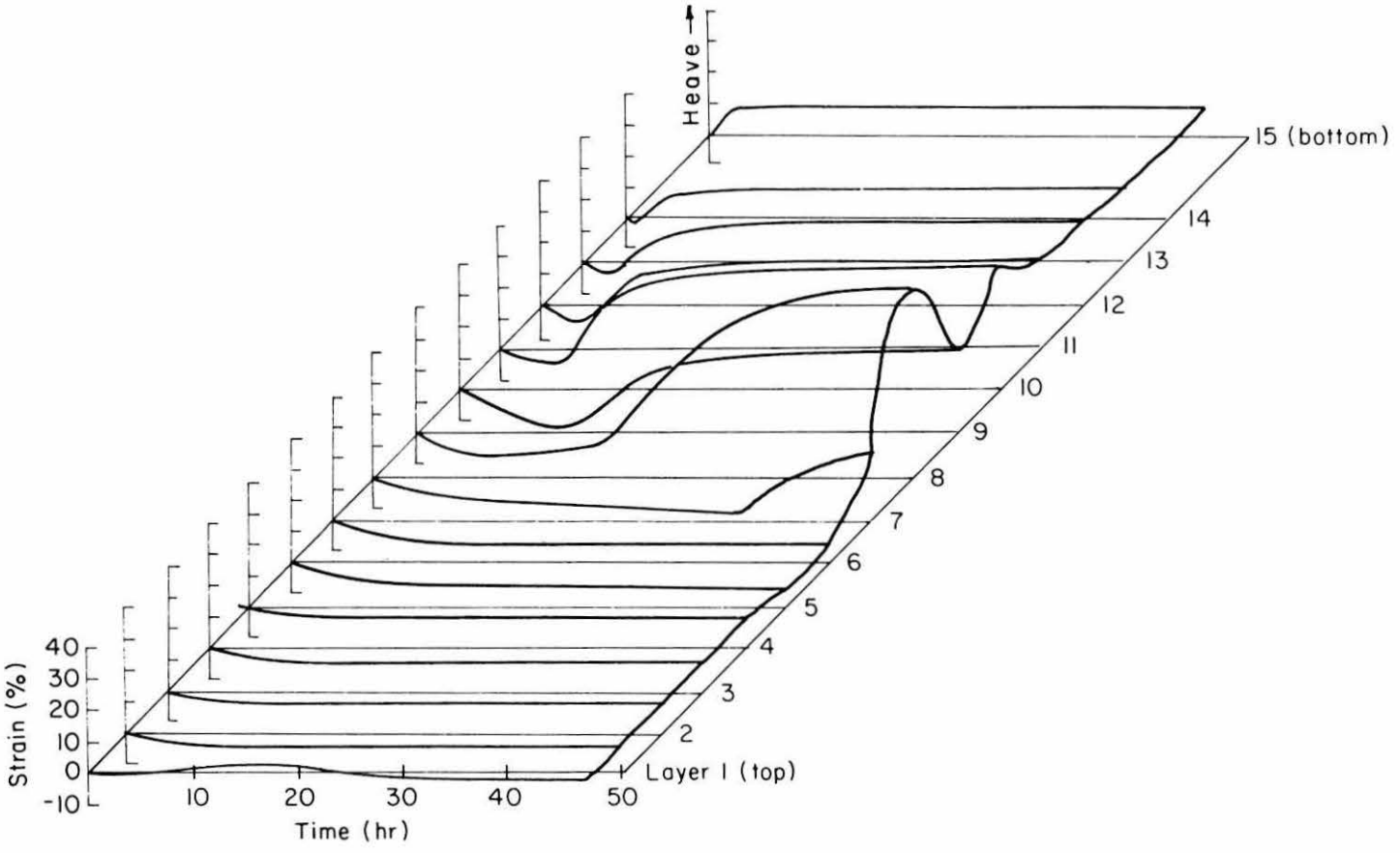

b. Test B.

Figure 13 (cont'd).

cold side. Since the ice lenses in the specimen were not concave but were rather flat, this lateral heat flow was not causing enough thermal disturbance to seriously affect ice lens formation, especially at the warmest ice lens, where segregation was presumably most active. However, these comparisons suggest that the measurement error has to be recognized when temperature profiles are measured from the side surface of the specimen.

A much more fundamental problem is whether or not linear interpolations of the temperature profile from the warm-side and cold-side temperatures are acceptable. Of course the validity of the interpolation will depend on how precise a temperature reading is necessary for the specific study. However, from the temperature profiles in Figure 12, the linear interpolation seems to be unacceptable during the early part of the transient freezing and most of the stationary freezing if thick ice lens segregation is expected or recorded.

Strain developed by freezing in each soil layer

Figure 13 shows the expansion change in percent strain for each layer. To calculate strain, two adjacent lead spheres at time t were identified as (t,n) and $(t,n+1)$. The Z coordinates for these spheres were written as $Z(t,n)$ and $Z(t,n+1)$. The conventional strain ε in a soil layer was then calculated as follows:

$$\varepsilon\,(n,t) = \frac{[Z\,(t,n) - Z\,(t,n+1)] - [Z\,(0,n) - Z\,(0,n+1)]}{Z\,(0,n) - Z(0,n+1)} \,. \qquad (1)$$

Expansive strain is assumed to be positive. Appendix B shows the strain change in each soil layer, and Appendix C shows the strain distribution at times when X-ray photos were taken.

In Test A, since the strain at 0.5 hours is treated as the initial value, the strain developed between 0 and 0.5 hours is ignored; 0 hours is treated as the initial value in Test B. Because of this difference, no strain was shown in Layer 15 of Test A, located between Sphere 14 and the cold plate, because the temperature of Sphere 14 had already dropped to –2°C at 0.5 hours and about 70% of the water had frozen by then. Since only 1–2% of the unfrozen water would be expected to freeze during a further temperature drop in this layer, no expansion was measured during the experiment.

These experimental results show that expansive (heaving) strain progressed from the lower layers to the upper layers as time elapsed following penetration of the 0°C isotherm. As the 0°C isotherm penetration rate decreased, expansive strain became greater, and negative (consolidation) strain in the unfrozen soil appeared clearly before the expansion took place.

All of the unfrozen soil layers consistently shrank in thickness during the first freezing stage. This kind of shrinkage has been observed by Taber (1929) and studied by Nixon and Morgenstern (1973) and Chamberlain and Gow (1979); however, this report might be the first description of when, where and how much shrinkage is taking place. The earlier studies concluded that this shrinkage may be caused by the increase in effective pressure caused by the decrease in pore water pressure at the freezing front. The magnitude of the shrinkage observed in the unfrozen layers in this study tended to be greater in the layer nearest the warmest ice lens than in the layer nearest the warm plate. This tendency supports the conclusions of Taber, Nixon and Chamberlain that there is a pore water depression at the boundary of the warm side of the warmest ice lens. The maximum shrinkage is so high (about 10% in strain) that it results in much greater preconsolidation stress of the clay. The preconsolidation stress for this soil has been observed at a strain of about 5% by consolidation tests (Fig. 14).

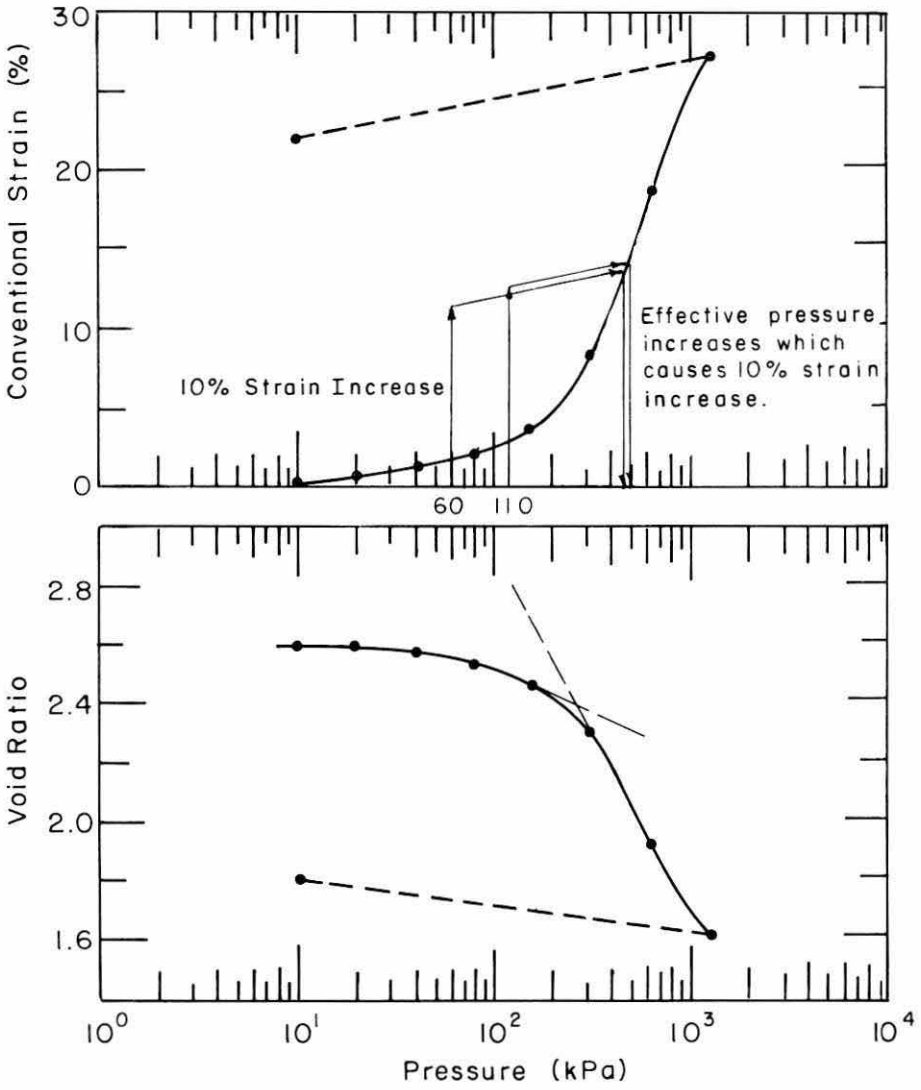

Figure 14. Consolidation properties of the test soil and nomographic pore water pressure of segregating ice.

The maximum shrinkage strain of 10% observed in this study would be caused by an increase of effective pressure of about 0.4 MPa. This increase of effective pressure may be understood to be the result of negative pore water pressures in the unfrozen layers. Since the magnitude of the pore water pressure depression is the mean pore pressure in the layer, and the pore water pressure may have a gradient, the maximum depression should be greater than the revealed value.

In addition, even though the shrinkage had been studied earlier, many frost heave tests have been conducted without concern for this aspect. In other words, frost heave studies using total heave amount or heave rate may cause confusion because the total heave measured may consist of both heave and shrinkage, particularly in clay soils. Figure 15 shows the positive expansion (real heave amount) and the negative expansion (real shrinkage) observed in the tests. The time-dependent properties of the real heaving and shrinkage in Test A and Test B are identical qualitatively and quantitatively if we consider the initial time difference mentioned above. The strong shrinkage took place during the first 3–4 hours, and a slight recovery was seen between 4 and 20 hours. This drastic shrinkage in the early stages of freezing is clearly reflected in a negative peak in the total

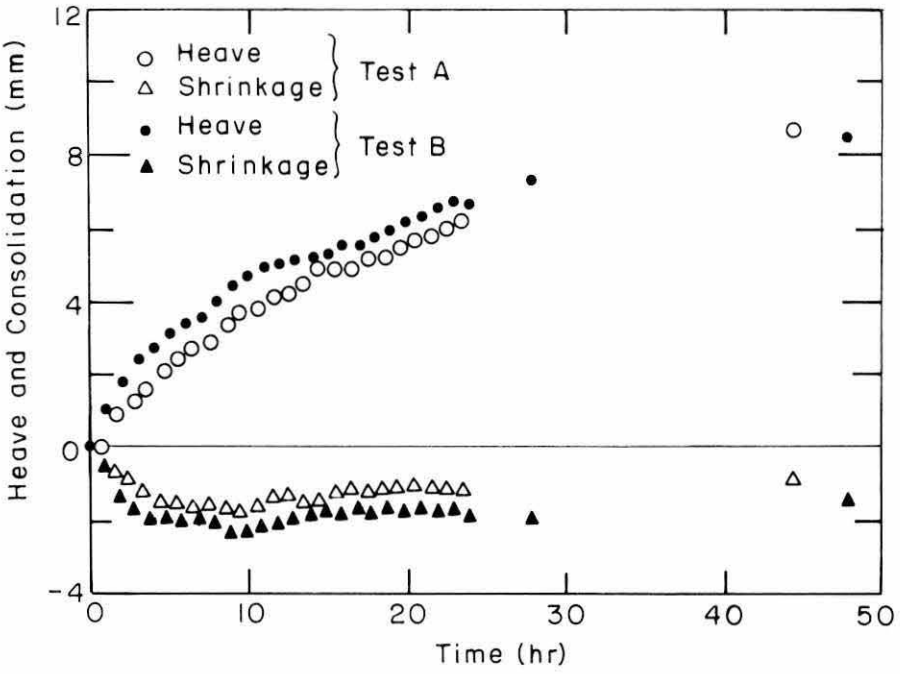

a. First 50 hours.

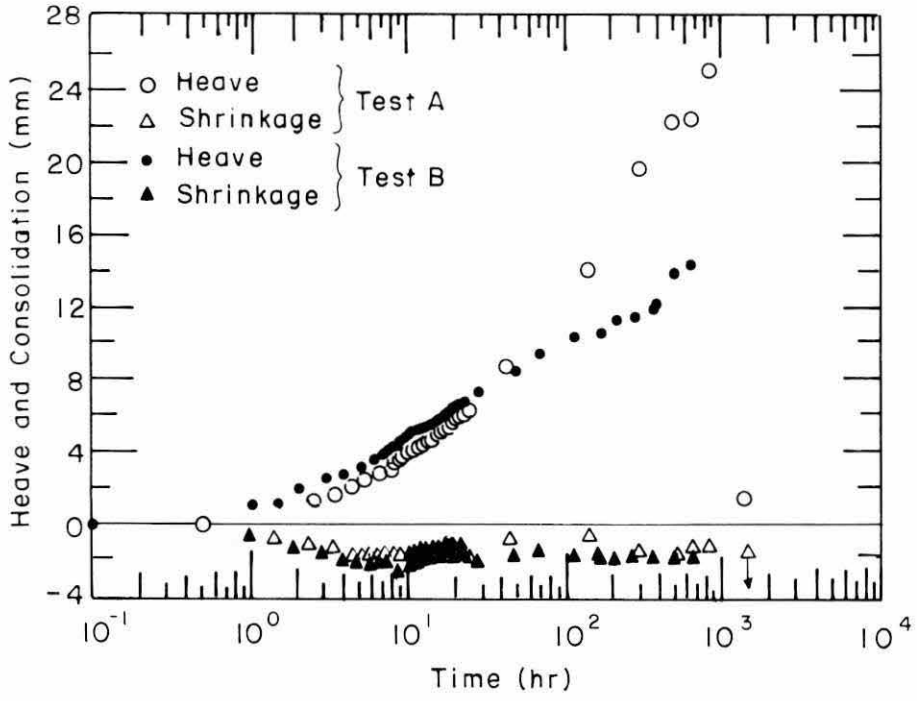

b. All hours.

Figure 15. Expansion (heave) and shrinkage (consolidation) in the freezing soil.

heave rate curves shown in Figure 16, which shows the heave properties in the early part of freezing. This negative peak has been observed even in freezing rocks (Akagawa et al. 1988).

Therefore, without knowing the amount of shrinkage, the total heave amount will demonstrate nothing for this time period. Of course this time period and the magnitude of shrinkage may vary with test conditions and soil properties. This period is related to a period of transient freezing that is characterized by a penetration of the 0°C isotherm. In other words, the total heave observed during stationary frost heaving that is characterized by the dominant growth of the final ice lens may show the real growth amount of the ice lenses, as is seen in Figure 15b, because no shrinkage is seen during this period. In addition, the effect of the overburden pressure on the heaving amount becomes clear during stationary frost heaving, but the effect is not clear during transient heaving (Fig. 15b).

Strain rate of each soil layer

Figure 17 shows the time-dependent expansion rate change in each layer. To calculate the strain rate, two adjacent lead spheres at time t were identified as (t_1,n) and $(t_1,n+1)$. The Z coordinates for these spheres were written as $Z(t_1,n)$ and $Z(t_1,n+1)$. The mean true strain rate at a period between t_1 and t_2, $(d\varepsilon/dt)$, is defined as

$$\frac{d\varepsilon((t_1,n)}{dt} = \frac{[Z(t_2,n) - Z(t_2,n+1)] - [Z(t_1,n) - Z(t_1,n+1)]}{[Z(t_1,n) - Z(t_1,n+1)] \cdot (t_2 - t_1)} . \quad (2)$$

Expansive strain rate is assumed to be positive. Appendix D shows the strain rate change in each soil layer, and Appendix E shows the strain rate distribution at times when X-ray photos were taken.

Figure 17, a smoothed version of Appendix D, clearly shows the deformation activity (heave and consolidation) due to freezing. The expansive strain began in the lower (colder) layers at the early stages of freezing and moved to the upper layers as the freezing zone reached each layer. In the early stages of freezing, unfrozen Layers 6–11 in Test A and 9–13 in Test B shrunk strongly. Layers 1–5 in Test A and 1–8 in Test B, which remained unfrozen throughout the tests, shrank slightly during the first 20–30 hours; this corresponds to the period of transient heaving.

A discussion about pore water migration during transient heaving, the deformation activity shown in Figure 17, and the temperature-dependent unfrozen water content listed in Table 2 has been published by Akagawa (1988a) regarding the location and dominance of in-situ and segregation freezing.

Apparent temperature range of the frozen fringe

From the temperature profiles and the location of the warm side of the warmest ice lens shown in Appendices C and E, the apparent temperature of the segregating ice lens T_s was determined (Fig. 18). During Test A, T_s tended to rise with time, from –1° to –0.4°C, during constant overburden pressure and boundary temperatures; during Test B, T_s tended to remain constant at slightly below –0.8°C during constant test conditions. Figure 19 shows the difference in T_s between Test A and Test B when the test conditions were kept constant. It is uncertain whether there is a difference in T_s in the first 30 hours because the accuracy of the T_s values for the the warm side of the warmest ice lens is questionable.

After 329 hours in Test A and 383 hours in Test B the overburden pressure was changed several times, and after 360, 377, 930.5 and 1006 hours in Test A and 111 and 167 hours in Test B the boundary temperatures were changed to see the effect on T_s. However, the data

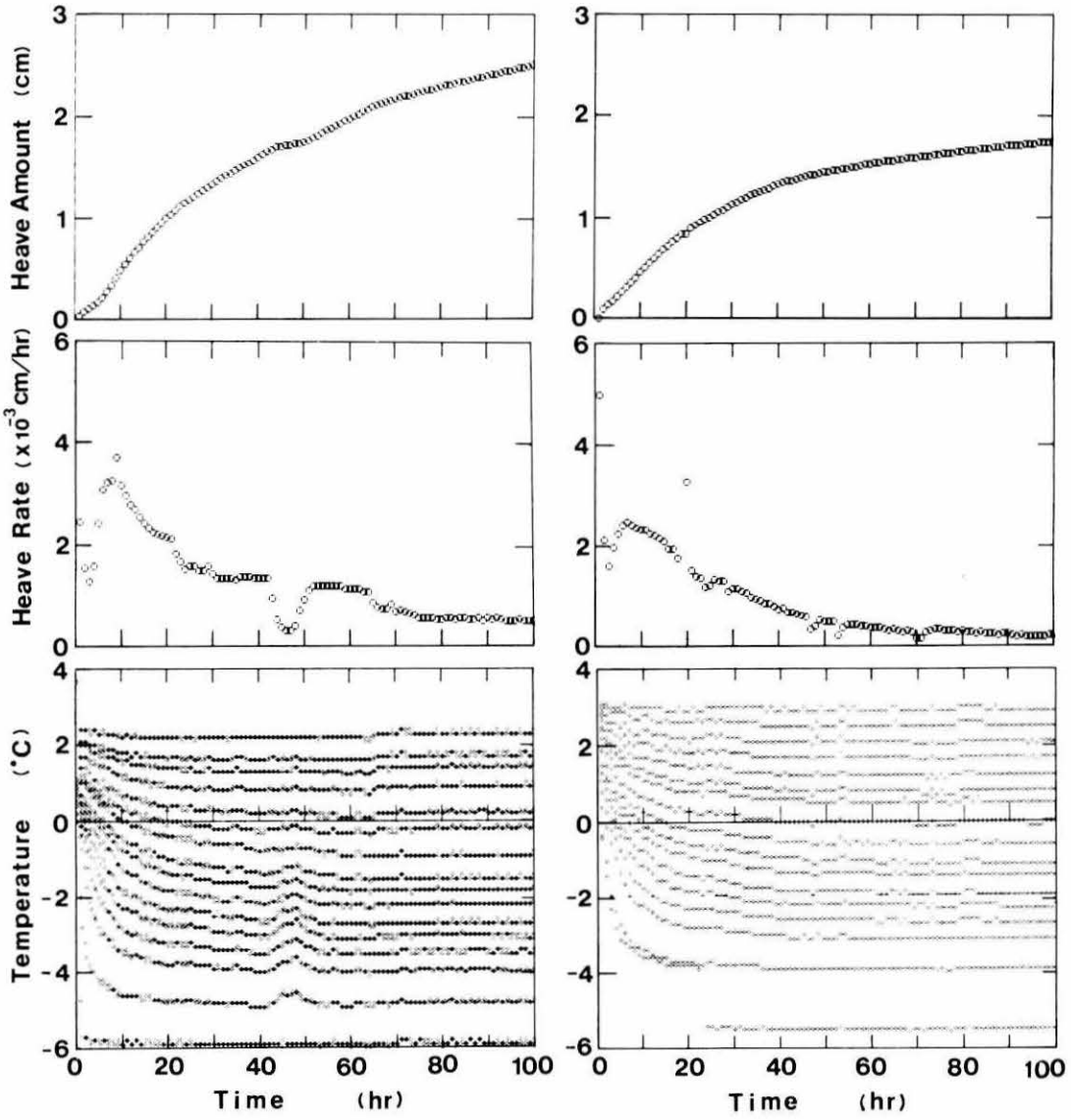

a. Test A. *b. Test B.*

Figure 16. Heave properties in the early stage of freezing.

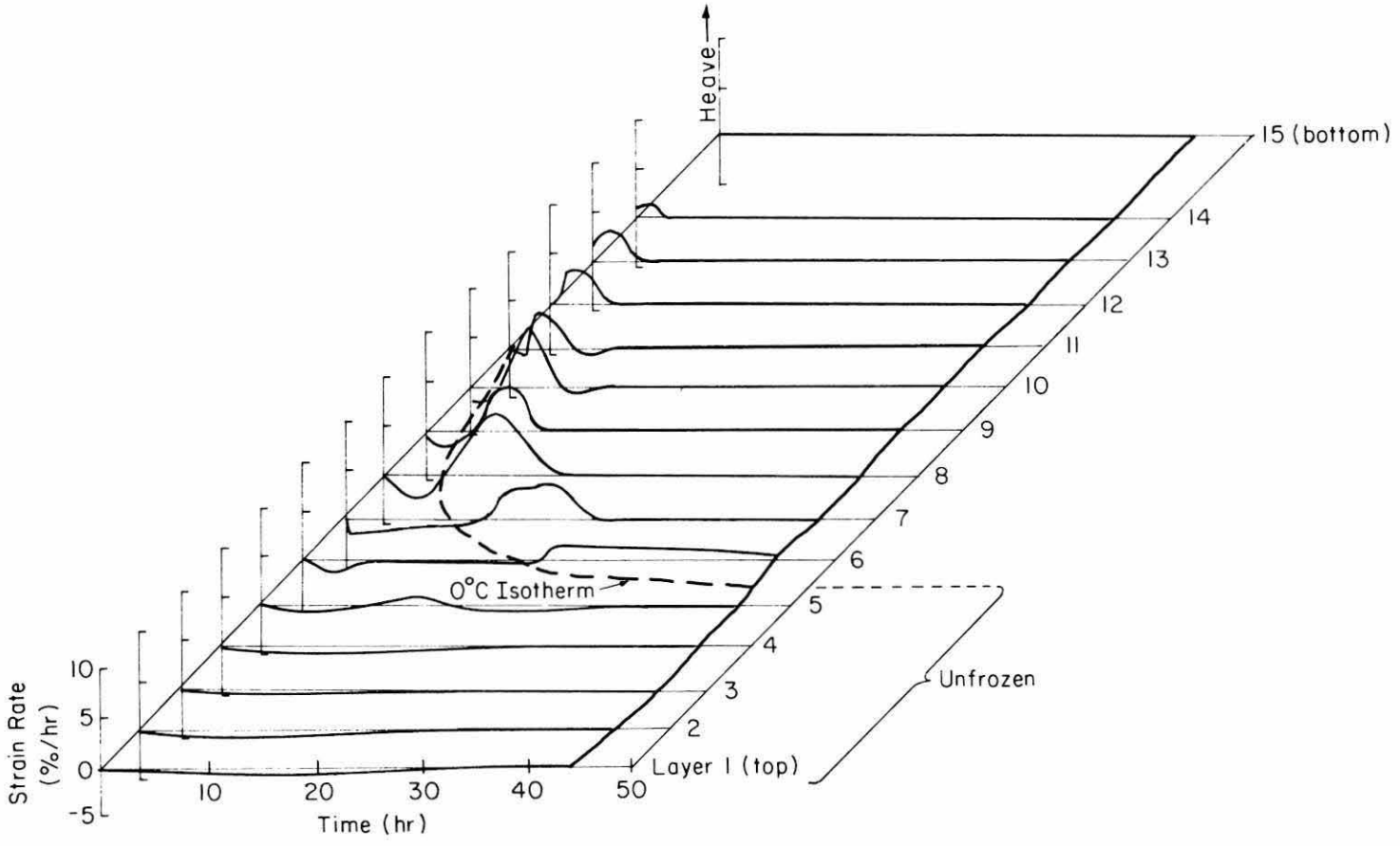

a. Test A.

Figure 17. Strain rate development in the freezing soil. Heave is positive.

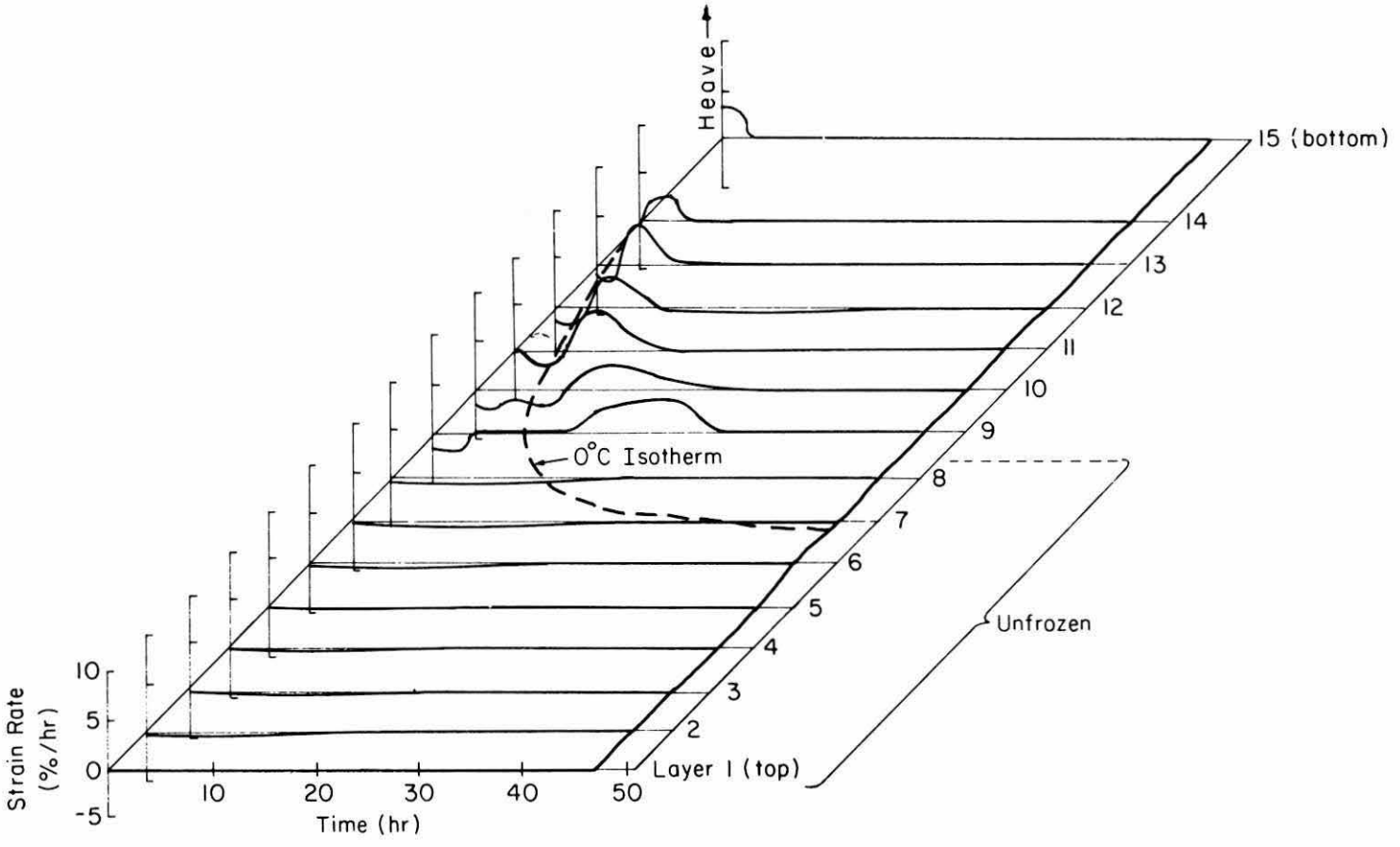

b. Test B.

Figure 17 (cont'd).

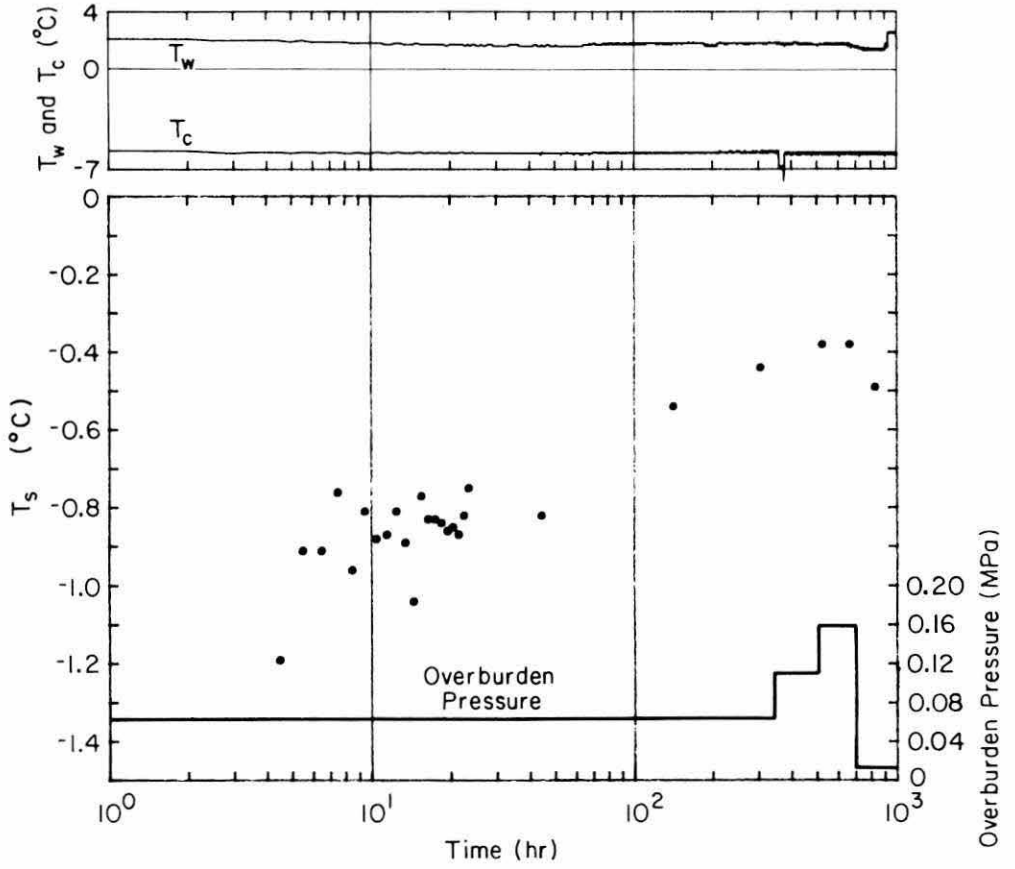

a. Test A.

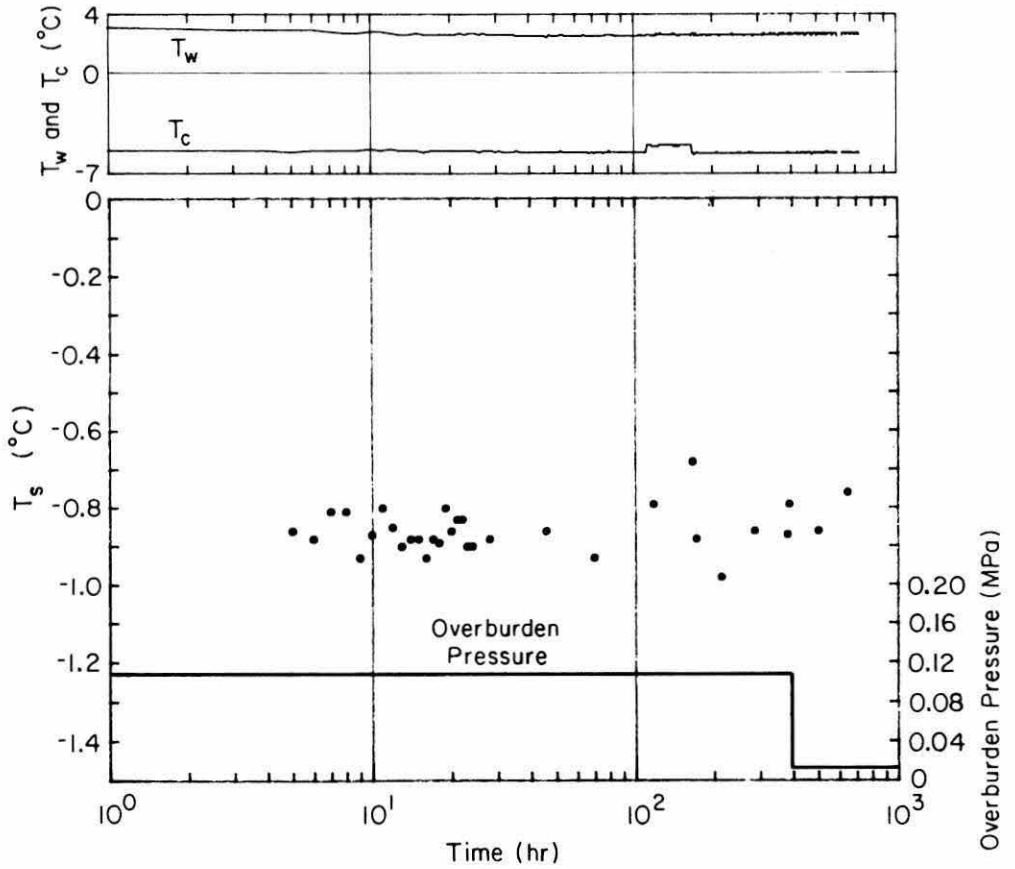

b. Test B.

Figure 18. Apparent segregation temperature.

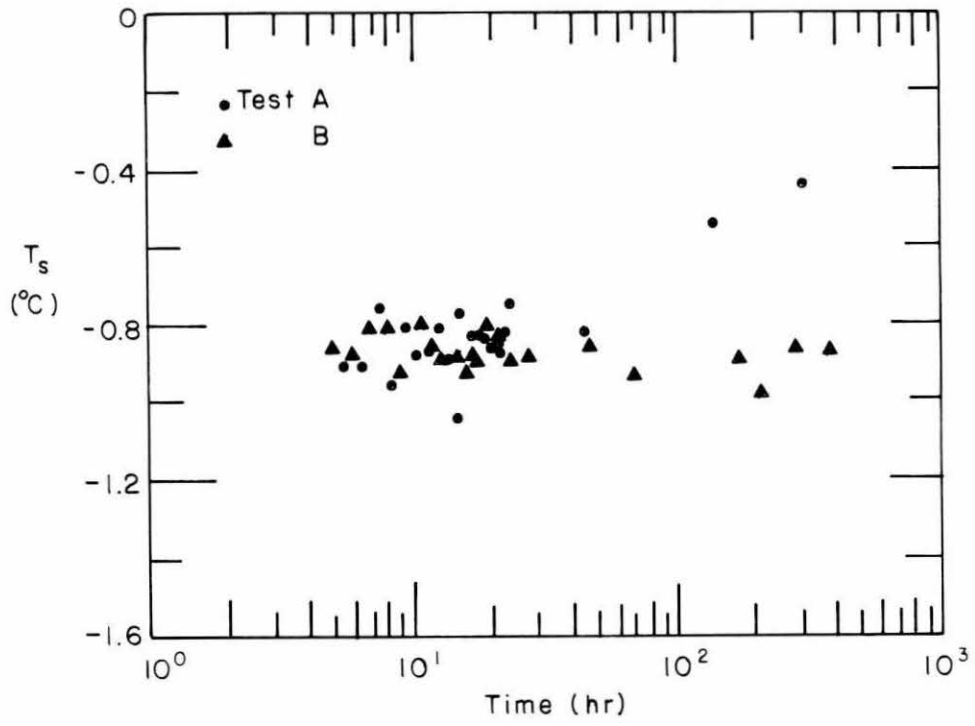

Figure 19. Comparison of T_s *in Test A and Test B.*

points in this report might not be adequate to describe a general trend for the effects of overburden pressure and boundary temperature on T_s. Therefore, the data are shown only for reference.

Apparent thickness of the frozen fringe

From the 0°C isotherm depth and the location of the warmest ice lens, shown in Appendices C and E, the apparent thickness of the frozen fringe L_{ff} was observed (Fig. 20). During Test A, L_{ff} tended to become thinner with time, from 1.1 to 0.5 cm, during constant overburden pressure and boundary temperatures; during Test B, L_{ff} showed the same tendency as in Test A for the first 30 hours but then seemed to stay at about 1 cm during constant test conditions between 30 and 100 hours. Figure 21 shows the difference in L_{ff} between Test A and Test B. Again, the data may not be adequate to describe the effects of overburden pressure and boundary temperature on L_{ff}.

Thermal conductivity of the frozen fringe during stationary heaving

During stationary heaving the latent and sensible heat at the 0°C isotherm are negligible. The thermal conductivity of the frozen fringe during stationary heaving can be demonstrated as follows. The heat balance at the 0°C isotherm where no ice growth is expected is

$$Q_u = Q_{ff} \tag{3}$$

where Q_u and Q_{ff} are heat fluxes in unfrozen soil and the frozen fringe, respectively. Equation 3 can be rewritten in terms of thermal conductivity and temperature gradient as

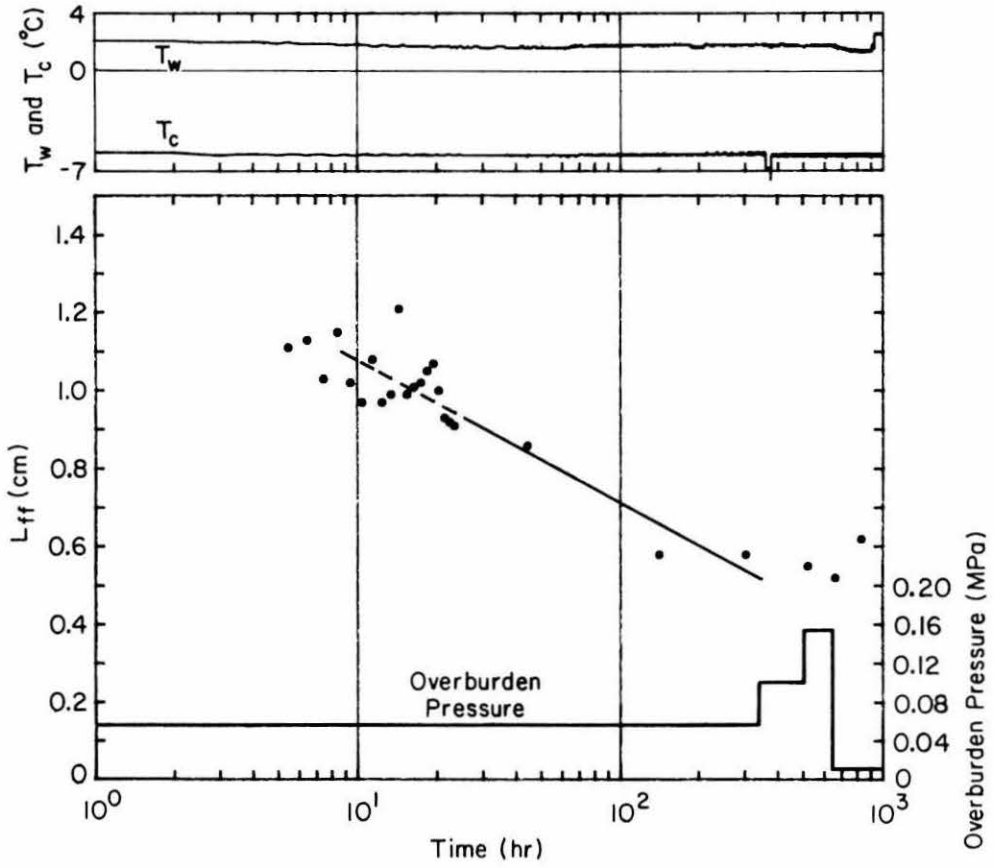

a. Test A.

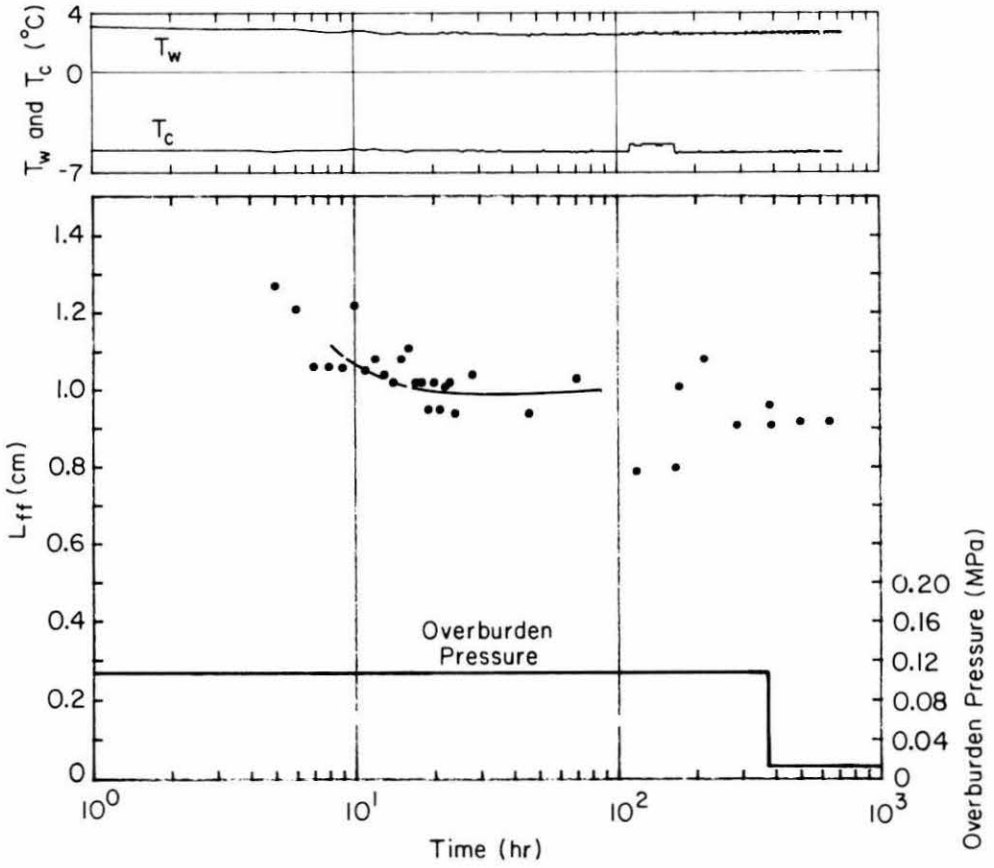

b. Test B.

Figure 20. Apparent thickness of the frozen fringe.

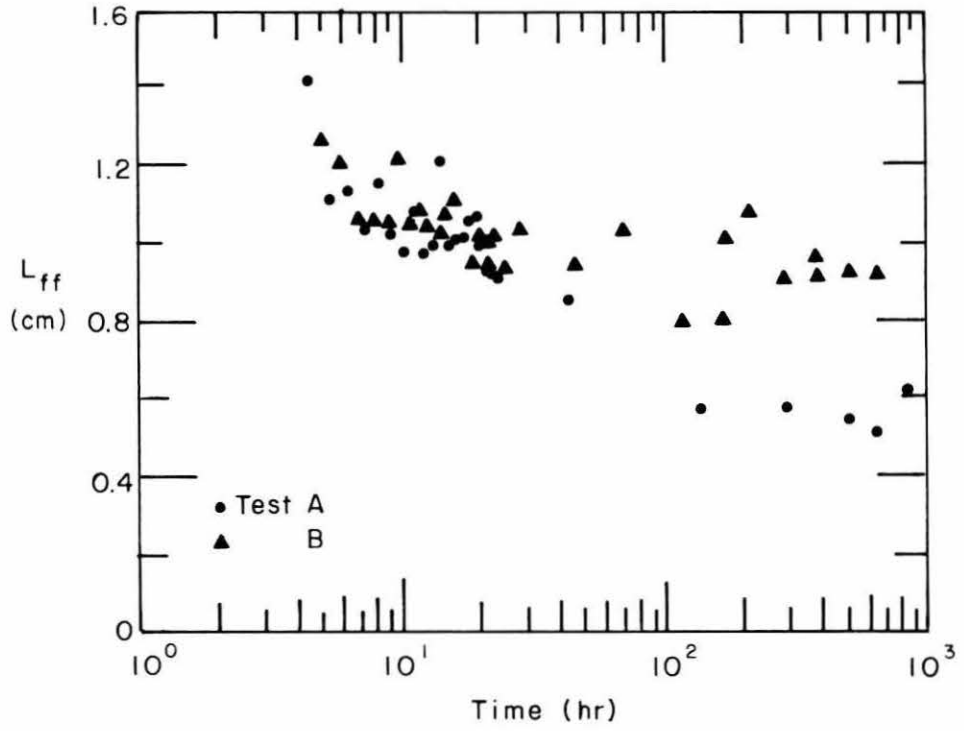

Figure 21. Comparison of L_{ff} in Test A and Test B.

$$K_u(d\theta/dz)_u = K_{ff}(d\theta/dz)_{ff} \quad (4)$$

where K is the thermal conductivity of the soil and $(d\theta/dz)$ is the temperature gradient of the soil. The subscripts "u" and "ff" stand for unfrozen soil and frozen fringe, respectively. The thermal conductivity of the unfrozen soil has been measured by the thermal probe method (Penner 1975), as shown in Table 2. The temperature gradients within the unfrozen soil $(d\theta/dz)_u$ and the frozen fringe $(d\theta/dz)_{ff}$ were calculated from the data listed in Appendix A. The heat flow density $K_u(d\theta/dz)_u$ in unfrozen soil was determined by using the measured thermal conductivity from Table 2 and the mean temperature gradient in unfrozen soil calculated from Appendix A.

Most of the temperature gradients in the frozen fringe were calculated using the coordinates and temperatures of two lead spheres. These spheres were located below the 0°C isotherm and above the warmest ice lens in a zone where no expansive strain was observed. However, since the frozen fringe was too thin to contain the two spheres between 44.5 and 832.5 hours in Test A, $(d\theta/dz)_{ff}$ was calculated by another procedure for this layer. First the 0°C isotherm depth was extrapolated by assuming a linear temperature profile within the unfrozen soil. By using the depth of the 0°C isotherm and the temperature and coordinates of a lead sphere located in the shrinking zone in the frozen fringe, $(d\theta/dz)_{ff}$ was calculated for this period. In this way, the thermal conductivity of the frozen fringe K_{ff} where there was no expansive strain was calculated by substituting values for K_u, $(d\theta/dz)_u$, and $(d\theta/dz)_{ff}$ in eq 4:

$$K_{ff} = K_u\left[(d\theta/dz)_u / (d\theta/dz)_{ff}\right]. \quad (5)$$

Again, since the 0°C isotherm was no longer penetrating into the unfrozen soil (i.e. there was no temperature change at the vicinity of the 0°C isotherm) in this stationary heaving

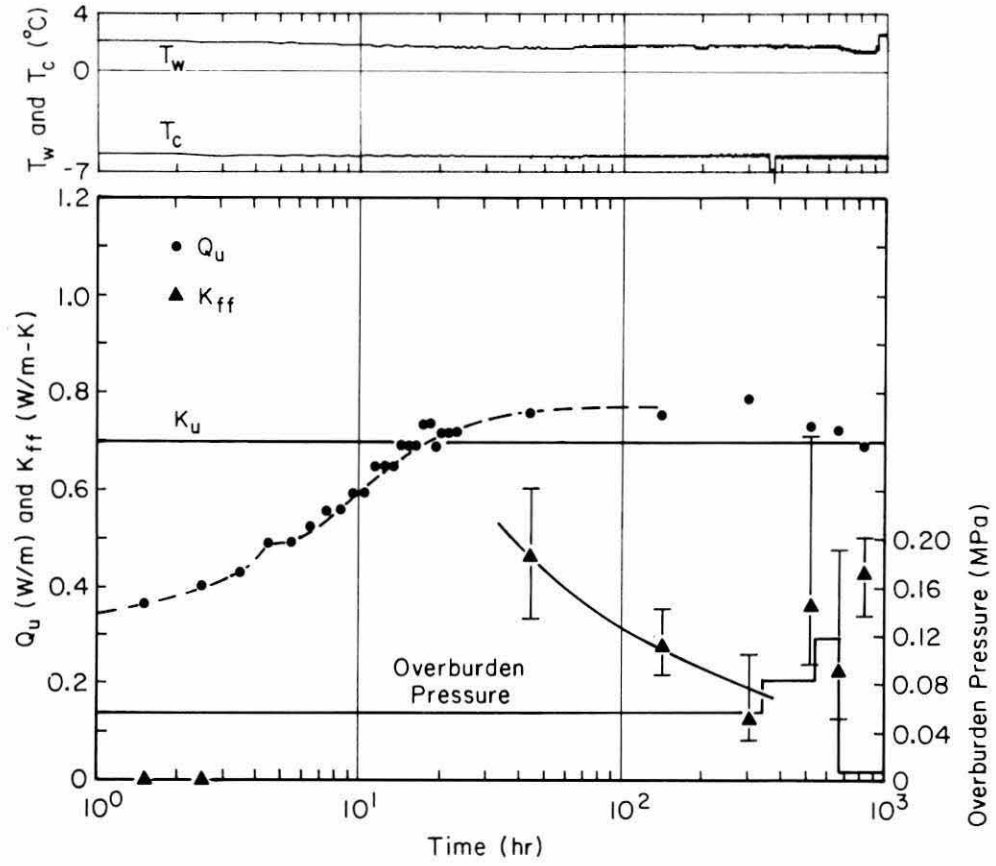

a. Test A.

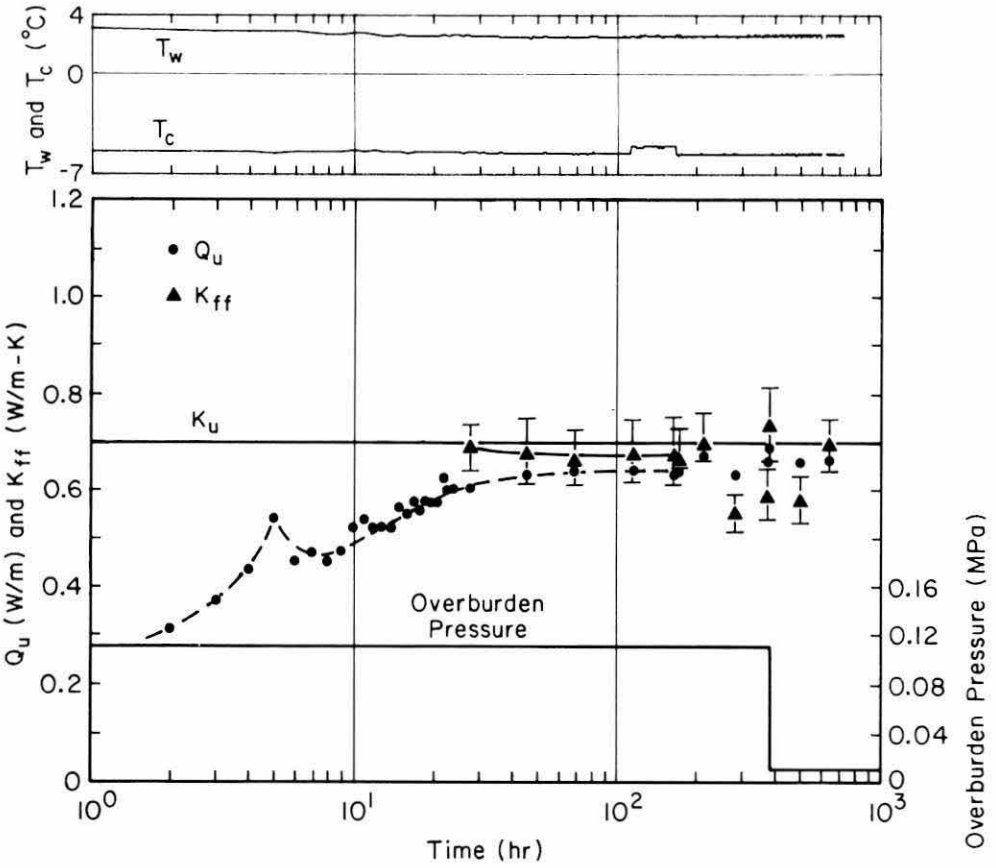

b. Test B.

Figure 22. Heat flow density in the unfrozen soil and thermal conductivity of the frozen fringe. K_u is the thermal conductivity of the unfrozen soil observed by the thermal probe method.

phase and no ice growth in the shrinking zone was expected, the latent heat and the sensible heat at the 0°C isotherm were neglected in this analysis.

Figure 22 shows the calculated heat flow density and thermal conductivity in unfrozen soil. The heat flow density in unfrozen soil increases with time up to about 30 hours and then stabilizes. After the first 30 hours, during a period when the overburden pressures were maintained at 0.06 MPa for Test A and 0.11 MPa for Test B, the thermal conductivity of the frozen fringe in Test A decreased greatly from the value for unfrozen soil (K_u), whereas there was little decrease from K_u in Test B. However, the expected error in temperature measurement, shown as the length of the bar at each data point, suggests that more data are needed for a general understanding of the thermal properties during freezing.

After 329 hours in Test A and 111 hours in Test B, the overburden pressure and the cold-side temperature were changed several times. However, there was no clear correlation with the thermal conductivity.

In conclusion, the thermal conductivity in the shrinking zone of the frozen fringe during the growth of the final ice lens is similar to or lower than that of the unfrozen soil (Fig. 22).

Problems in determining T_s and L_{ff}

So far, T_s has been assumed to be the temperature at the warm side of the visible warmest ice lens. However, much of the data in Appendix E may not support this assumption, especially during transient heaving. Many figures in Appendix E, which demonstrate strain rate distributions, show the expanding layer(s) between the locations of the warmest ice lens and the 0°C isotherm, especially during transient heaving. The existence of this expanding layer may mean that the visible ice lens does not indicate the real ice segregation location but only the result of the ice segregation.

Another empirical result that supports this understanding is shown in Figure 23 (Akagawa 1988b), obtained from the intensity profile of the X-ray photos. This figure

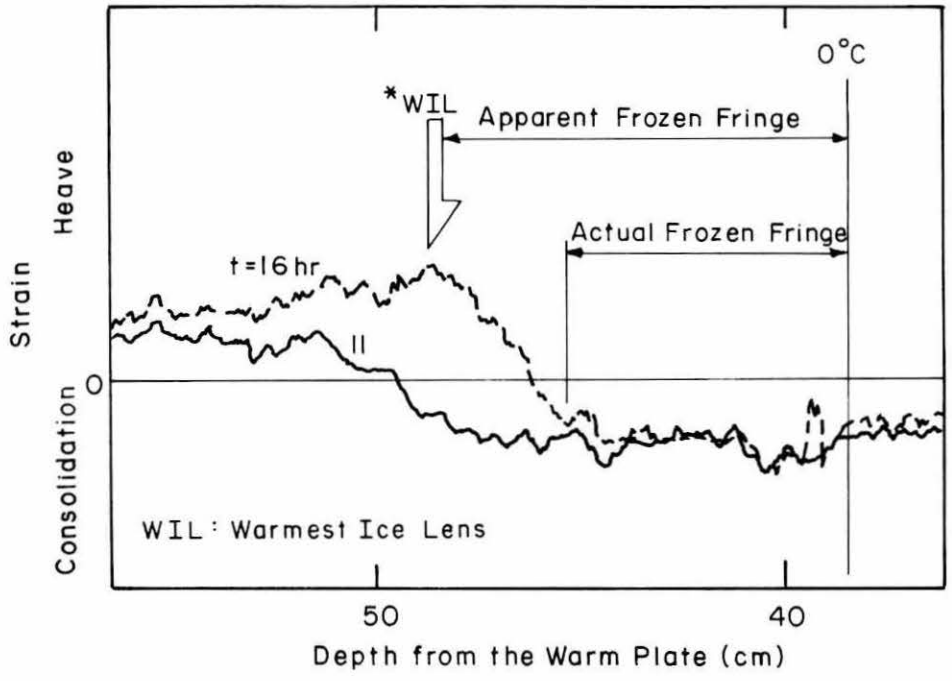

a. Test A.

Figure 23. Difference in frozen fringe location determined from the location of the warm side of the warmest ice lens and from the expansion rate profile converted from the intensity profile of the X-ray photo.

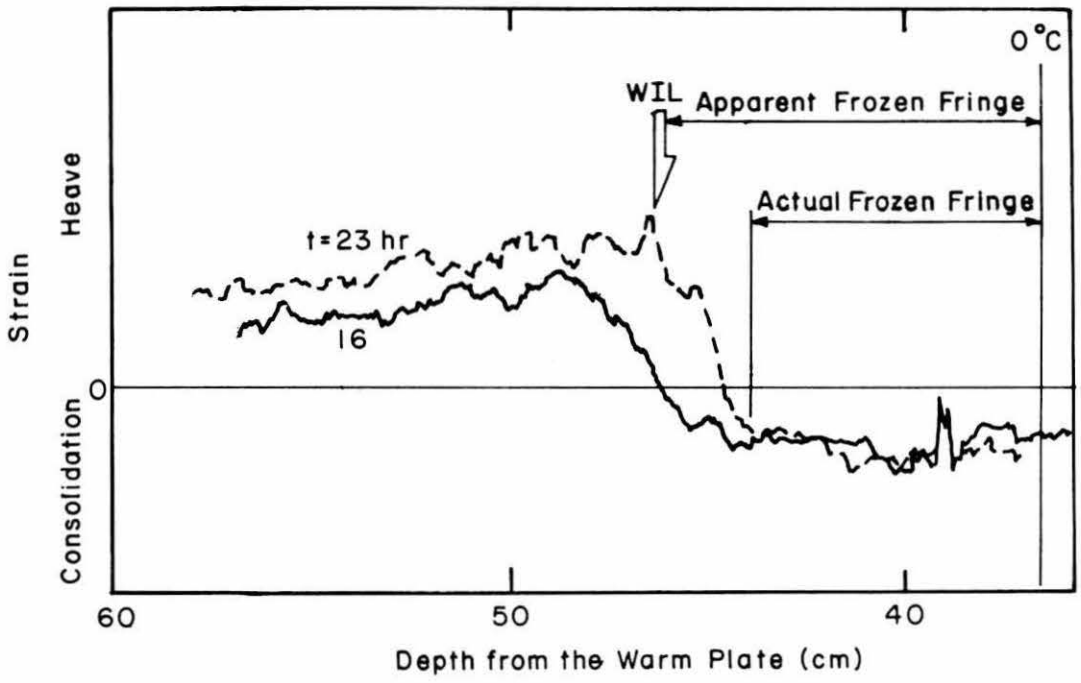

b. Test B.

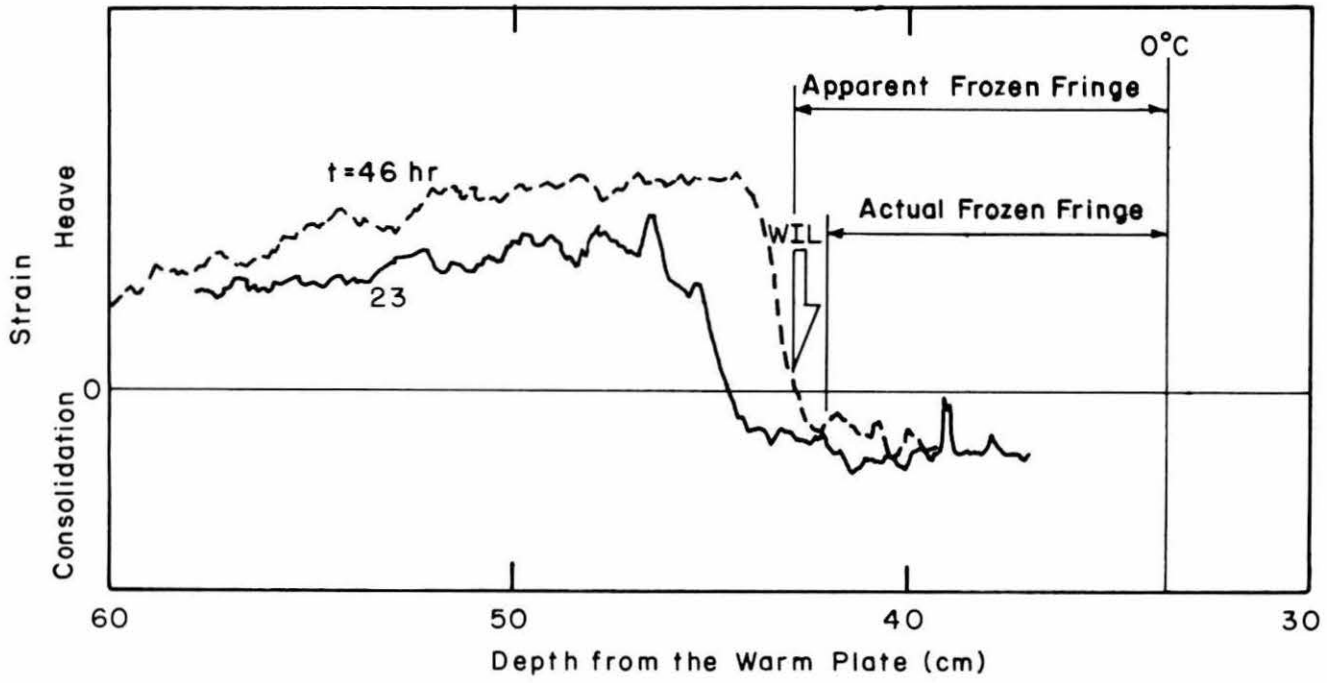

c. Test C.

Figure 23 (cont'd).

shows the continuous strain field over the specimen, along with the locations of the 0°C isotherm and the warm side of the visible ice lens. The location of the warm side of the visible ice lens is somewhat behind the location where expansion is taking place. Unfortunately it is not certain what is causing the expansion in this area. The expansion may be caused by the early stages of the segregation freezing, but there is no proof of this. By analyzing the shape of the intensity profile between the 0°C isotherm and the location of the warmest ice lens, it might be possible to define what is causing the expansion.

However, until it becomes clear, the determination of the T_s and L_{ff} has to rely on the location of the warm side of the visible warmest ice lens, and T_s and L_{ff} have to be called "apparent T_s and L_{ff}." This is the reason that qualitative or theoretical analyses have not been presented in this report.

SUMMARY AND CONCLUSIONS

The X-ray radiograph technique is effective for studying freezing soil behavior, especially when the lead spheres contain thermocouples. The lead spheres enable us to determine the temperature profiles, and the X-ray photographs clearly show the ice lens distribution. This information allows us to determine the apparent segregation temperature and the thickness of the frozen fringe. From the sphere coordinates, the strain and strain rate for each soil layer between adjacent lead spheres can be calculated, and then the distributions of strain and strain rate over the specimen can be determined.

The tests showed that the frost heave activity in the soil while freezing is as follows. Before the 0°C isotherm penetrates through a soil layer, the soil layer shrinks and then expands during transient heaving. The amount and duration of this shrinkage and expansion seem to be closely related to the rate of the 0°C isotherm penetration, which in turn has a close relation with the net heat flow at the freezing front. However, simple comparisons between the 0°C isotherm penetration and the total heave or total heave rate may cause confusing results because of the shrinkage. During this period when the 0°C isotherm is penetrating into unfrozen soil, not all of the net heat flow is expended for ice lens growth (segregation freezing); some is expended for in-situ freezing, which will not result in ice lens formation. (Evaluations of expansion amounts due to in-situ and segregation freezing are important for determining the correlation between the expansion rate and the 0°C isotherm penetration rate).

The maximum amount of the shrinkage is as high as 10% in strain, well beyond the preconsolidation strain of this soil. From an analysis of the magnitude and distribution of the shrinkage with load and porosity data obtained from a consolidation test, the magnitude of the local pore water pressure depression was found to be greater than 0.4 MPa. This magnitude should have a close relation with the frost heaving force. Unfrozen soil also shrinks during transient freezing; this might be caused by a pore water pressure gradient created by the steep pore water drop at the segregating ice.

This study shows the following limitations for studying frost heave using conventional frost heave tests. Since during a period when a 0°C isotherm is penetrating (transient heaving) the frozen fringe and the unfrozen soil may shrink, the amount of shrinkage has to be determined in order to describe the frost heave properties. Some lateral heat flow may not be avoidable during the test, so the temperature measured at the side of the specimen may contain errors caused by radial heat flow. Since the temperature profile in frozen soil is not linear, the assumption of a linear temperature profile may result in an error of some tenths of a degree in the temperature measurements.

The test has the following limitations for the experimental study of the frozen fringe. The direct strain measurement using position markers like lead spheres, as in this study, might not be precise enough for studying the frozen fringe. However, if the conversion from intensity of the X-ray photos to strain proposed by Akagawa (1988b) is introduced, strain observations in a small area, such as the frozen fringe, may become accurate enough. After the structure of the frozen fringe is clearly observed, the accuracy of the temperature measurements demonstrated in this study may be sufficient. However, without the experimentally proven structure of the frozen fringe, the absolute accuracy of 0.1°C seems to be inadequate. Therefore, the most crucial breakthrough in the study of

frost heaving will be the study of the frozen fringe structure: the distribution of water in this zone and its state relative to the thermal, mechanical and chemical conditions.

LITERATURE CITED

Akagawa, S. (1983) Relation between frost heave and specimen length. Shimizu Technical Research Bulletin No. 4, p. 1–7 (formally presented at 4th International Conference on Permafrost).

Akagawa, S. (1985) Frost heave characteristics and scale effect of stationary frost heave. *Proceedings, Fourth International Symposium on Ground Freezing*, p. 137–143.

Akagawa, S. (1988a) Experimental study of frozen fringe characteristics. *Journal of Cold Regions Science and Technology*, **15**: 209–223.

Akagawa, S. (1988b) Evaluation of the X-ray radiography efficiency for heaving and consolidation observation. *Proceedings, Fifth International Symposium on Ground Freezing*, p. 23–28.

Akagawa, S., S. Goto and A. Saito (1988) Segregation freezing observed in welded tuff by open system frost heave test. *Proceedings, Fifth International Conference on Permafrost*, p. 1030–1035.

Beskow, G. (1935) Soil freezing and frost heaving with special application to roads and railroads. The Swedish Geological Society, Series C, No. 375, 26th Yearbook, No. 3. (Translated by J.O. Osterberg; Published by Technical Institute, Northwestern University, November, 1947).

Chamberlain, E.J. and A. J. Gow (1979) Effect of freezing and thawing on the permeability and structure of soils. *Engineering Geology*, **13**:73–92.

Gilpin, R.R. (1980) A model for the prediction of ice lensing and frost heave in soils. *Water Research*, **16**: 918–930.

Ishizaki, T. (1985) Experimental study of frost heaving of saturated soil under overburden pressure. PhD. Thesis, Hokkaido University, Sapporo, Japan.

Nixon, J.F. and N.R. Morgenstern (1973) The residual stress in thawing soils. *Canadian Geotechnical Journal*, **10**(4): 571–580.

O'Neill, K. and R. D. Miller (1982) Numerical solutions for a rigid-ice model of secondary frost heave. USA Cold Regions Research and Engineering Laboratory, CRREL Report 82-13.

Patterson, D.E. and Smith, M.W. (1981) The measurement of unfrozen water content by time domain reflectometry: Results from laboratory tests. *Canadian Geotechnical Journal*, **18**:131–144.

Penner, E. (1975) Thermal conductivity laboratory studies of some Mackenzie Highway soils. *Canadian Geotechnical Journal*, **12**(3): 271–288.

Svec, O.J. (1986) Performance of a frost heave cell for low-temperature-gradient experiments. *Proceedings, Fifth International Offshore Mechanics and Arctic Engineering Symposium*, Vol. IV, p. 53–58.

Taber, S. (1929) Frost heaving. *Journal of Geology*, **37**:428–461.

APPENDIX A: Z COORDINATES AND TEMPERATURES.

TEST A

Time (hr):	0.5		1.5		2.5		3.5		4.5	
	Z (mm)	Tmp. (°C)	Z (mm)	Tmp. (°C)	Z (mm)	Tmp. (°C)	Z (mm)	Tmp. (°C)	Z (mm)	Tmp. (°C)
No.										
Tw	82.74	2.4	82.8	2.4	82.89	2.4	82.99	2.4	83.17	2.3
1	77.19	2.1	77.24	2.1	77.3	2	77.44	2	77.63	2
2	74.14	2	74.18	2	74.26	1.9	74.41	1.8	74.63	1.8
3	69.95	1.7	70.01	1.7	70.11	1.6	70.27	1.6	70.5	1.5
4	63.47	1.4	63.58	1.2	63.71	1.3	63.94	1.1	64.19	1
5	60.52	1.1	60.6	1.1	60.76	0.9	60.98	0.9	61.27	0.7
6	55.18	1	55.25	1	55.47	0.8	55.76	0.7	56.13	0.5
7	49.26	0.7	49.42	0.6	49.71	0.4	50.07	0.3	50.47	0.1
8	45.64	0.5	45.78	0.4	46.13	0.2	46.55	0.1	47.05	-0.1
9	40.86	0.4	41.05	0.2	41.48	0	41.96	-0.2	42.5	-0.4
10	35.82	0.2	36.07	0	36.55	-0.3	37.06	-0.6	37.47	-0.9
11	31.41	-0.1	31.61	-0.2	32.1	-0.7	32.44	-1	32.71	-1.4
12	27.63	-0.1	27.82	-0.5	28.17	-1.2	28.34	-1.7	28.48	-2
13	22.31	-0.4	22.38	-1.2	22.52	-2.1	22.52	-2.5	22.59	-2.8
14	11.9	-2	11.9	-3.2	11.9	-3.8	11.9	-4	11.9	-4.2
Tc	0	-4.7	0	-5.7	0	-5.8	0	-5.8	0	-5.8

Time (hr):	5.5		6.5		7.5		8.5		9.5	
	Z (mm)	Tmp. (°C)	Z (mm)	Tmp. (°C)	Z (mm)	Tmp. (°C)	Z (mm)	Tmp. (°C)	Z (mm)	Tmp. (°C)
No.										
Tw	83.43	2.4	83.74	2.3	84.02	2.3	84.29	2.2	84.59	2.2
1	77.89	2	78.19	1.9	78.48	1.9	78.75	1.8	79.04	1.8
2	74.91	1.8	75.23	1.7	75.53	1.7	75.81	1.6	76.1	1.6
3	70.76	1.5	71.07	1.4	71.36	1.3	71.69	1.2	71.97	1.2
4	64.54	1.1	64.83	0.8	65.14	0.9	65.41	0.7	65.77	0.7
5	61.63	0.7	61.98	0.5	62.32	0.4	62.61	0.4	62.95	0.3
6	56.47	0.5	56.84	0.3	57.19	0.2	57.57	0.1	57.91	0
7	50.89	0.1	51.29	-0.1	51.66	-0.2	51.99	-0.4	52.35	-0.4
8	47.52	-0.2	47.9	-0.4	48.29	-0.5	48.6	-0.6	48.88	-0.7
9	42.95	-0.5	43.32	-0.7	43.51	-0.8	43.61	-1.1	43.66	-1.2
10	37.71	-1	37.72	-1.3	37.64	-1.4	37.59	-1.7	37.64	-1.8
11	32.81	-1.5	32.79	-1.8	32.73	-1.9	32.7	-2.2	32.72	-2.3
12	28.5	-2.1	28.47	-2.4	28.37	-2.5	28.34	-2.8	28.38	-2.8
13	22.63	-2.9	22.55	-3.1	22.39	-3.1	22.14	-3.4	22.17	-3.4
14	11.9	-4.2	11.9	-4.4	11.9	-4.4	11.9	-4.6	11.9	-4.6
Tc	0	-5.8	0	-5.9	0	-5.8	0	-5.9	0	-5.9

Time (hr):	10.5		11.5		12.5		13.5		14.5	
	Z (mm)	Tmp. (°C)	Z (mm)	Tmp. (°C)	Z (mm)	Tmp. (°C)	Z (mm)	Tmp. (°C)	Z (mm)	Tmp. (°C)
No.										
Tw	84.94	2.3	85.25	2.2	85.47	2.3	85.71	2.2	85.97	2.2
1	79.39	1.8	79.74	1.7	80.02	1.8	80.31	1.7	80.55	1.7
2	76.45	1.6	76.81	1.5	77.08	1.5	77.38	1.5	77.65	1.4
3	72.3	1.2	72.69	1.1	72.99	1.1	73.25	1.1	73.41	1
4	66.09	0.7	66.45	0.6	66.72	0.6	67.01	0.6	67.26	0.5
5	63.3	0.4	63.64	0.2	63.91	0.3	64.17	0.2	64.42	0.1
6	58.25	0	58.56	-0.1	58.85	-0.1	59.13	-0.1	59.4	-0.3
7	52.68	-0.5	53.02	-0.6	53.33	-0.6	53.61	-0.7	53.82	-0.8
8	49.01	-0.8	49.07	-0.9	49.13	-0.9	49.23	-1	49.31	-1.2
9	43.7	-1.3	43.73	-1.4	43.74	-1.4	43.78	-1.5	43.82	-1.6
10	37.74	-1.8	37.78	-2	37.85	-1.9	37.86	-2	37.91	-2.2
11	32.8	-2.3	32.79	-2.4	32.84	-2.4	32.89	-2.5	32.91	-2.6
12	28.42	-2.9	28.41	-3	28.4	-2.9	28.46	-3	28.5	-3.1
13	22.25	-3.4	22.41	-3.6	22.5	-3.5	22.53	-3.6	22.63	-3.7
14	11.9	-4.6	11.9	-4.6	11.9	-4.6	11.9	-4.6	11.9	-4.7
Tc	0	-5.8	0	-5.9	0	-5.8	0	-5.9	0	-5.9

TEST A (CONT'D).

Time (hr):	15.5		16.5		17.5		18.5		19.5	
	Z (mm)	Tmp. (°C)	Z (mm)	Tmp. (°C)	Z (mm)	Tmp. (°C)	Z (mm)	Tmp. (°C)	Z (mm)	Tmp. (°C)
No.										
Tw	86.22	2.2	86.34	2.2	86.49	2.2	86.72	2.2	86.98	2.2
1	80.84	1.7	81.05	1.7	81.26	1.7	81.48	1.7	81.69	1.6
2	77.91	1.5	78.03	1.4	78.18	1.4	78.42	1.4	78.69	1.4
3	73.7	1	73.96	1	74.15	0.9	74.36	0.9	74.55	0.9
4	67.55	0.5	67.79	0.5	68.05	0.4	68.31	0.4	68.51	0.3
5	64.68	0.1	64.89	0.1	65.11	0	65.36	0	65.6	-0.1
6	59.69	-0.2	59.93	-0.3	60.13	-0.4	60.36	-0.4	60.57	-0.4
7	53.94	-0.7	54	-0.8	54.06	-0.9	54.11	-0.9	54.12	-1
8	49.36	-1.1	49.36	-1.2	49.4	-1.3	49.44	-1.3	49.45	-1.4
9	43.87	-1.6	43.87	-1.7	43.85	-1.8	43.88	-1.8	43.9	-1.8
10	37.9	-2.1	37.92	-2.2	37.93	-2.3	37.99	-2.3	37.99	-2.4
11	32.9	-2.6	32.79	-2.6	32.8	-2.7	32.87	-2.7	32.93	-2.8
12	28.52	-3.1	28.51	-3.1	28.47	-3.2	28.48	-3.2	28.46	-3.3
13	22.59	-3.6	22.59	-3.7	22.6	-3.7	22.63	-3.8	22.66	-3.8
14	11.9	-4.6	11.9	-4.7	11.9	-4.7	11.9	-4.8	11.9	-4.8
Tc	0	-5.8	0	-5.9	0	-5.9	0	-5.9	0	-5.9

Time (hr):	20.5		21.5		22.5		23.5		44.5	
	Z (mm)	Tmp. (°C)	Z (mm)	Tmp. (°C)	Z (mm)	Tmp. (°C)	Z (mm)	Tmp. (°C)	Z (mm)	Tmp. (°C)
No.										
Tw	87.21	2.2	87.38	2.2	87.56	2.2	87.65	2.2	90.48	2.2
1	81.9	1.7	82.07	1.7	82.26	1.7	82.37	1.7	85.15	1.6
2	78.93	1.4	79.1	1.4	79.29	1.4	79.39	1.4	82.32	1.3
3	74.74	0.9	74.93	0.9	75.13	0.9	75.24	0.9	78.2	0.8
4	68.68	0.4	68.85	0.4	69.04	0.4	69.15	0.4	72.06	0.2
5	65.79	0	65.99	0	66.18	0	66.31	0	69.18	-0.2
6	60.8	-0.4	60.98	-0.5	61.19	-0.4	61.3	-0.4	62.39	-0.8
7	54.09	-1	54.12	-1.1	54.16	-1.1	54.21	-1	54.41	-1.3
8	49.42	-1.4	49.42	-1.4	49.44	-1.4	49.49	-1.4	49.64	-1.6
9	43.91	-1.8	43.89	-1.9	43.91	-1.8	43.94	-1.8	44.09	-2.1
10	37.9	-2.3	37.82	-2.3	37.87	-2.3	37.97	-2.3	38.09	-2.4
11	32.89	-2.7	32.81	-2.8	32.81	-2.7	32.83	-2.7	32.97	-2.8
12	28.48	-3.2	28.44	-3.2	28.62	-3.2	28.73	-3.2	28.48	-3.3
13	22.52	-3.8	22.47	-3.7	22.5	-3.7	22.62	-3.7	22.64	-3.7
14	11.9	-4.7	11.9	-4.7	11.9	-4.7	11.9	-4.7	11.9	-4.6
Tc	0	-5.9	0	-5.9	0	-5.8	0	-5.9	0	-6

Time (hr):	141.5		304.5		524.5		664.5		832.5	
	Z (mm)	Tmp. (°C)	Z (mm)	Tmp. (°C)	Z (mm)	Tmp. (°C)	Z (mm)	Tmp. (°C)	Z (mm)	Tmp. (°C)
No.										
Tw	95.89	2.3	101.03	2.4	103.39	2.2	103.96	2.2	106.52	1.9
1	90.62	1.8	95.81	1.8	97.67	1.7	98.25	1.7	100.87	1.3
2	87.88	1.4	93.17	1.5	95.06	1.4	95.66	1.3	98.35	1
3	83.55	0.9	88.32	1	91.3	0.9	91.11	0.9	94.34	0.7
4	77.36	0.3	82.4	0.3	85.28	-0.3	85.31	0.3	88.31	0.1
5	74.34	-0.2	79.43	-0.1	82.43	-0.1	82.33	-0.1	85.34	-0.3
6	62.59	-1	62.67	-1.1	62.94	-1.2	62.89	-1.2	62.99	-1.3
7	54.12	-1.5	54.19	-1.6	---	---	---	---	---	---
8	49.85	-1.8	---	---	---	---	---	---	---	---
9	44.23	-2.2	44.31	-2.3	45.05	-2.3	45.06	-2.3	45.25	-2.3
10	38.01	-2.7	38.1	-2.8	38.89	-2.8	38.73	-2.8	38.72	-2.8
11	32.98	-3.1	33.34	-3.1	33.77	-2.9	33.58	-2.9	33.56	-2.8
12	28.61	-3.5	28.44	-3.5	29.26	-3.5	29.11	-3.4	29.11	-3.4
13	22.29	-3.9	22.47	-3.9	23.54	-4.1	22.93	-4	22.66	-4.1
14	11.9	-4.8	11.9	-4.7	11.9	-4.7	11.9	-4.7	11.9	-4.7
Tc	0	-5.8	0	-5.8	0	-5.9	0	-5.9	0	-5.9

TEST B

Time (hr):	Ref		0		1		2		3	
No.	Z (mm)	Tmp. (°C)	Z (mm)	Tmp. (°C)	Z (mm)	Tmp. (°C)	Z (mm)	Tmp. (°C)	Z (mm)	Tmp. (°C)
Tw	98.27	3.2	97.83	3.1	98.35	3	98.32	3.1	98.5	3
0	92.34	3.1	91.9	3	92.43	3.1	92.4	3	92.57	2.9
1	87.18	3.1	86.76	2.9	87.47	2.9	87.34	2.8	87.52	2.6
2	82.72	3.1	82.31	2.8	83	2.8	82.95	2.6	83.15	2.4
3	77.91	3	77.66	2.7	78.38	2.7	78.34	2.4	78.48	2.1
4	72.89	3	72.69	2.7	73.25	2.5	73.36	2.2	73.56	1.9
5	69.6	3	69.35	2.6	70	2.4	70.07	2.1	70.25	1.7
6	63.3	2.9	63.21	2.5	63.93	2.2	64.1	1.8	64.25	1.4
7	57.65	2.9	57.5	2.4	58.1	1.9	58.35	1.5	58.67	1.1
8	52.46	2.9	52.24	2.5	52.82	1.9	53.23	1.2	53.51	0.8
9	49.29	2.8	49.19	2.1	49.82	1.5	50.22	1.1	50.66	0.6
10	42.62	2.7	42.42	2	43.04	1.3	43.85	0.9	44.31	0.4
11	38.23	2.7	38.13	1.9	38.57	1.1	39.51	0.6	40.02	0.1
12	33.09	2.6	33.05	1.6	33.51	0.8	34.62	0.3	35.12	-0.2
13	27.76	2.5	27.71	1.2	28.1	0.4	29.4	-0.1	30.05	-0.5
14	17.51	2.2	17.59	0.3	18.02	-0.3	19.31	-1	19.28	-1.9
Tc	0	2.2	0	0	0	-5.4	0	-5.4	0	-5.4

Time (hr):	4		5		6		7		8	
No.	Z (mm)	Tmp. (°C)	Z (mm)	Tmp. (°C)	Z (mm)	Tmp. (°C)	Z (mm)	Tmp. (°C)	Z (mm)	Tmp. (°C)
Tw	98.58	3	99.04	3	99.25	3.1	99.53	3.1	99.85	3
0	92.65	2.9	93.12	2.9	93.33	2.9	93.6	2.8	93.92	2.7
1	87.68	2.6	87.95	2.5	88.16	2.6	88.5	2.4	88.78	2.3
2	83.34	2.3	83.61	2.2	83.9	2.3	84.18	2.1	84.39	2
3	78.7	2	78.92	1.9	79.34	2	79.54	1.8	79.8	1.7
4	73.86	1.8	74.04	1.7	74.24	1.7	74.64	1.5	74.94	1.4
5	70.56	1.5	70.88	1.5	71.11	1.5	71.39	1.3	71.72	1.2
6	64.58	1.2	64.91	1	65.03	1	65.38	0.9	65.75	0.8
7	58.99	0.8	59.34	0.7	59.67	0.7	59.96	0.5	60.29	0.4
8	53.92	0.6	54.31	0.4	54.69	0.4	54.95	0.2	55.31	0.2
9	51.06	0.3	51.47	0.2	51.82	0.2	52.05	0	52.47	-0.2
10	44.74	0.1	45.18	-0.1	45.6	-0.2	45.98	-0.4	46.45	-0.6
11	40.41	-0.1	41.03	-0.3	41.35	-0.4	41.59	-0.8	41.87	-0.9
12	35.67	-0.4	36.06	-0.7	36.22	-0.9	36.24	-1.3	36.44	-1.5
13	30.36	-0.9	30.43	-1.3	30.4	-1.6	30.41	-1.9	30.52	-2.1
14	19.49	-2.4	19.38	-2.7	19.5	-2.9	19.29	-3.1	19.3	-3.3
Tc	0	-5.4	0	-5.4	0	-5.4	0	-5.4	0	-5.4

Time (hr):	9		10		11		12		13	
No.	Z (mm)	Tmp. (°C)	Z (mm)	Tmp. (°C)	Z (mm)	Tmp. (°C)	Z (mm)	Tmp. (°C)	Z (mm)	Tmp. (°C)
Tw	99.95	3	100.28	3	100.56	3	100.79	3	101.03	3
0	94.02	2.7	94.36	2.8	94.64	2.8	94.87	2.7	95.1	2.6
1	88.98	2.3	89.21	2.4	89.38	2.4	89.68	2.3	89.88	2.3
2	84.65	2.1	84.87	2.1	84.98	2.1	85.41	2	85.59	1.9
3	80.07	1.7	80.26	1.7	80.48	1.7	80.79	1.6	81.05	1.6
4	75.23	1.4	75.47	1.4	75.62	1.3	75.96	1.3	76.17	1.2
5	71.99	1.2	72.18	1.1	72.3	1.1	72.7	1	72.88	1
6	66.05	0.7	66.33	0.7	66.62	0.6	66.77	0.6	67.19	0.5
7	60.65	0.4	60.93	0.3	61.13	0.2	61.46	0.2	61.74	0.1
8	55.64	0.1	55.97	-0.1	56.16	-0.1	56.5	-0.2	56.85	-0.3
9	52.76	-0.2	53.07	-0.4	53.35	-0.4	53.59	-0.5	53.97	-0.6
10	46.89	-0.7	47.14	-0.7	47.22	-0.8	47.43	-0.9	47.53	-1.1
11	42.06	-1.1	42.05	-1.1	42.14	-1.2	42.19	-1.3	42.25	-1.5
12	36.41	-1.6	36.44	-1.7	36.5	-1.8	36.52	-1.9	36.64	-2
13	30.49	-2.2	30.41	-2.2	30.5	-2.3	30.52	-2.4	30.59	-2.5
14	19.44	-3.3	19.34	-3.4	19.35	-3.4	19.39	-3.5	19.46	-3.6
Tc	0	-5.4	0	-5.4	0	-5.4	0	-5.4	0	-5.4

TEST B (CONT'D).

Time (hr):	14		15		16		17		18	
	Z (mm)	Tmp. (°C)	Z (mm)	Tmp. (°C)	Z (mm)	Tmp. (°C)	Z (mm)	Tmp. (°C)	Z (mm)	Tmp. (°C)
No.										
Tw	101.29	3	101.39	2.9	101.55	2.9	101.73	2.9	101.82	3
0	95.36	2.6	95.47	2.7	95.63	2.6	95.8	2.6	95.89	2.6
1	90.18	2.3	90.24	2.3	90.35	2.2	90.74	2.2	90.87	2.2
2	85.84	1.9	85.92	2	86.14	1.9	86.41	1.8	86.5	1.9
3	81.22	1.6	81.54	1.6	81.65	1.5	81.89	1.5	82.06	1.5
4	76.38	1.2	76.61	1.2	76.8	1.1	77.01	1.1	77.17	1.1
5	73.11	1	73.32	0.9	73.48	0.9	73.84	0.8	73.92	0.8
6	67.35	0.5	67.52	0.4	67.74	0.4	68	0.3	68.36	0.4
7	61.93	0.1	62.15	0	62.35	-0.1	62.59	-0.1	62.83	-0.1
8	57.04	-0.3	57.25	-0.4	57.54	-0.4	57.79	-0.5	58.03	-0.5
9	54.13	-0.6	54.38	-0.7	54.61	-0.8	54.76	-0.8	54.95	-0.8
10	47.6	-1.1	47.58	-1.1	47.7	-1.2	47.69	-1.3	47.78	-1.3
11	42.2	-1.5	42.21	-1.5	42.31	-1.7	42.36	-1.7	42.38	-1.7
12	36.54	-2.1	36.56	-2.1	36.53	-2.2	36.52	-2.2	36.68	-2.2
13	30.56	-2.6	30.6	-2.6	30.63	-2.7	30.56	-2.7	30.59	-2.7
14	19.4	-3.6	19.32	-3.6	19.51	-3.7	19.46	-3.7	19.43	-3.7
Tc	0	-5.4	0	-5.4	0	-5.4	0	-5.4	0	-5.4

Time (hr):	19		20		21		22		23	
	Z (mm)	Tmp. (°C)	Z (mm)	Tmp. (°C)	Z (mm)	Tmp. (°C)	Z (mm)	Tmp. (°C)	Z (mm)	Tmp. (°C)
No.										
Tw	102.2	2.9	102.28	2.9	102.48	3	102.65	3	102.9	2.9
0	96.27	2.6	96.35	2.6	96.56	2.6	96.72	2.7	96.98	2.6
1	91.12	2.2	91.09	2.1	91.35	2.2	91.46	2.2	91.71	2.2
2	86.88	1.8	86.92	1.8	87.09	1.8	87.14	1.9	87.39	1.8
3	82.27	1.5	82.27	1.4	82.52	1.4	82.49	1.5	83	1.4
4	77.49	1.1	77.52	1	77.67	1	77.85	1	78.07	1
5	74.19	0.8	74.38	0.8	74.44	0.8	74.62	0.8	74.88	0.7
6	68.44	0.3	68.56	0.3	68.68	0.3	68.8	0.2	69.01	0.2
7	63.05	-0.1	63.19	-0.2	63.32	-0.2	63.52	-0.2	63.64	-0.2
8	58.21	-0.5	58.35	-0.6	58.53	-0.6	58.73	-0.6	58.89	-0.6
9	55.04	-0.8	55.13	-0.9	55.19	-0.9	55.22	-0.9	55.3	-1
10	47.76	-1.4	47.91	-1.4	47.85	-1.4	47.86	-1.4	47.85	-1.5
11	42.34	-1.8	42.38	-1.8	42.41	-1.8	42.37	-1.8	42.41	-1.9
12	36.62	-2.3	36.63	-2.3	36.58	-2.3	36.62	-2.3	36.62	-2.3
13	30.6	-2.8	30.64	-2.8	30.62	-2.8	30.62	-2.8	30.58	-2.8
14	19.32	-3.7	19.3	-3.7	19.32	-3.7	19.32	-3.8	19.32	-3.8
Tc	0	-5.4	0	-5.4	0	-5.4	0	-5.4	0	-5.4

Time (hr):	24		28		46		70		118	
	Z (mm)	Tmp. (°C)	Z (mm)	Tmp. (°C)	Z (mm)	Tmp. (°C)	Z (mm)	Tmp. (°C)	Z (mm)	Tmp. (°C)
No.										
Tw	102.73	2.9	103.24	3	104.82	3	105.74	2.9	106.64	2.9
0	96.8	2.7	97.31	2.6	98.89	2.5	99.82	2.5	100.72	2.5
1	91.81	2.3	92.36	2.2	93.93	2.1	94.79	2	95.59	2
2	87.46	1.9	88.05	1.9	89.6	1.7	90.54	1.6	91.45	1.6
3	82.95	1.5	83.5	1.4	85.07	1.2	85.95	1.2	86.88	1.2
4	78.09	1.1	78.64	1	80.23	0.8	81.16	0.8	82.14	0.8
5	74.84	0.8	75.4	0.8	77.02	0.5	77.93	0.5	78.97	0.5
6	69.09	0.3	69.61	0.2	71.3	0	72.16	-0.1	73.18	0
7	63.74	-0.2	64.3	-0.3	65.97	-0.5	66.91	-0.6	67.93	-0.5
8	58.95	-0.7	59.58	-0.7	60.32	-1	60.59	-1.1	60.96	-1
9	55.33	-1	55.47	-1	55.85	-1.3	56.13	-1.4	56.54	-1.3
10	47.89	-1.4	48.03	-1.5	48.2	-1.8	48.43	-1.9	48.72	-1.7
11	42.4	-1.8	42.51	-1.9	42.65	-2.2	42.77	-2.2	43.05	-2.1
12	36.62	-2.3	36.66	-2.4	36.75	-2.6	36.88	-2.7	37.05	-2.4
13	30.63	-2.8	30.63	-2.9	30.69	-3.1	30.8	-3.1	30.84	-2.8
14	19.39	-3.7	19.57	-3.8	19.5	-3.9	19.61	-3.9	19.62	-3.6
Tc	0	-5.4	0	-5.4	0	-5.4	0	-5.5	0	-5.1

TEST B (CONT'D).

Time (hr):	166		172		214		286		382	
	Z (mm)	Tmp. (°C)	Z (mm)	Tmp. (°C)	Z (mm)	Tmp. (°C)	Z (mm)	Tmp. (°C)	Z (mm)	Tmp. (°C)
No.										
Tw	106.79	2.9	106.76	2.9	107.37	2.9	107.69	2.9	108.1	3
0	100.86	2.6	100.83	2.5	101.44	2.6	101.76	2.5	102.18	2.6
1	95.94	2.1	95.84	2	96.41	2.1	96.59	2.1	97.15	2.1
2	91.62	1.7	91.6	1.6	92.26	1.7	92.45	1.7	92.95	1.7
3	87.05	1.3	87.13	1.2	87.7	1.2	87.88	1.2	88.34	1.2
4	82.25	0.9	82.26	0.8	82.92	0.8	83.13	0.8	83.57	0.8
5	79	0.6	79.08	0.5	79.73	0.5	79.89	0.5	80.4	0.5
6	73.3	0.1	73.34	-0.1	74.04	-0.1	74.17	0	74.69	0
7	68	-0.4	68.1	-0.6	68.82	-0.6	68.97	-0.6	69.38	-0.6
8	61.2	-0.9	61.27	-1.1	61.52	-1.2	61.55	-1.1	61.85	-1.1
9	56.74	-1.2	56.82	-1.4	57.16	-1.5	57.23	-1.4	57.53	-1.4
10	48.91	-1.6	49.02	-1.9	49.17	-1.9	49.34	-1.9	49.69	-1.9
11	43.09	-2	43.15	-2.3	43.38	-2.3	43.53	-2.3	43.81	-2.3
12	37.05	-2.4	37.14	-2.7	37.27	-2.7	37.38	-2.7	37.74	-2.7
13	30.86	-2.8	30.98	-3.2	31.06	-3.1	31.19	-3.1	31.41	-3.1
14	19.49	-3.6	19.59	-4	19.77	-4	19.73	-4	20.02	-4
Tc	0	-5	0	-5.6	0	-5.6	0	-5.6	0	-5.6

Time (hr):	388		502		646	
	Z (mm)	Tmp. (°C)	Z (mm)	Tmp. (°C)	Z (mm)	Tmp. (°C)
No.						
Tw	108.23	3	110.04	3	110.46	2.9
0	102.3	2.7	104.12	2.6	104.53	2.6
1	97.58	2.2	99.39	2.1	99.81	2.1
2	93.31	1.8	95.09	1.7	95.55	1.7
3	88.62	1.3	90.33	1.2	90.8	1.3
4	83.83	0.9	85.55	0.8	86.01	0.9
5	80.56	0.6	82.32	0.5	82.86	0.6
6	74.91	0	76.49	0	77	0
7	69.58	-0.5	71.23	-0.6	71.75	-0.5
8	61.75	-1.1	62.12	-1.2	62.46	-1.1
9	57.54	-1.3	57.84	-1.4	58.25	-1.4
10	49.67	-1.8	49.93	-1.9	50.37	-1.9
11	43.8	-2.2	44.02	-2.3	44.35	-2.2
12	37.63	-2.6	37.99	-2.7	38.16	-2.6
13	31.28	-3.1	31.6	-3.1	31.8	-3.1
14	19.82	-3.9	20.06	-3.9	20.11	-3.9
Tc	0	-5.5	0	-5.6	0	-5.6

APPENDIX B: STRAIN OBSERVED IN THE SOIL LAYERS.

Positive strain represents heave and negative strain represents consolidation.

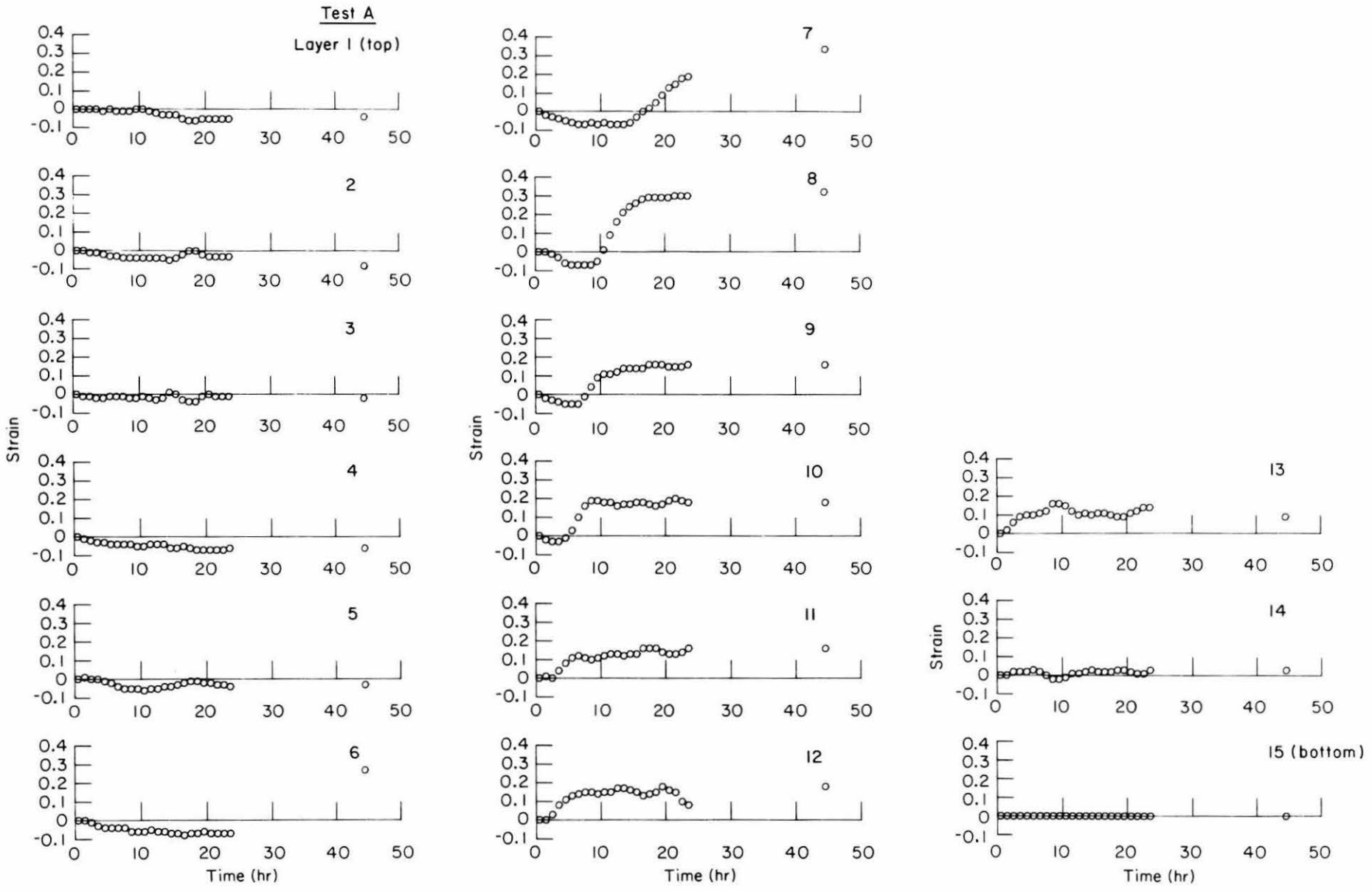

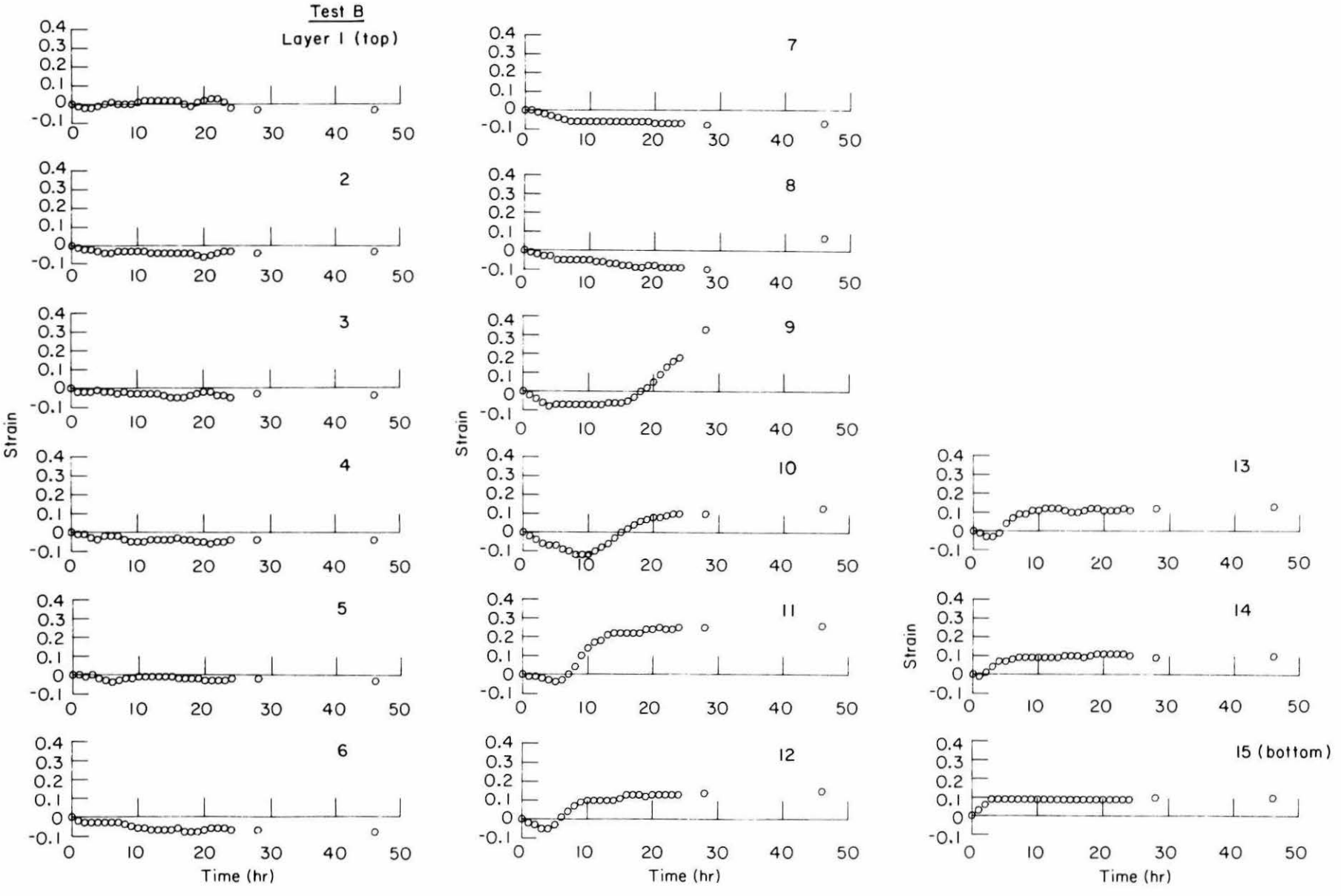
Test B
Layer 1 (top)
2
3
4
5
6
7
8
9
10
11
12
13
14
15 (bottom)
Strain
Time (hr)
0.4
0.3
0.2
0.1
0
-0.1
0
10
20
30
40
50

APPENDIX C: STRAIN DISTRIBUTION IN THE FREEZING SOIL.

Positive strain represents heave and negative strain represents consolidation.

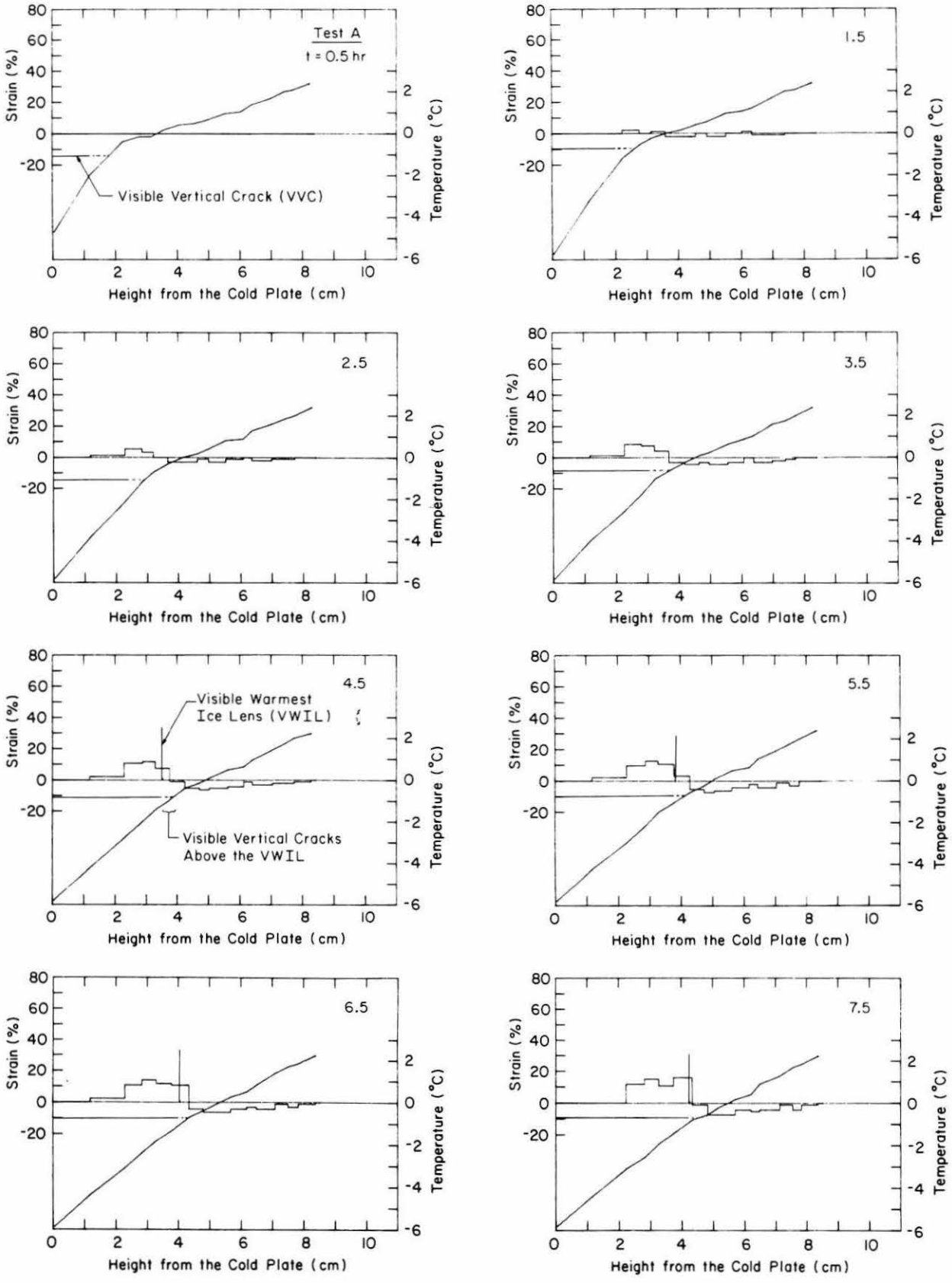

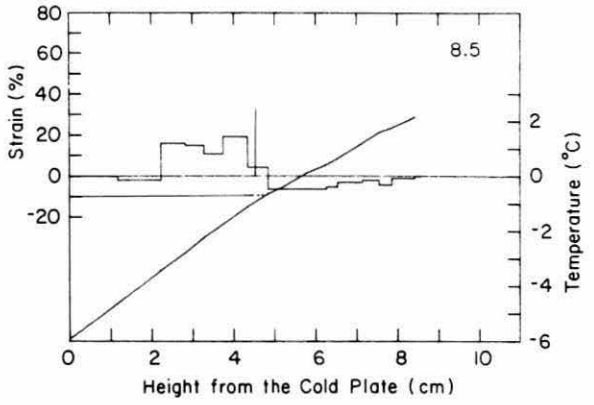
8.5
Strain (%)
Temperature (°C)
Height from the Cold Plate (cm)

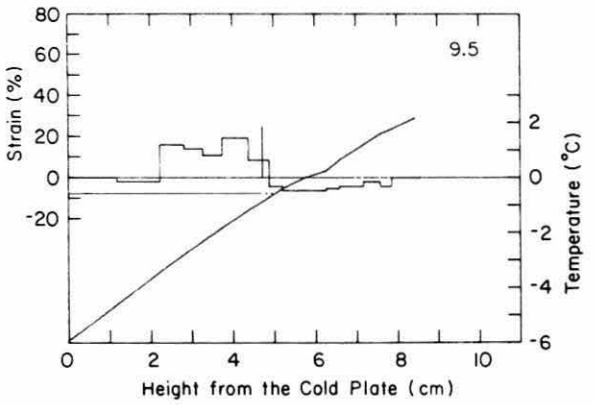
9.5
Strain (%)
Temperature (°C)
Height from the Cold Plate (cm)

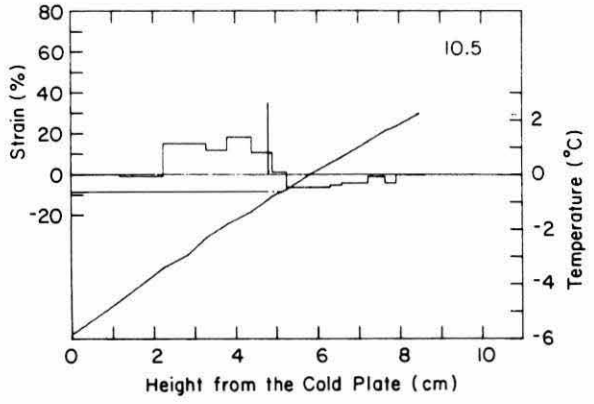
10.5
Strain (%)
Temperature (°C)
Height from the Cold Plate (cm)

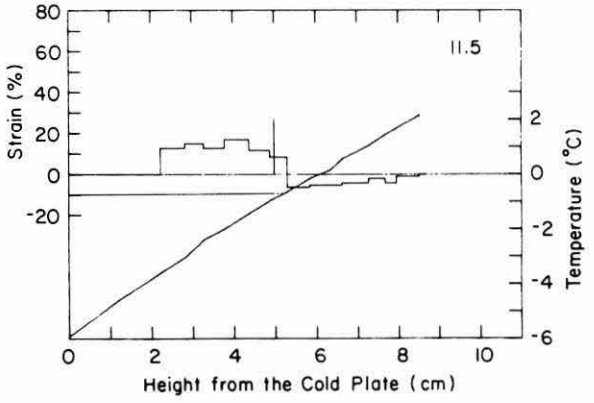
11.5
Strain (%)
Temperature (°C)
Height from the Cold Plate (cm)

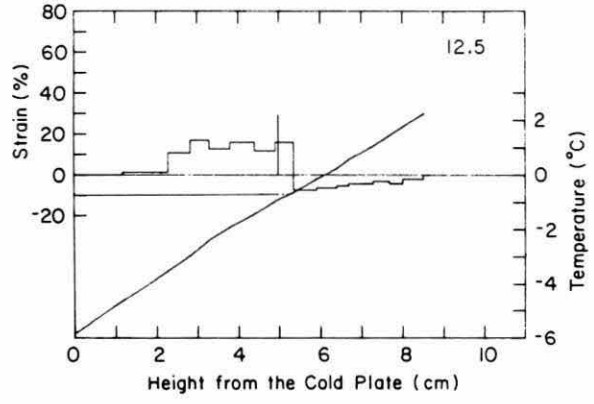
12.5
Strain (%)
Temperature (°C)
Height from the Cold Plate (cm)

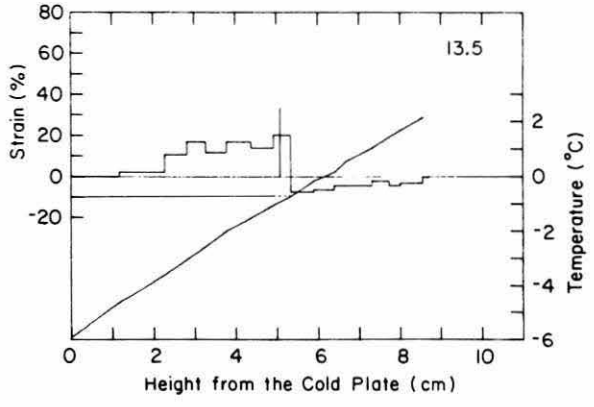
13.5
Strain (%)
Temperature (°C)
Height from the Cold Plate (cm)

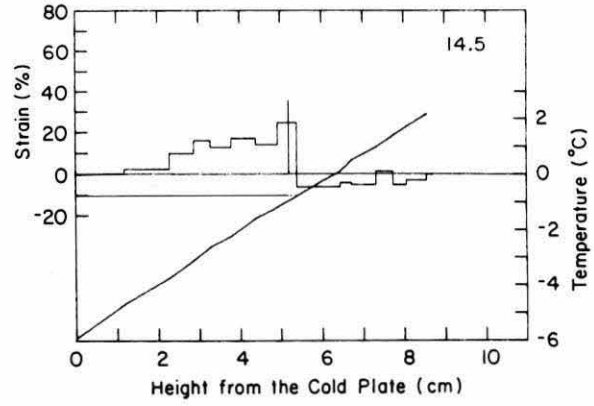
14.5
Strain (%)
Temperature (°C)
Height from the Cold Plate (cm)

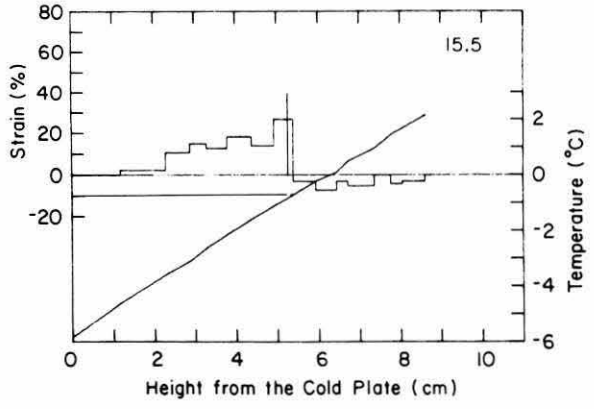
15.5
Strain (%)
Temperature (°C)
Height from the Cold Plate (cm)

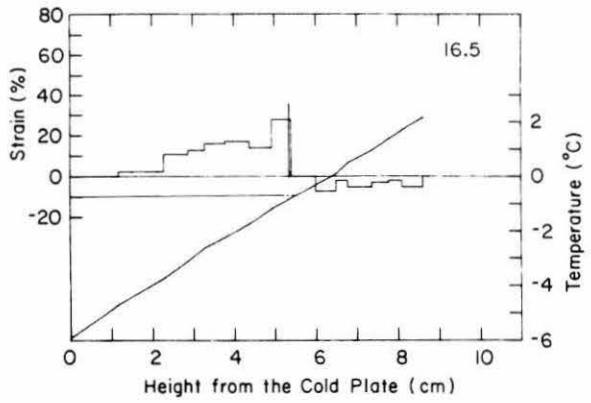
16.5
Strain (%)
Temperature (°C)
Height from the Cold Plate (cm)

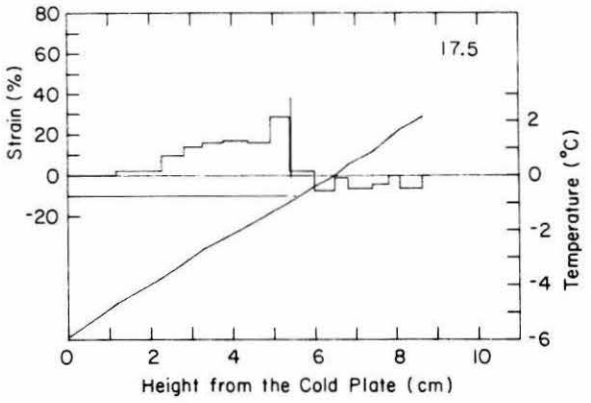
17.5
Strain (%)
Temperature (°C)
Height from the Cold Plate (cm)

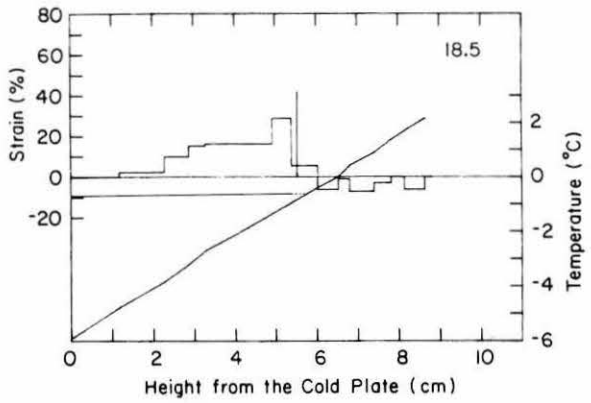
18.5
Strain (%)
Temperature (°C)
Height from the Cold Plate (cm)

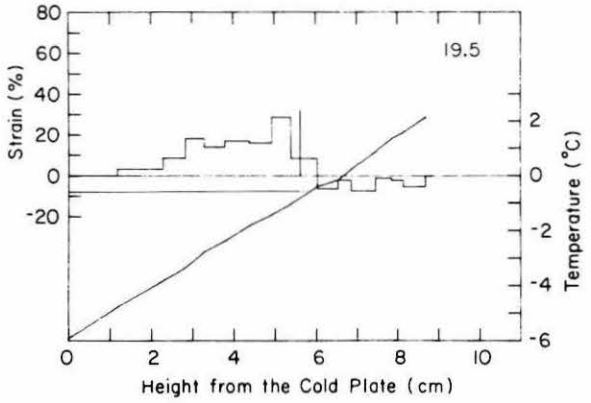
19.5
Strain (%)
Temperature (°C)
Height from the Cold Plate (cm)

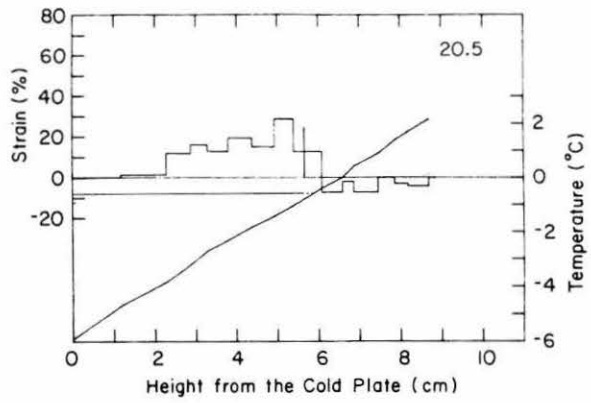
20.5
Strain (%)
Temperature (°C)
Height from the Cold Plate (cm)

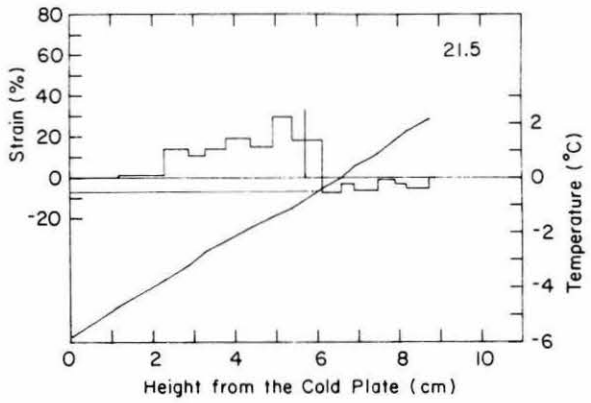
21.5
Strain (%)
Temperature (°C)
Height from the Cold Plate (cm)

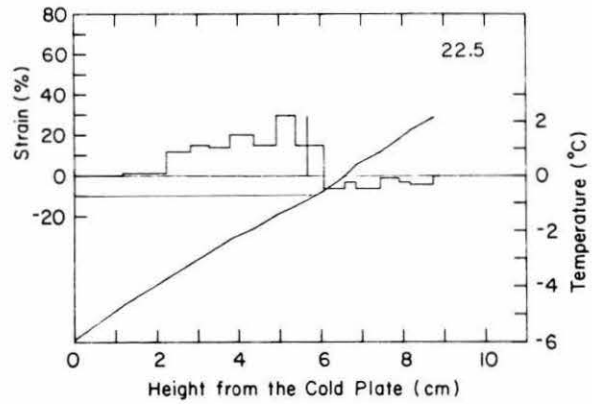
22.5
Strain (%)
Temperature (°C)
Height from the Cold Plate (cm)

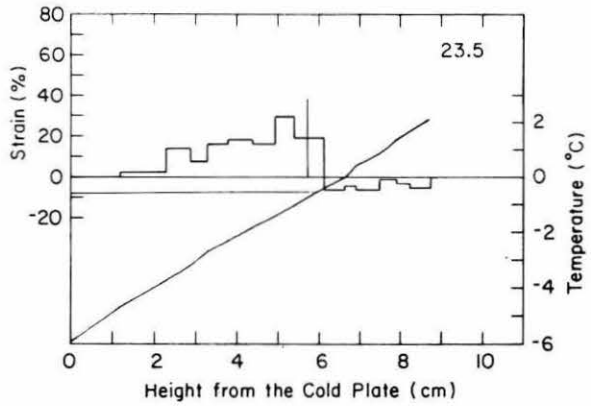
23.5
Strain (%)
Temperature (°C)
Height from the Cold Plate (cm)

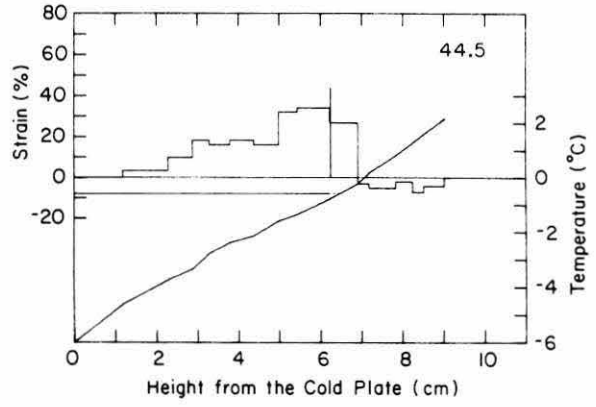
44.5
Strain (%)
Temperature (°C)
Height from the Cold Plate (cm)

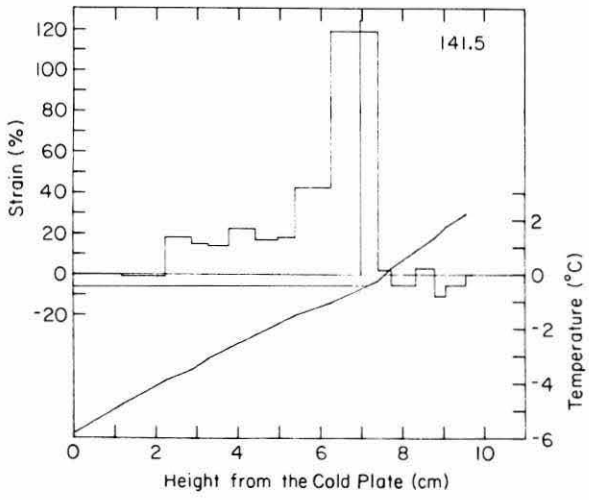
141.5
Strain (%)
Temperature (°C)
Height from the Cold Plate (cm)

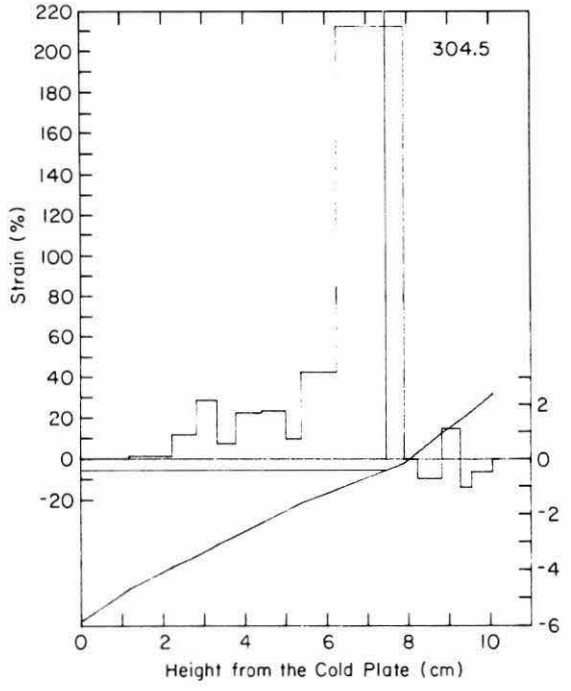
304.5
Strain (%)
Temperature (°C)
Height from the Cold Plate (cm)

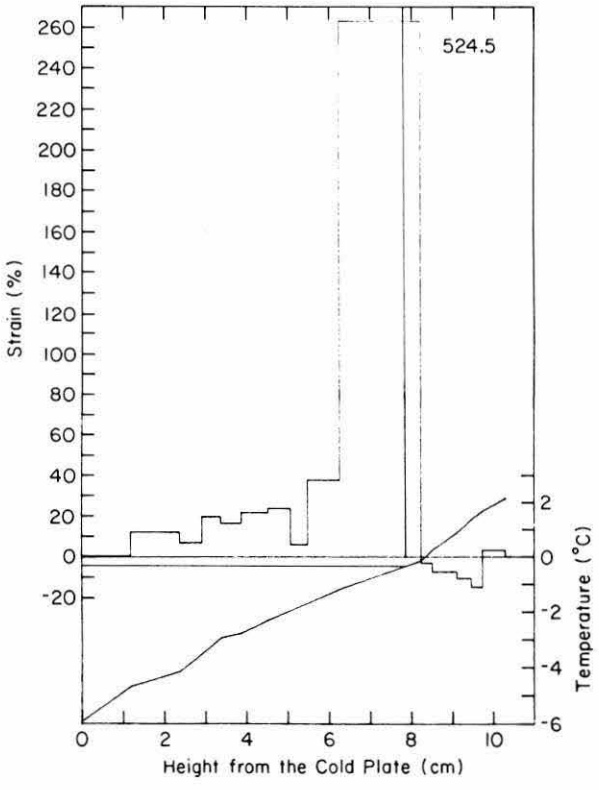
524.5
Strain (%)
Temperature (°C)
Height from the Cold Plate (cm)

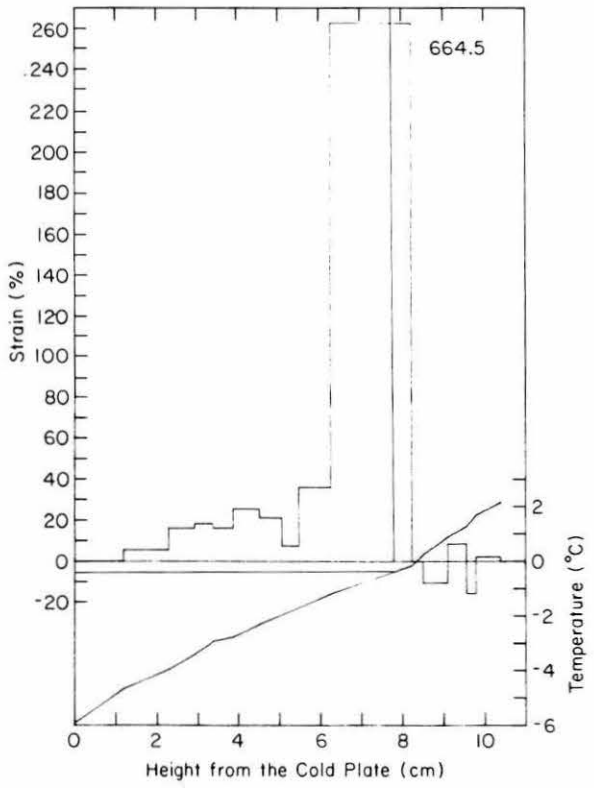
664.5
Strain (%)
Temperature (°C)
Height from the Cold Plate (cm)

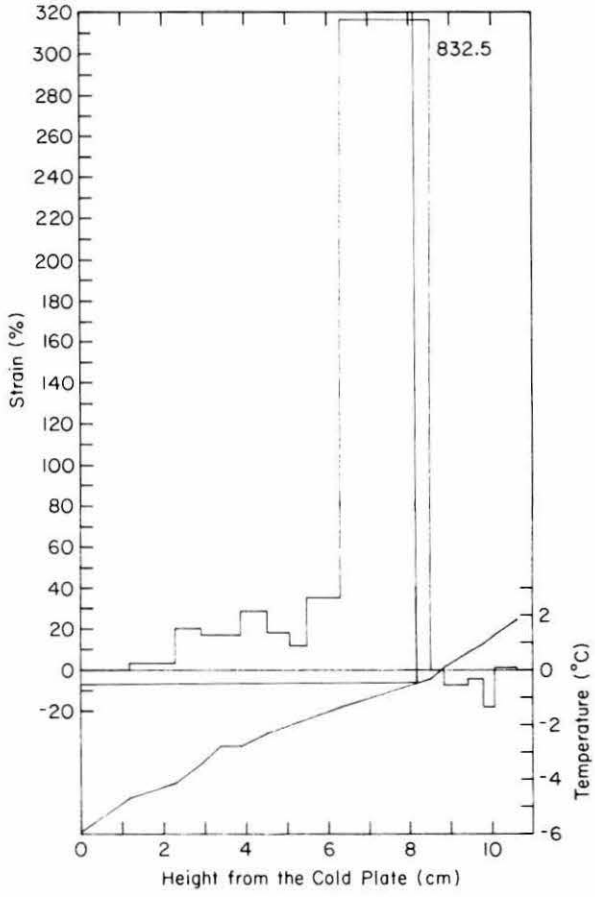
832.5
Strain (%)
Temperature (°C)
Height from the Cold Plate (cm)

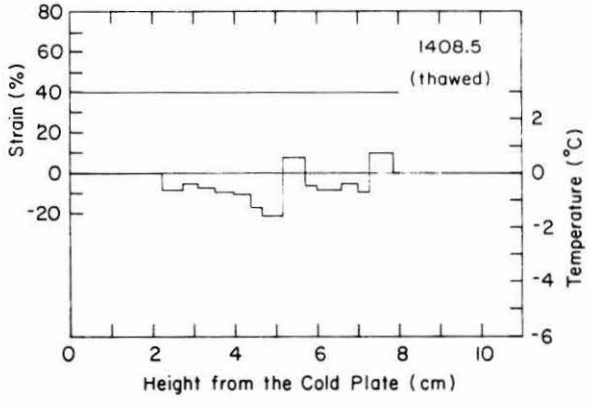
1408.5
(thawed)
Strain (%)
Temperature (°C)
Height from the Cold Plate (cm)

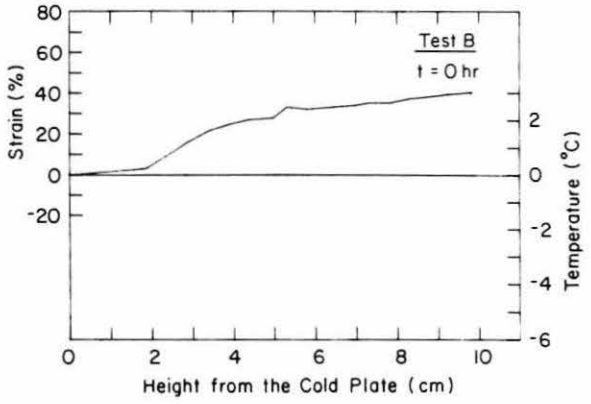
Test B
t = 0 hr
Strain (%)
Temperature (°C)
Height from the Cold Plate (cm)

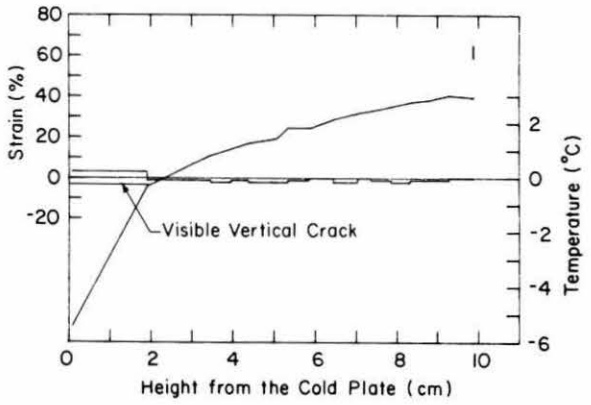
1
Visible Vertical Crack
Strain (%)
Temperature (°C)
Height from the Cold Plate (cm)

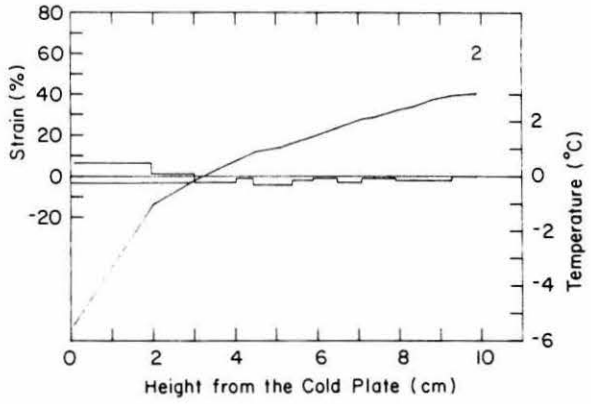
2
Strain (%)
Temperature (°C)
Height from the Cold Plate (cm)

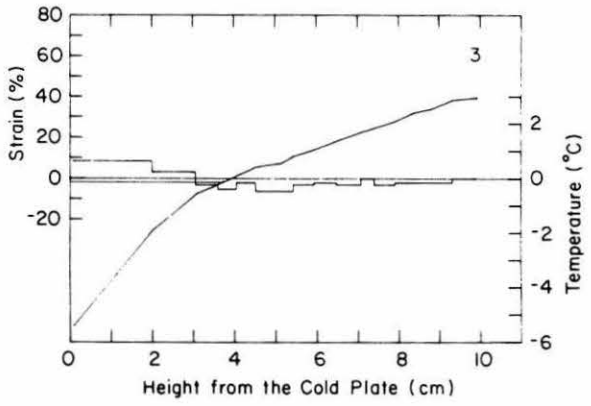
3
Strain (%)
Temperature (°C)
Height from the Cold Plate (cm)

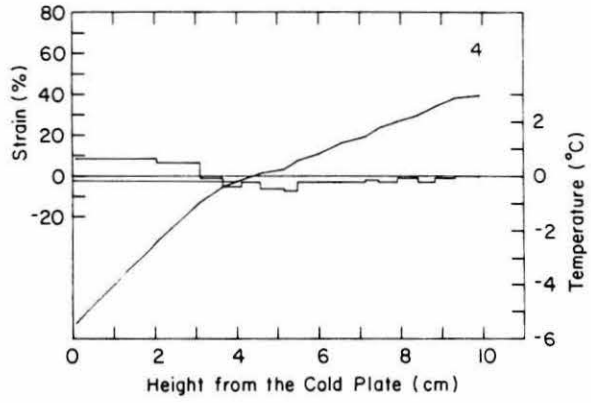
4
Strain (%)
Temperature (°C)
Height from the Cold Plate (cm)

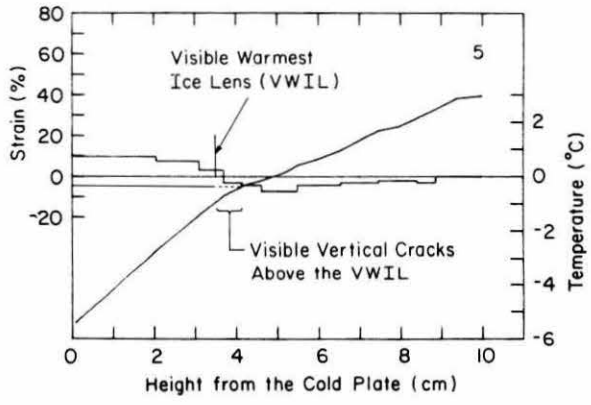
Visible Warmest
Ice Lens (VWIL)
5
Visible Vertical Cracks
Above the VWIL
Strain (%)
Temperature (°C)
Height from the Cold Plate (cm)

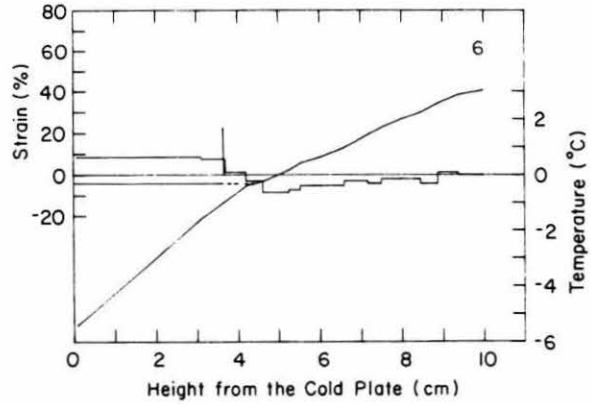
6
Strain (%)
Temperature (°C)
Height from the Cold Plate (cm)

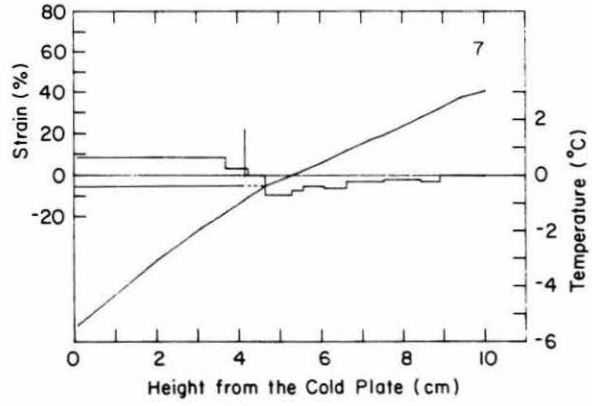
7
Strain (%)
Temperature (°C)
Height from the Cold Plate (cm)

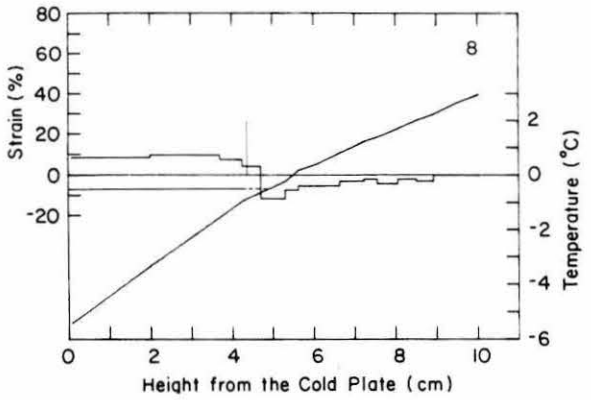
8
Strain (%)
Temperature (°C)
Height from the Cold Plate (cm)

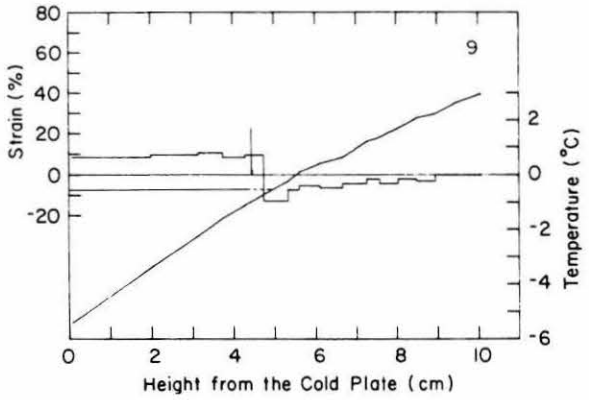
9
Strain (%)
Temperature (°C)
Height from the Cold Plate (cm)

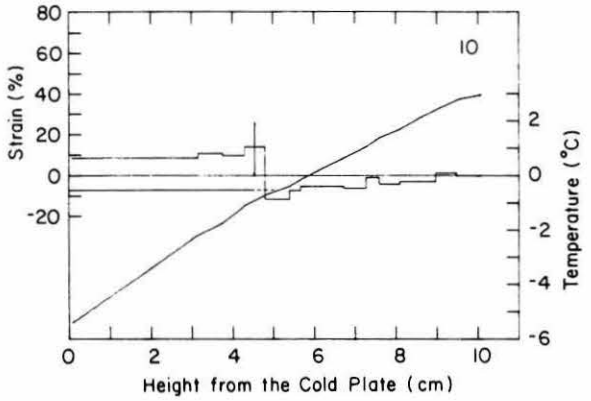
10
Strain (%)
Temperature (°C)
Height from the Cold Plate (cm)

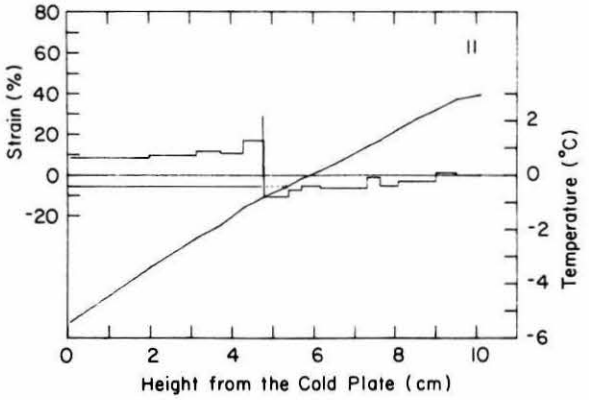
11
Strain (%)
Temperature (°C)
Height from the Cold Plate (cm)

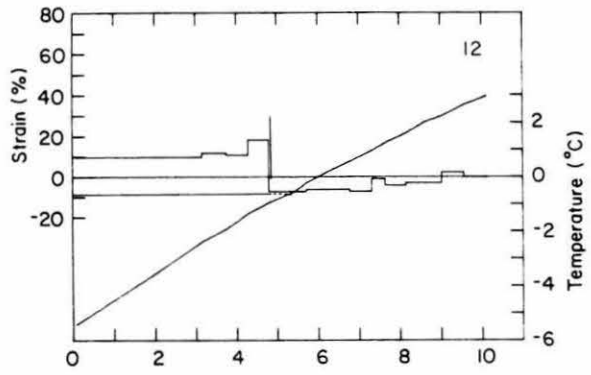
12
Strain (%)
Temperature (°C)

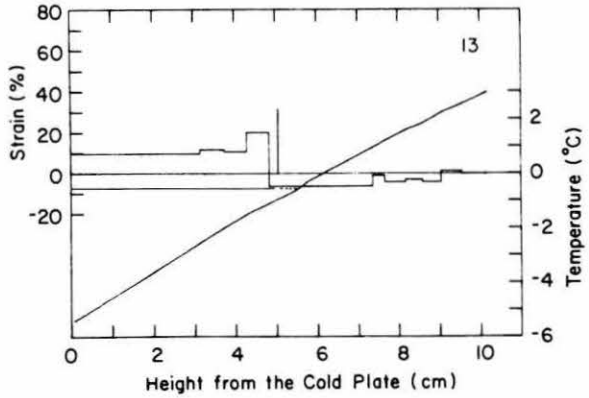
13
Strain (%)
Temperature (°C)
Height from the Cold Plate (cm)

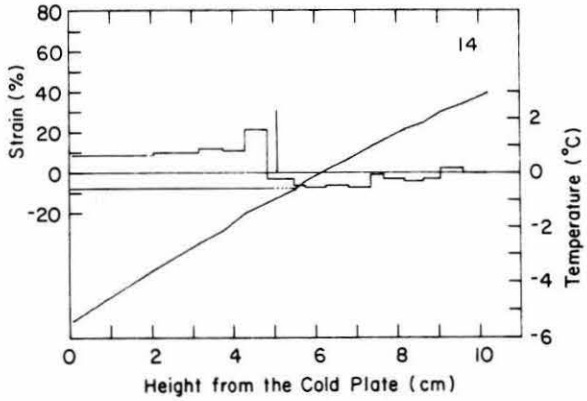
14
Strain (%)
Temperature (°C)
Height from the Cold Plate (cm)

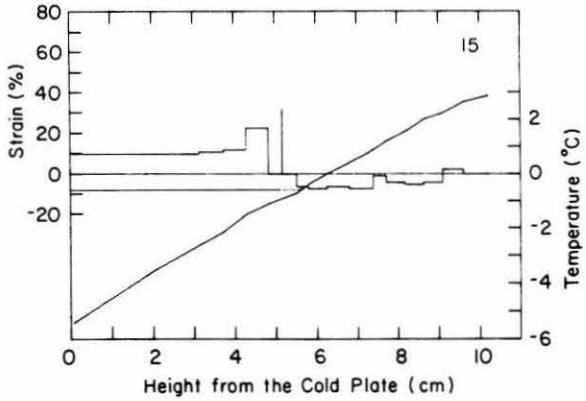
15
Strain (%)
Temperature (°C)
Height from the Cold Plate (cm)

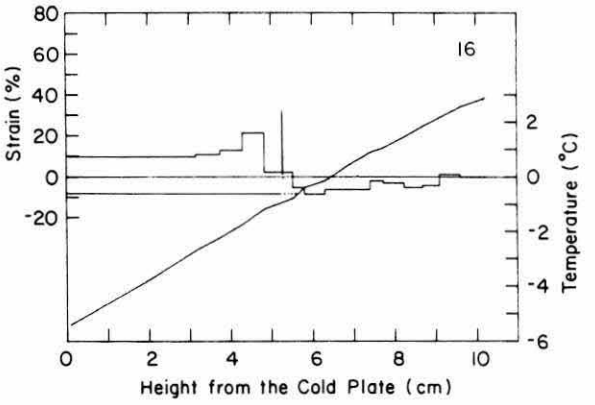
16
Strain (%)
Temperature (°C)
Height from the Cold Plate (cm)

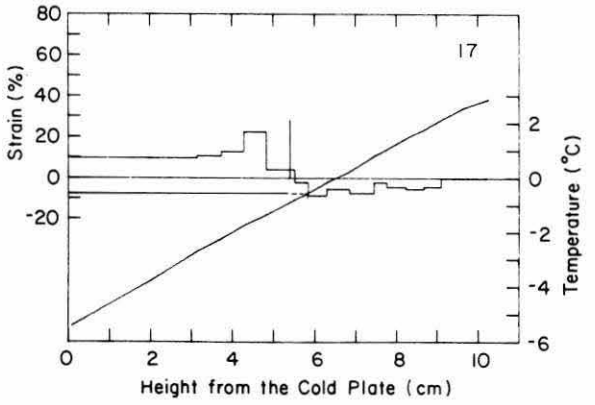
17
Strain (%)
Temperature (°C)
Height from the Cold Plate (cm)

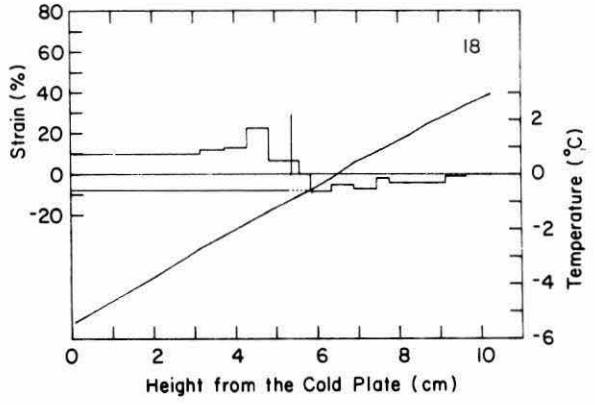
18
Strain (%)
Temperature (°C)
Height from the Cold Plate (cm)

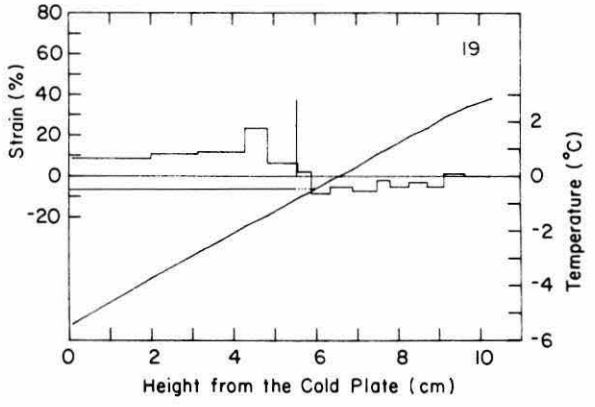
19
Strain (%)
Temperature (°C)
Height from the Cold Plate (cm)

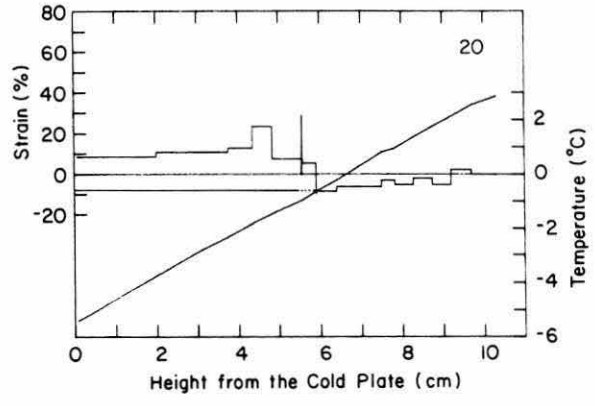
20
Strain (%)
Temperature (°C)
Height from the Cold Plate (cm)

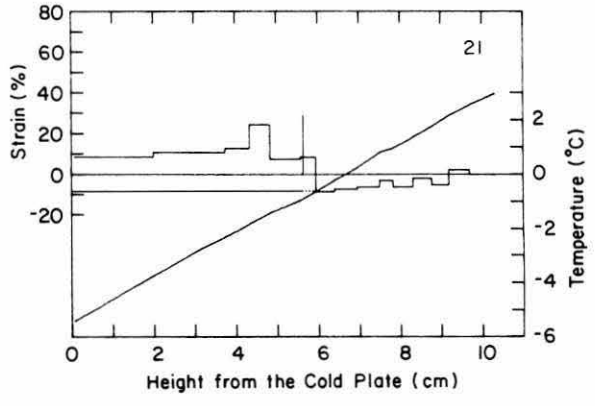
21
Strain (%)
Temperature (°C)
Height from the Cold Plate (cm)

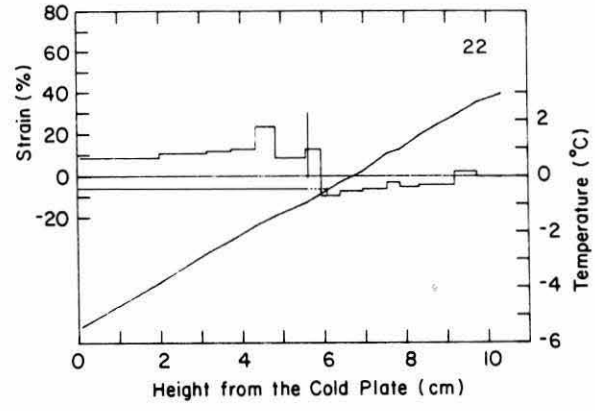
22
Strain (%)
Temperature (°C)
Height from the Cold Plate (cm)

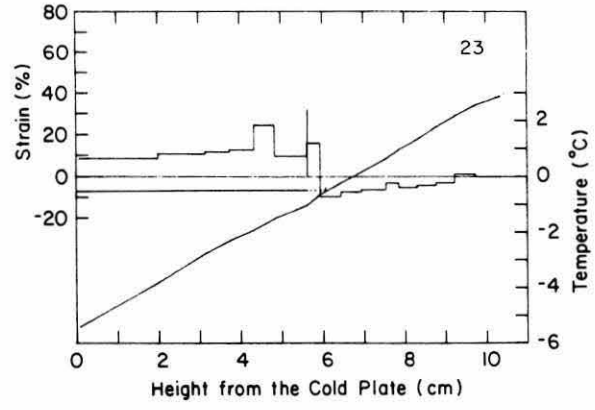
23
Strain (%)
Temperature (°C)
Height from the Cold Plate (cm)

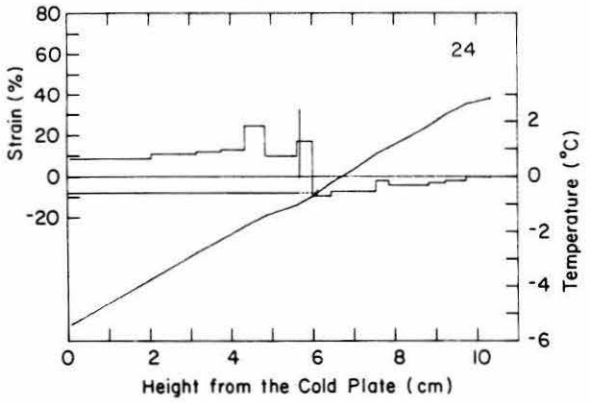
24
Strain (%)
Temperature (°C)
Height from the Cold Plate (cm)

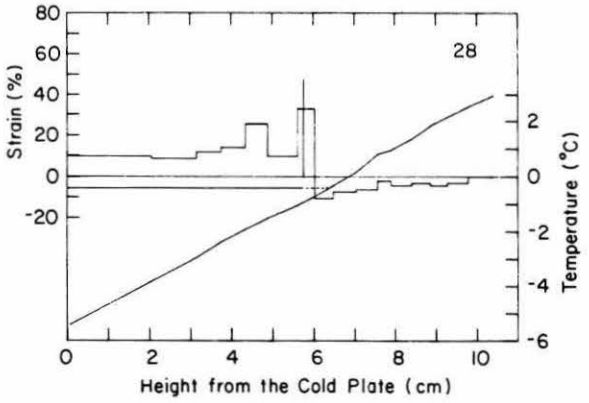
28
Strain (%)
Temperature (°C)
Height from the Cold Plate (cm)

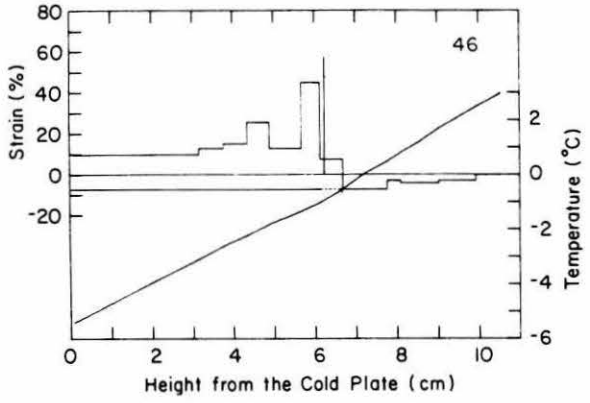
46
Strain (%)
Temperature (°C)
Height from the Cold Plate (cm)

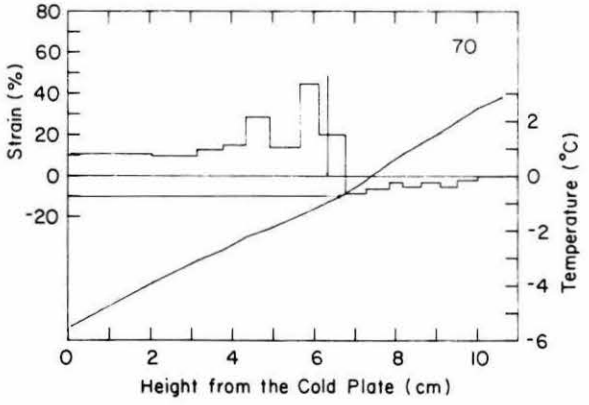
70
Strain (%)
Temperature (°C)
Height from the Cold Plate (cm)

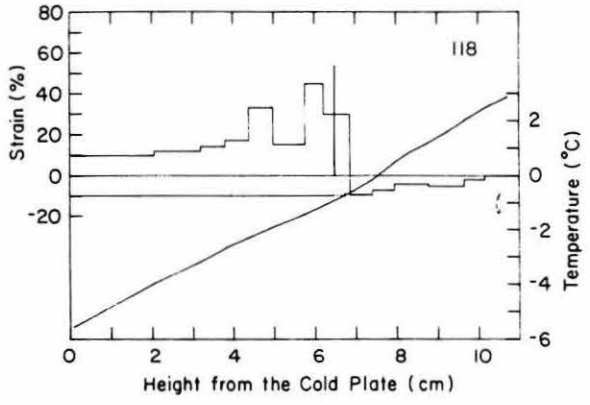
118
Strain (%)
Temperature (°C)
Height from the Cold Plate (cm)

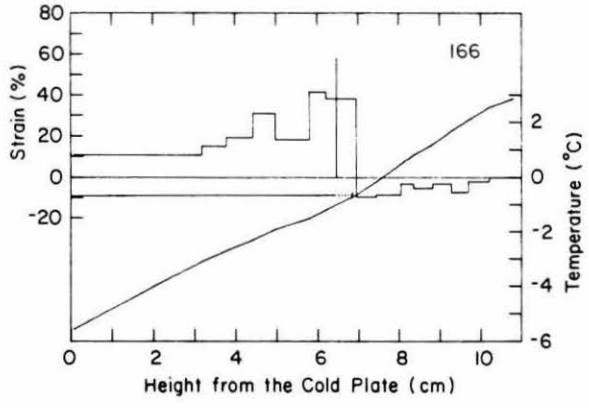
166
Strain (%)
Temperature (°C)
Height from the Cold Plate (cm)

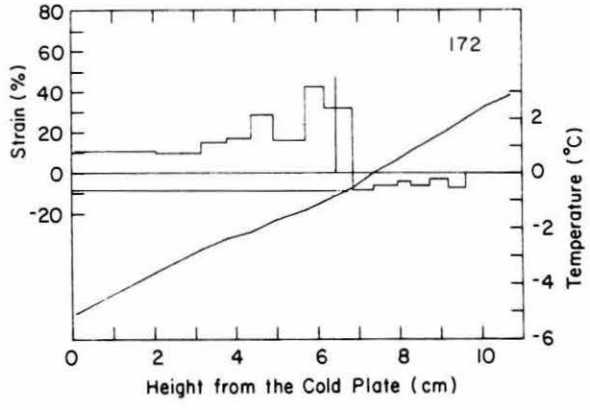
172
Strain (%)
Temperature (°C)
Height from the Cold Plate (cm)

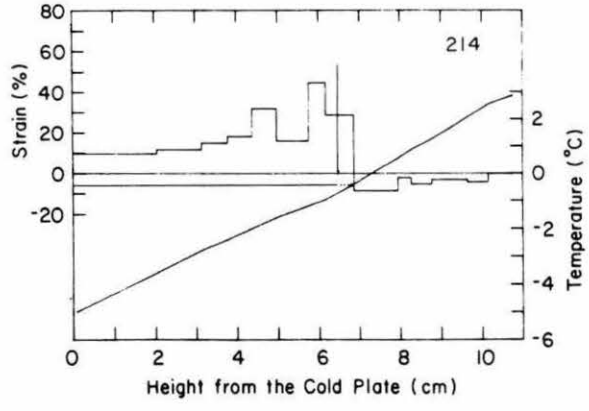
214
Strain (%)
Temperature (°C)
Height from the Cold Plate (cm)

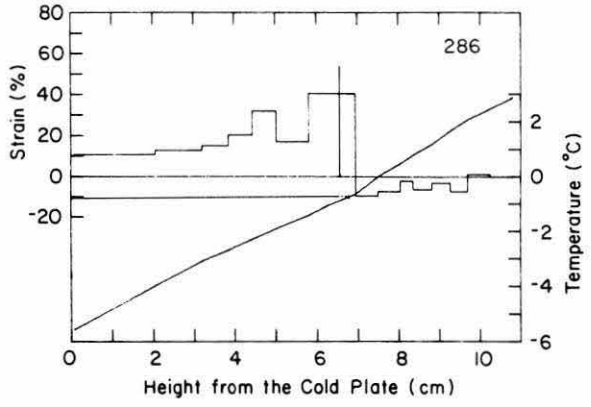
286
Strain (%)
Temperature (°C)
Height from the Cold Plate (cm)

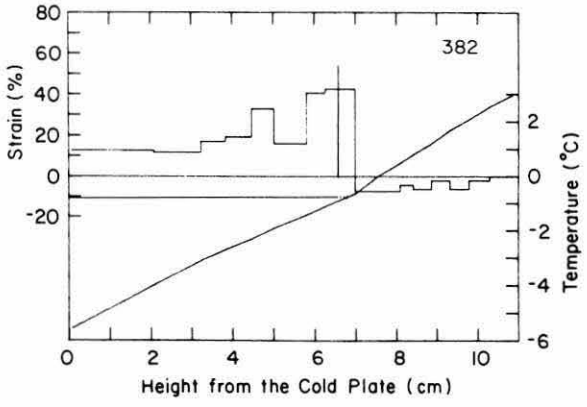
382
Strain (%)
Temperature (°C)
Height from the Cold Plate (cm)

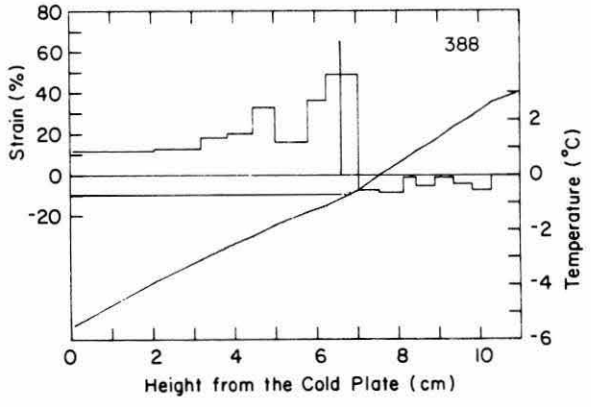
388
Strain (%)
Temperature (°C)
Height from the Cold Plate (cm)

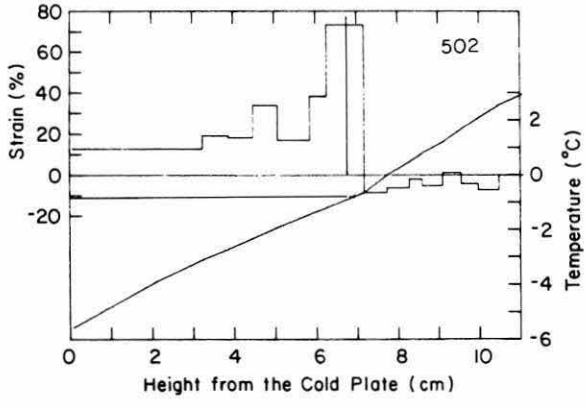
502
Strain (%)
Temperature (°C)
Height from the Cold Plate (cm)

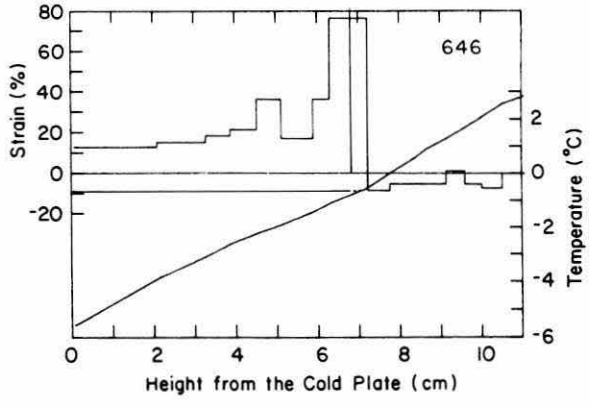
646
Strain (%)
Temperature (°C)
Height from the Cold Plate (cm)

APPENDIX D: STRAIN RATE OBSERVED IN THE SOIL LAYERS.

Positive strain rate represents heave and negative strain rate represents consolidation.

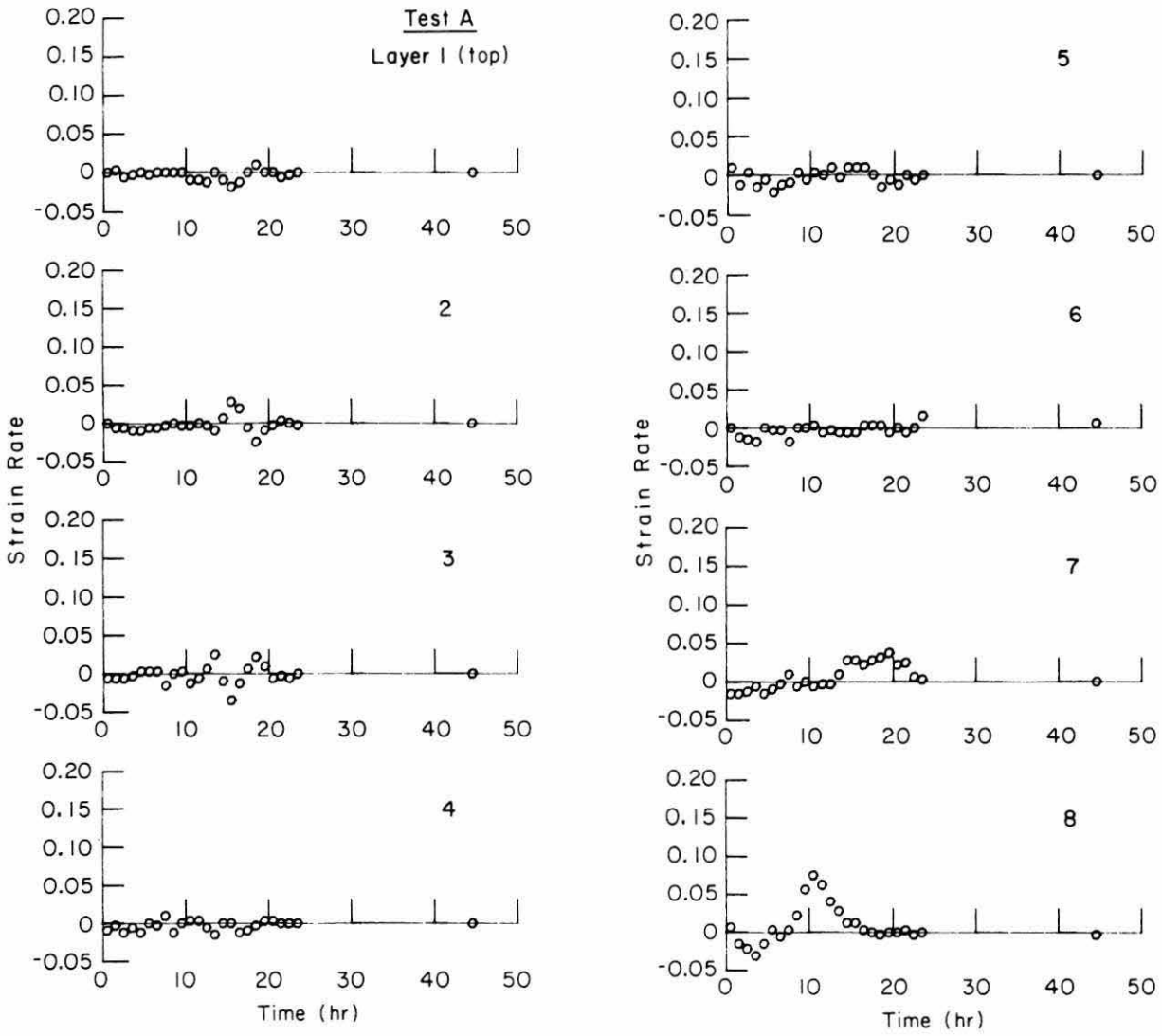

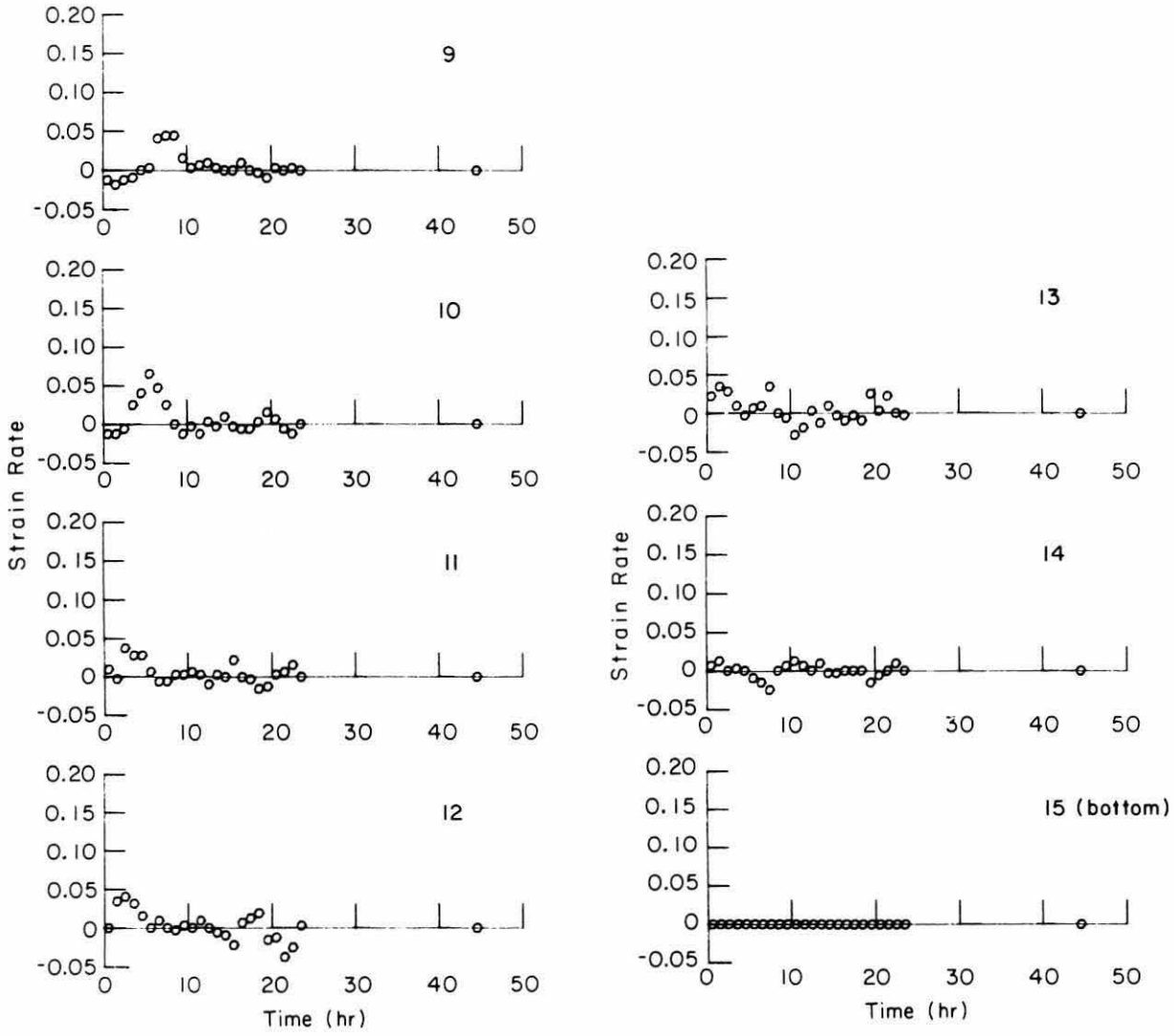
Strain Rate
0.20
0.15
0.10
0.05
0
-0.05
0
10
20
30
40
50
9
10
11
12
13
14
15 (bottom)
Time (hr)

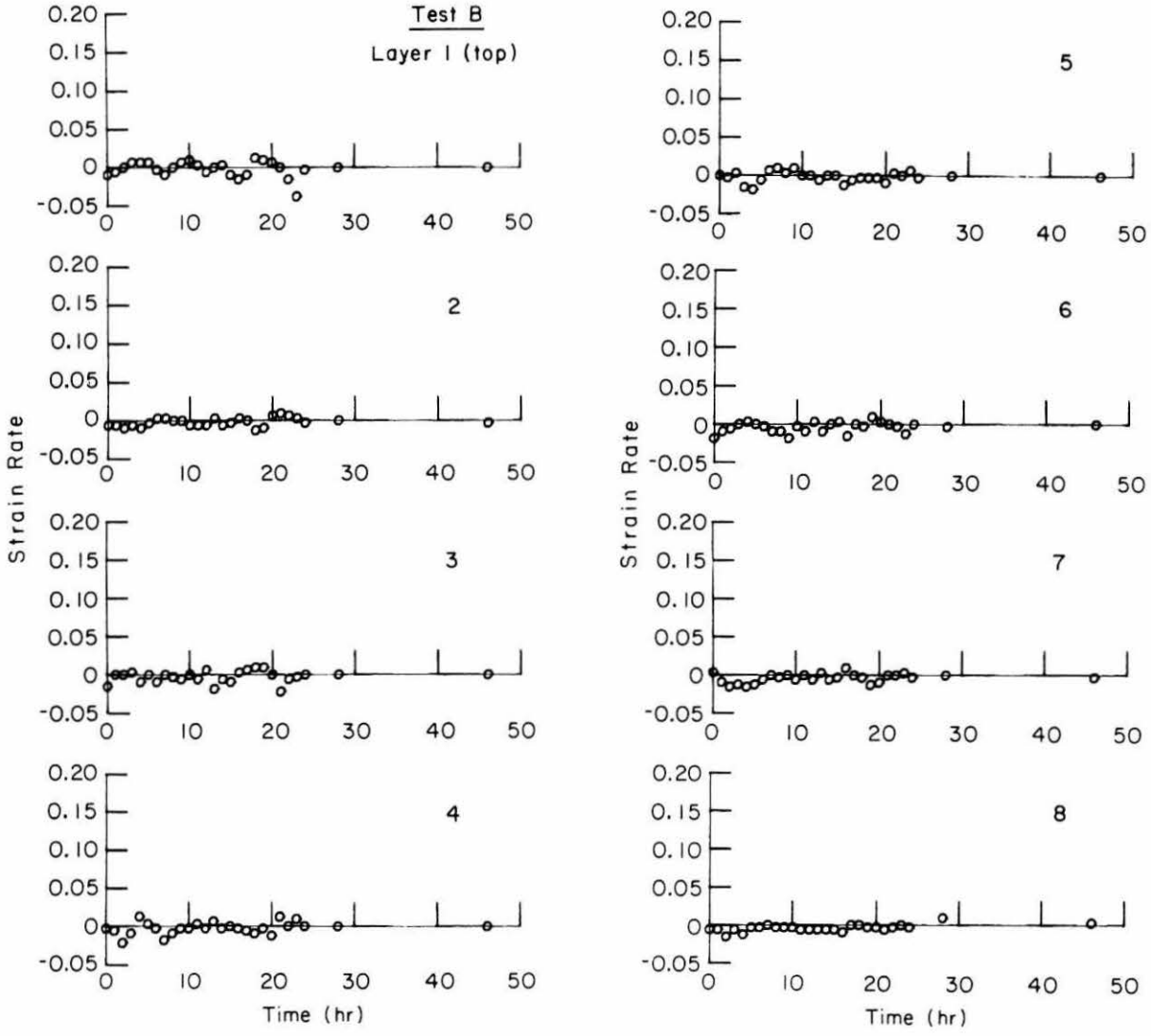
Test B
Layer 1 (top)
2
3
4
5
6
7
8
Strain Rate
Time (hr)
0.20
0.15
0.10
0.05
0
-0.05
0
10
20
30
40
50

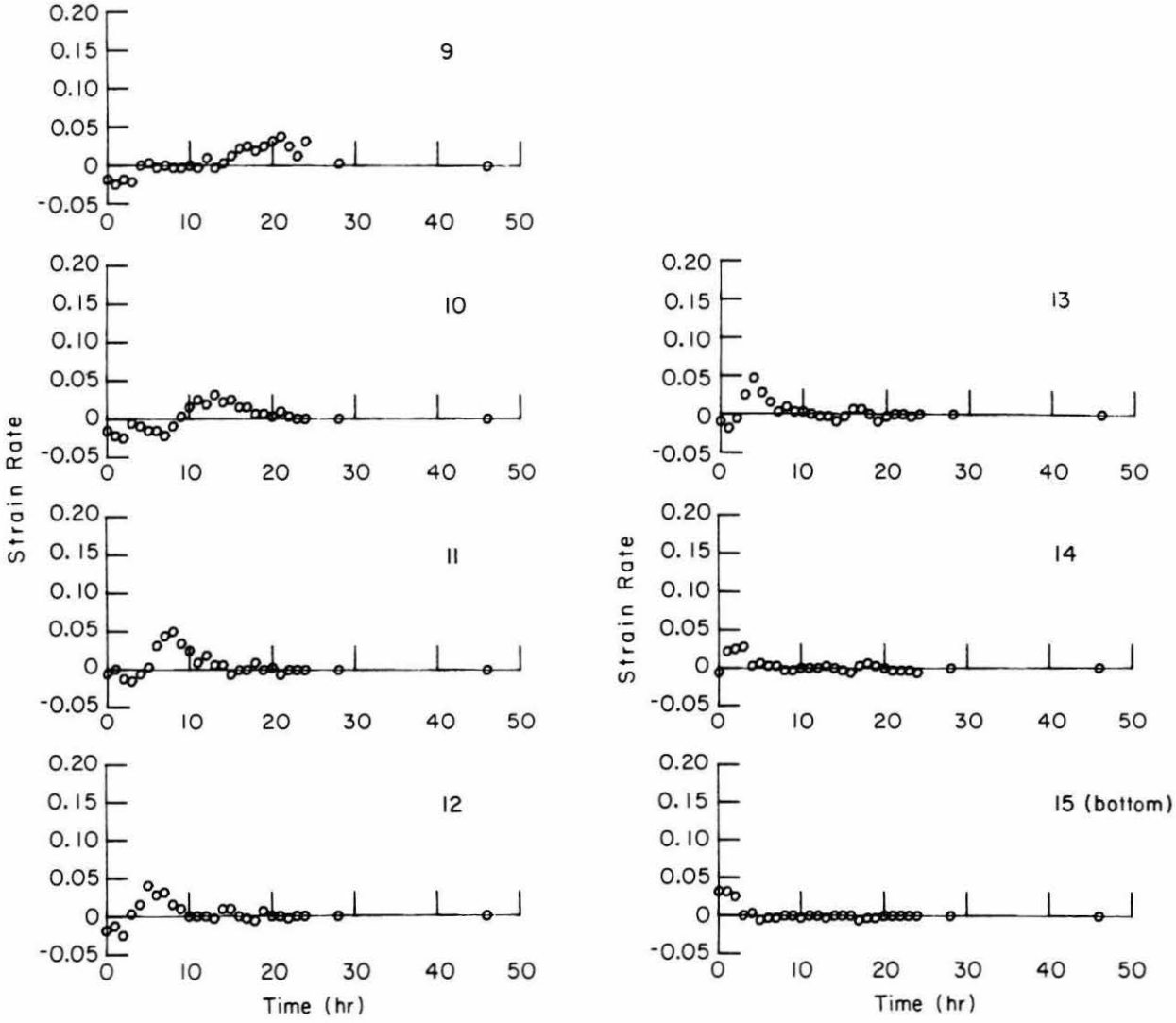
Strain Rate
0.20
0.15
0.10
0.05
0
-0.05
0
10
20
30
40
50
9
10
11
12
13
14
15 (bottom)
Time (hr)

APPENDIX E: STRAIN RATE DISTRIBUTION IN THE SOIL LAYERS.

Positive strain rate represents heave and negative strain rate represents consolidation.

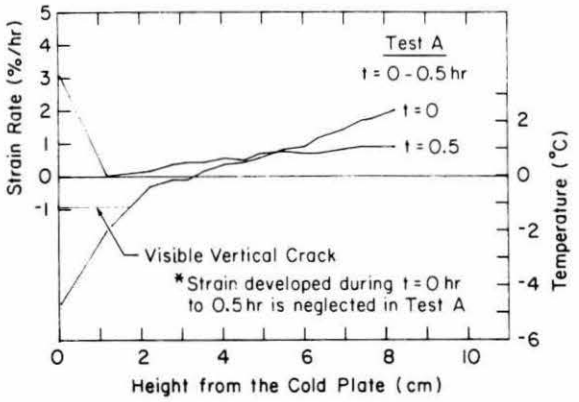

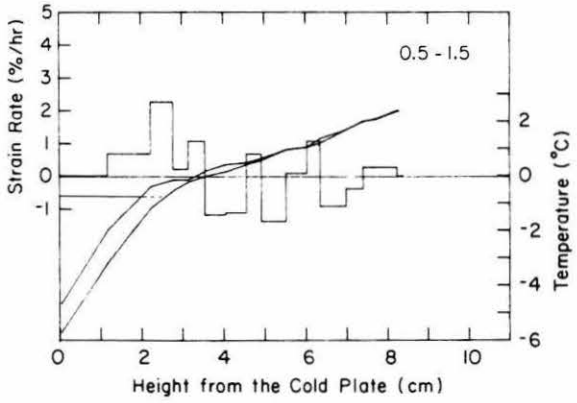

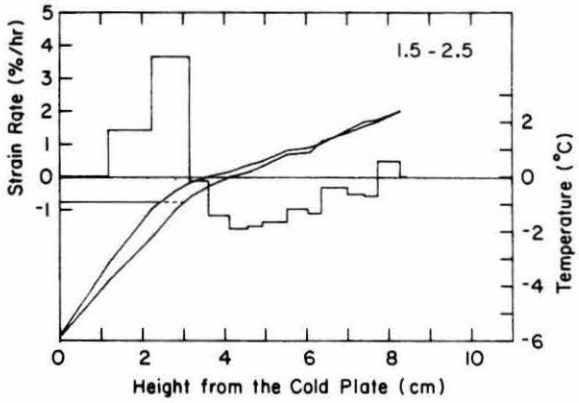

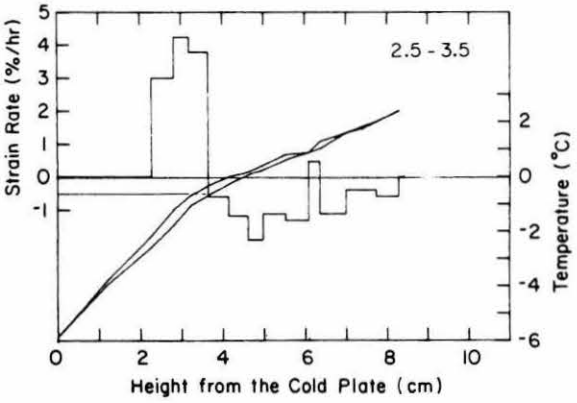

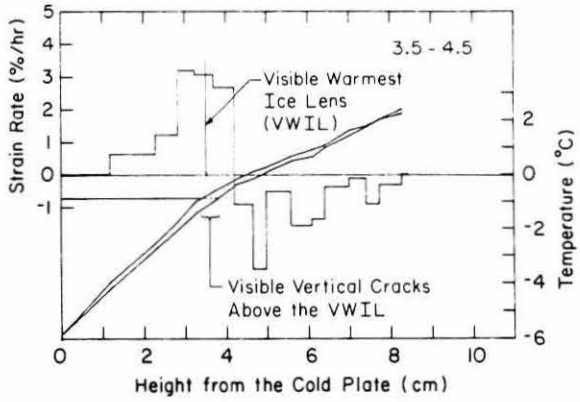

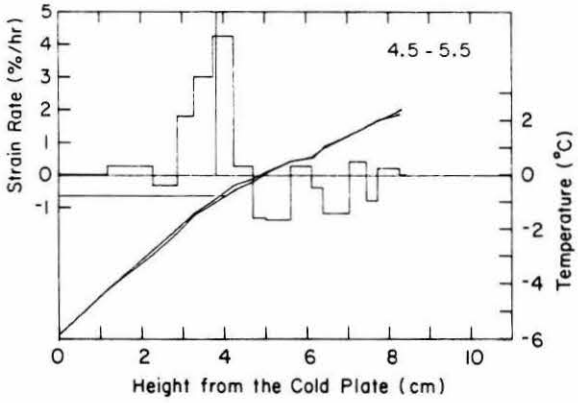

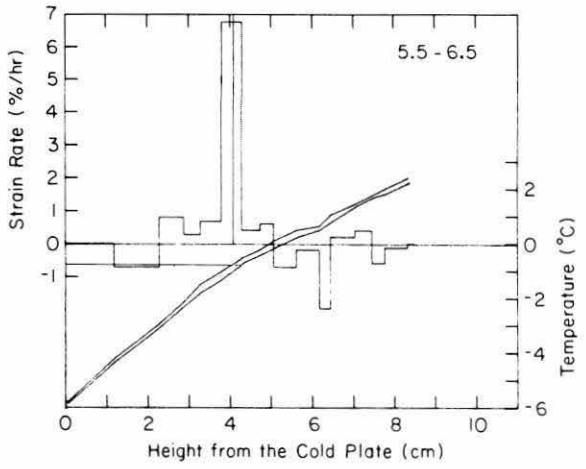
5.5 - 6.5
Strain Rate (%/hr)
Temperature (°C)
Height from the Cold Plate (cm)

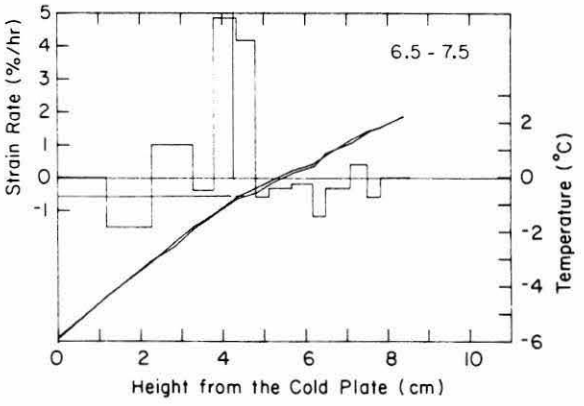
6.5 - 7.5
Strain Rate (%/hr)
Temperature (°C)
Height from the Cold Plate (cm)

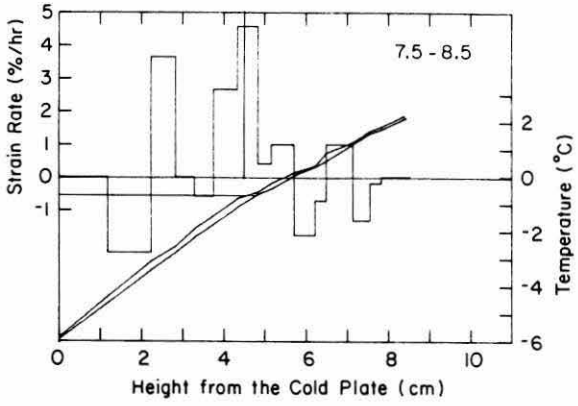
7.5 - 8.5
Strain Rate (%/hr)
Temperature (°C)
Height from the Cold Plate (cm)

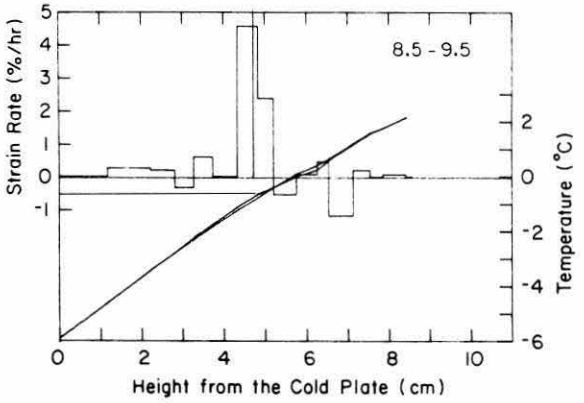
8.5 - 9.5
Strain Rate (%/hr)
Temperature (°C)
Height from the Cold Plate (cm)

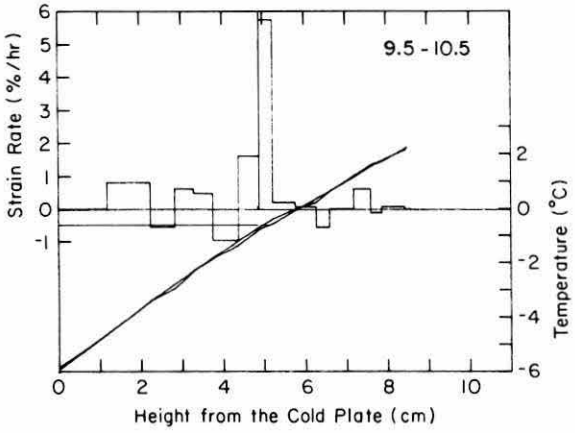
9.5 - 10.5
Strain Rate (%/hr)
Temperature (°C)
Height from the Cold Plate (cm)

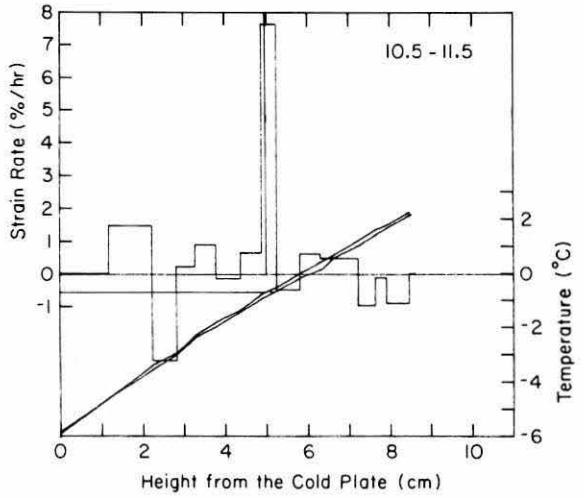
10.5 - 11.5
Strain Rate (%/hr)
Temperature (°C)
Height from the Cold Plate (cm)

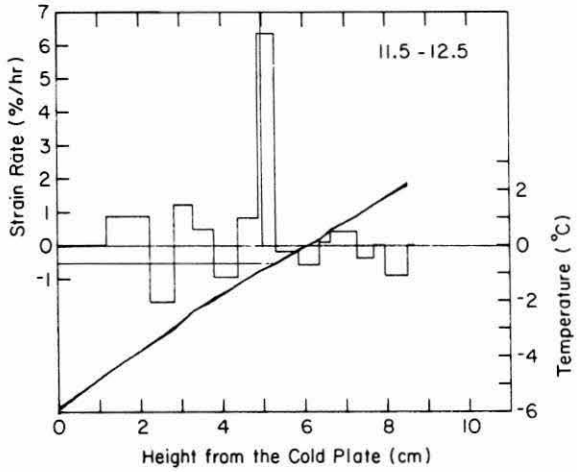
11.5 - 12.5
Strain Rate (%/hr)
Temperature (°C)
Height from the Cold Plate (cm)

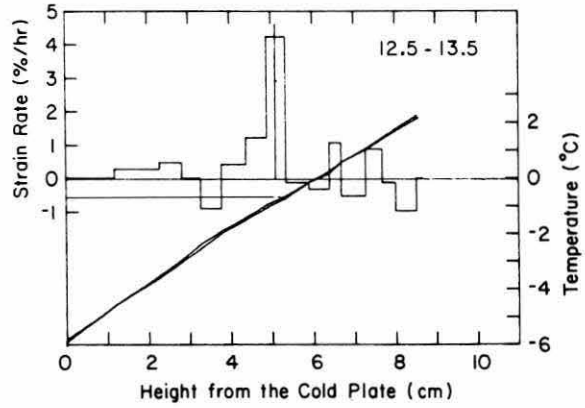
12.5 - 13.5
Strain Rate (%/hr)
Temperature (°C)
Height from the Cold Plate (cm)

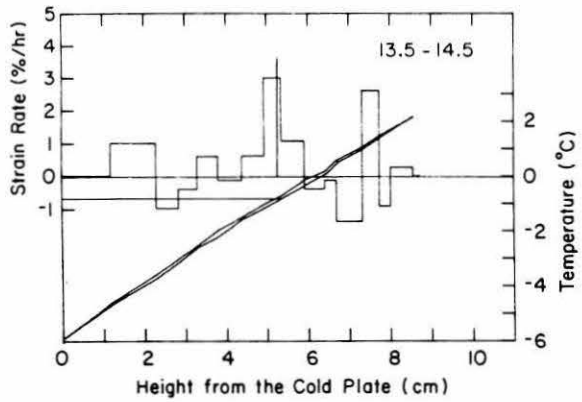
13.5 - 14.5
Strain Rate (%/hr)
Temperature (°C)
Height from the Cold Plate (cm)

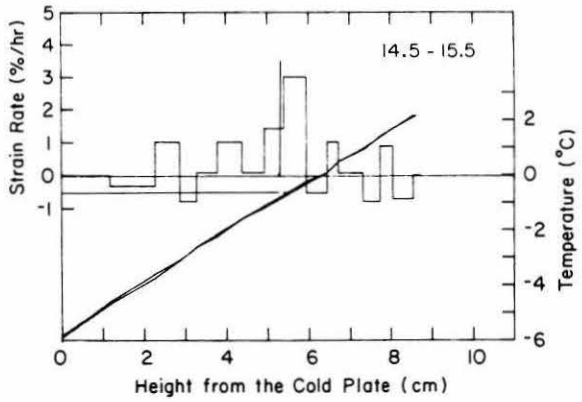
14.5 - 15.5
Strain Rate (%/hr)
Temperature (°C)
Height from the Cold Plate (cm)

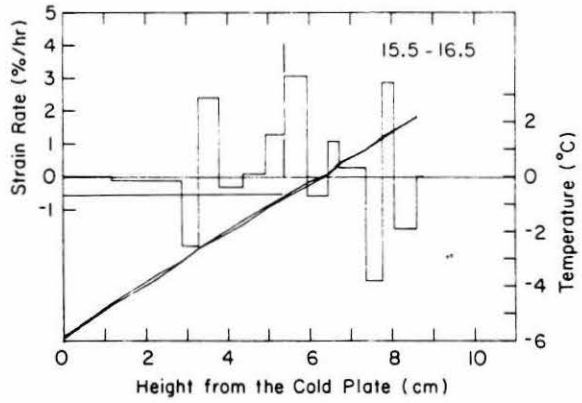
15.5 - 16.5
Strain Rate (%/hr)
Temperature (°C)
Height from the Cold Plate (cm)

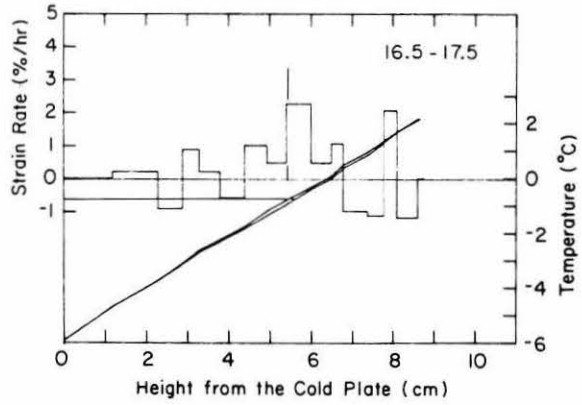
16.5 - 17.5
Strain Rate (%/hr)
Temperature (°C)
Height from the Cold Plate (cm)

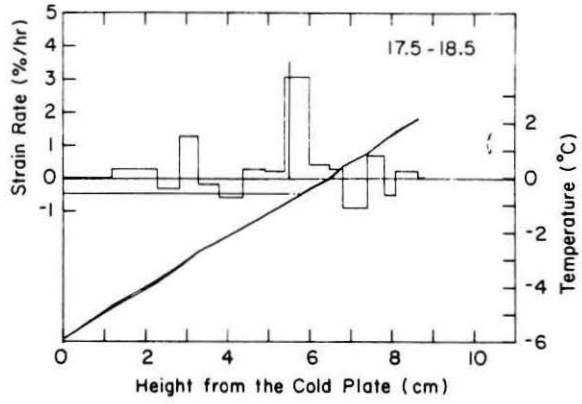
17.5 - 18.5
Strain Rate (%/hr)
Temperature (°C)
Height from the Cold Plate (cm)

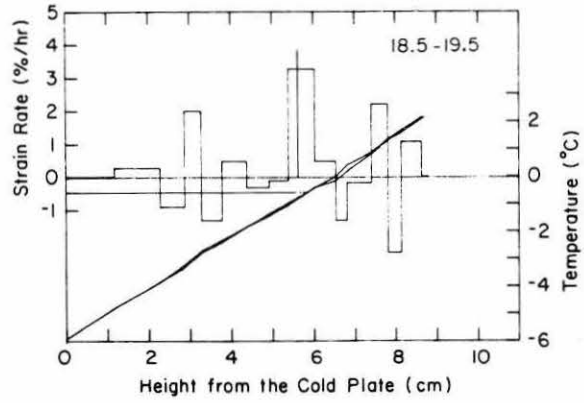
18.5 - 19.5
Strain Rate (%/hr)
Temperature (°C)
Height from the Cold Plate (cm)

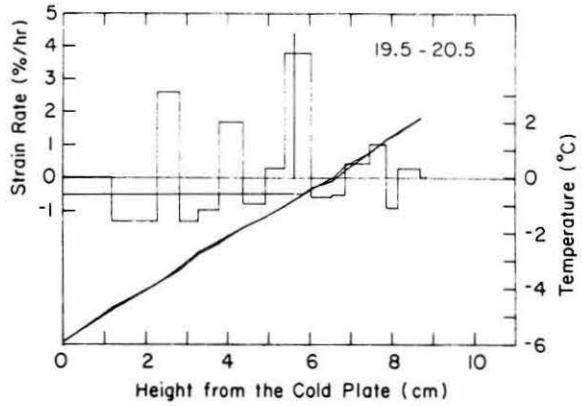
19.5 - 20.5
Strain Rate (%/hr)
Temperature (°C)
Height from the Cold Plate (cm)

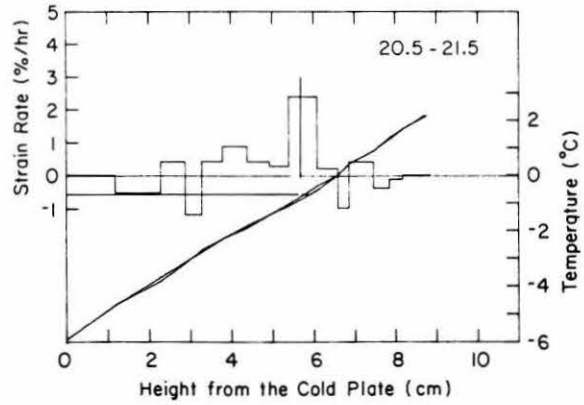
20.5 - 21.5
Strain Rate (%/hr)
Temperature (°C)
Height from the Cold Plate (cm)

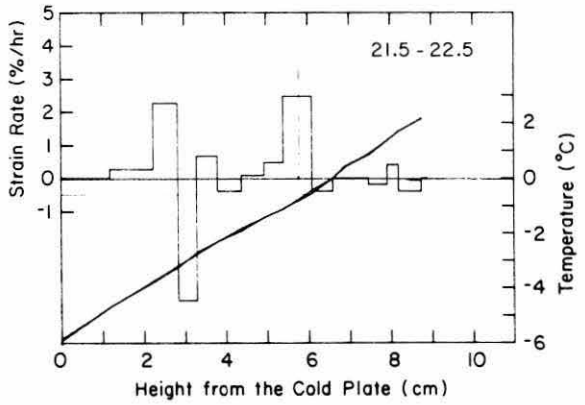
21.5 - 22.5
Strain Rate (%/hr)
Temperature (°C)
Height from the Cold Plate (cm)

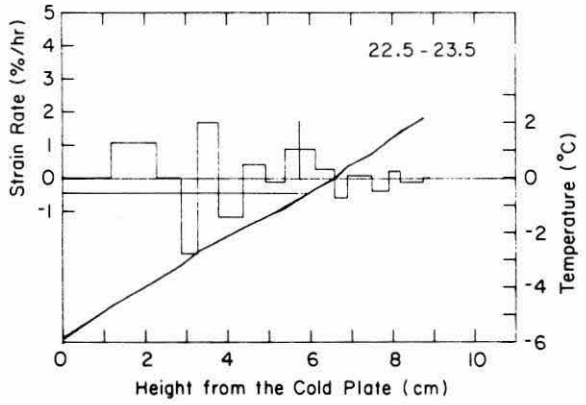
22.5 - 23.5
Strain Rate (%/hr)
Temperature (°C)
Height from the Cold Plate (cm)

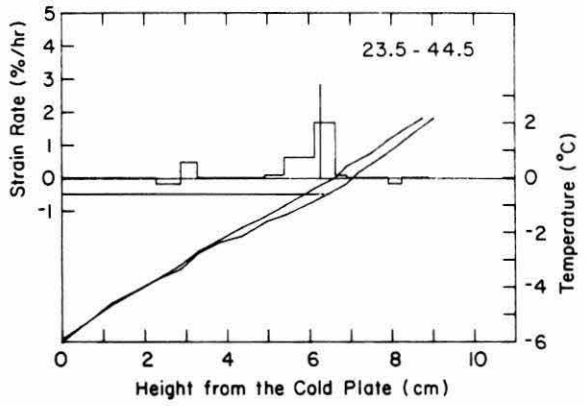
23.5 - 44.5
Strain Rate (%/hr)
Temperature (°C)
Height from the Cold Plate (cm)

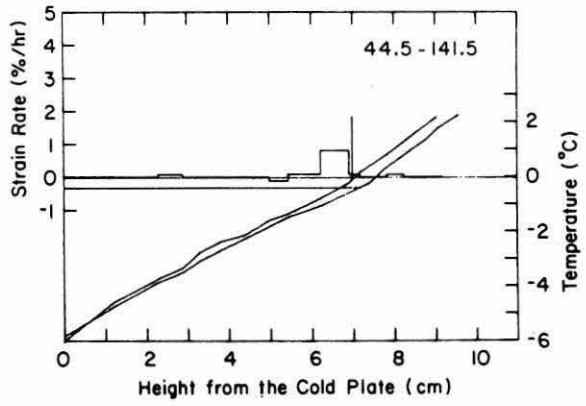
44.5 - 141.5
Strain Rate (%/hr)
Temperature (°C)
Height from the Cold Plate (cm)

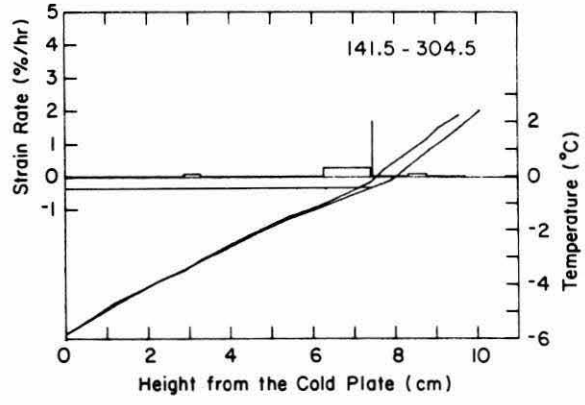
141.5 - 304.5
Strain Rate (%/hr)
Temperature (°C)
Height from the Cold Plate (cm)

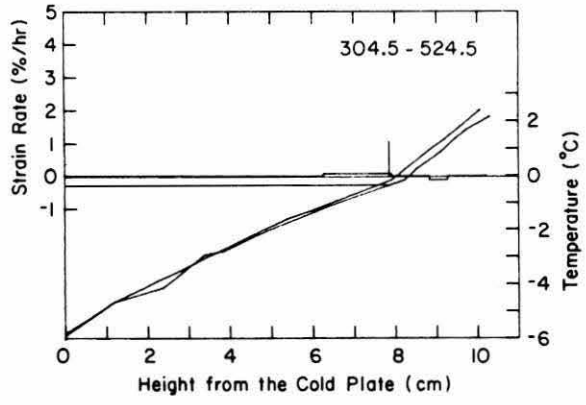
304.5 - 524.5
Strain Rate (%/hr)
Temperature (°C)
Height from the Cold Plate (cm)

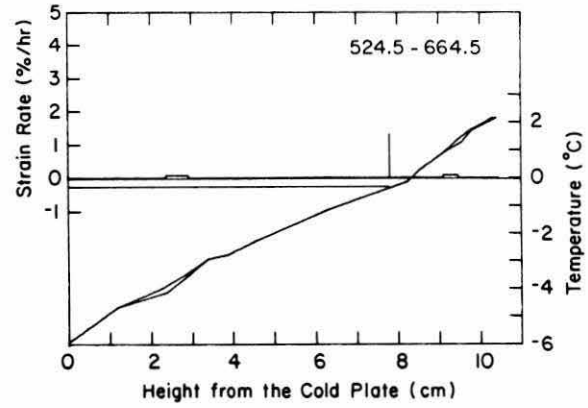
524.5 - 664.5
Strain Rate (%/hr)
Temperature (°C)
Height from the Cold Plate (cm)

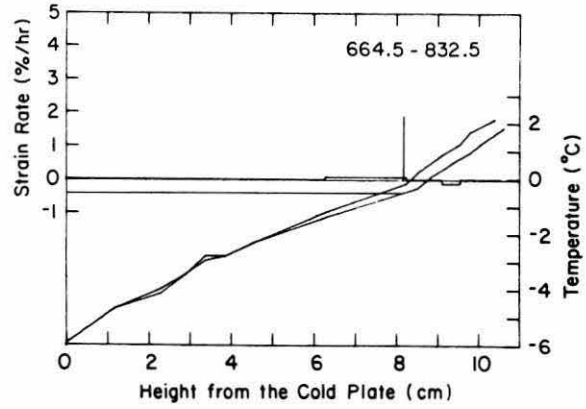
664.5 - 832.5
Strain Rate (%/hr)
Temperature (°C)
Height from the Cold Plate (cm)

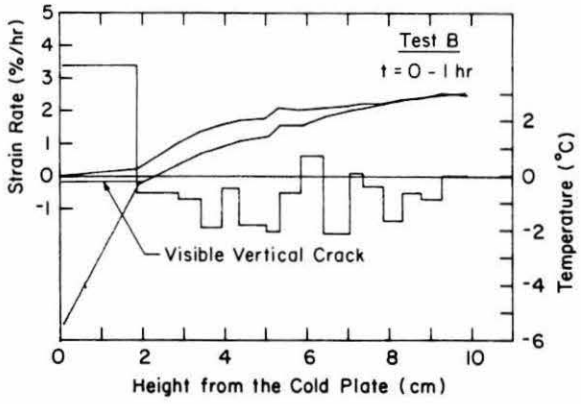
Test B
t = 0 - 1 hr
Visible Vertical Crack
Strain Rate (%/hr)
Temperature (°C)
Height from the Cold Plate (cm)

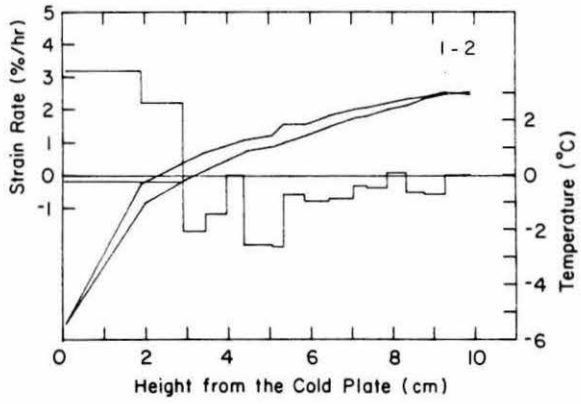
1 - 2
Strain Rate (%/hr)
Temperature (°C)
Height from the Cold Plate (cm)

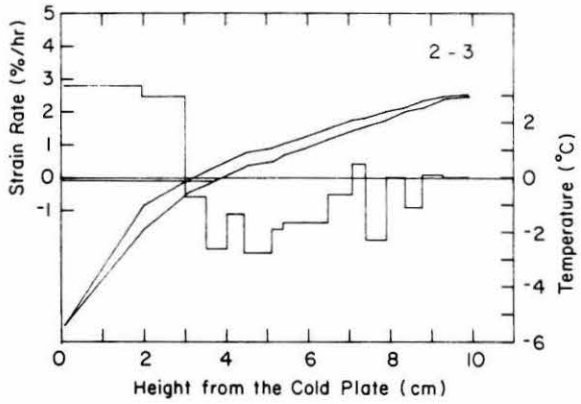
2 - 3
Strain Rate (%/hr)
Temperature (°C)
Height from the Cold Plate (cm)

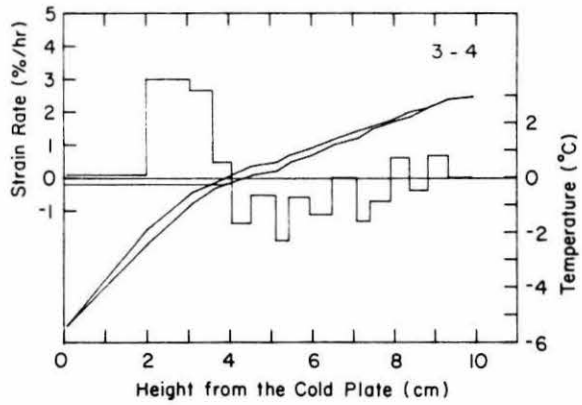
3 - 4
Strain Rate (%/hr)
Temperature (°C)
Height from the Cold Plate (cm)

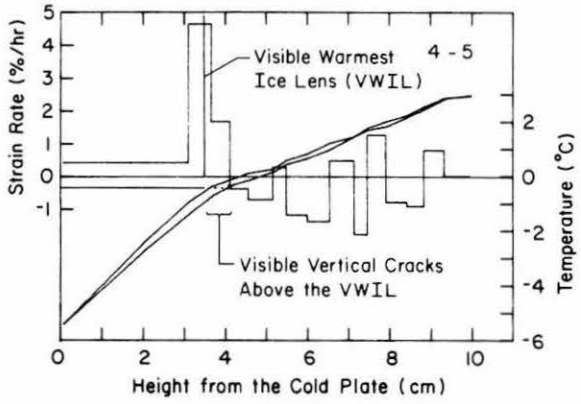
Visible Warmest
Ice Lens (VWIL)
4 - 5
Visible Vertical Cracks
Above the VWIL
Strain Rate (%/hr)
Temperature (°C)
Height from the Cold Plate (cm)

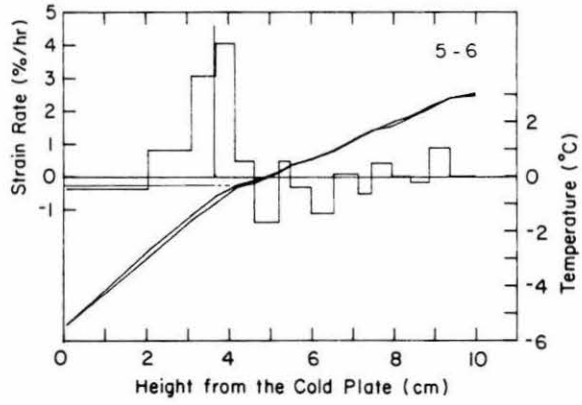
5 - 6
Strain Rate (%/hr)
Temperature (°C)
Height from the Cold Plate (cm)

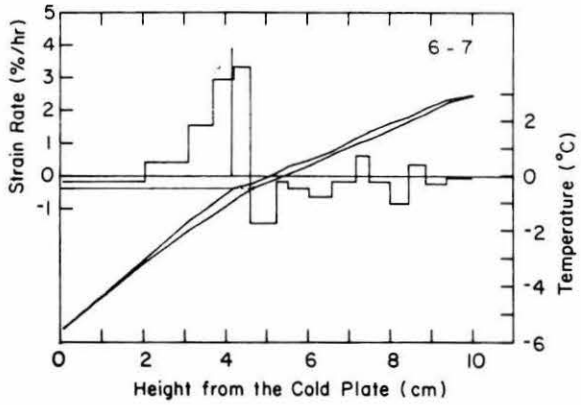
6 - 7
Strain Rate (%/hr)
Temperature (°C)
Height from the Cold Plate (cm)

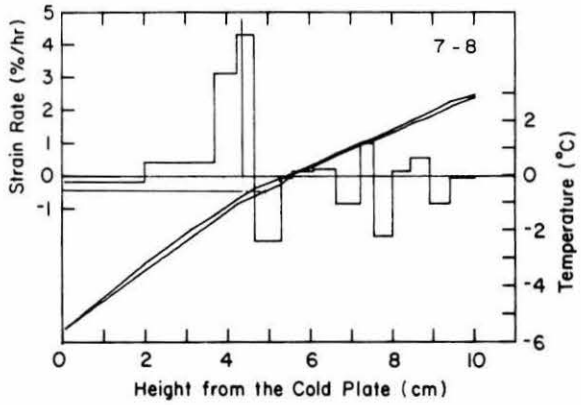
7 - 8
Strain Rate (%/hr)
Temperature (°C)
Height from the Cold Plate (cm)

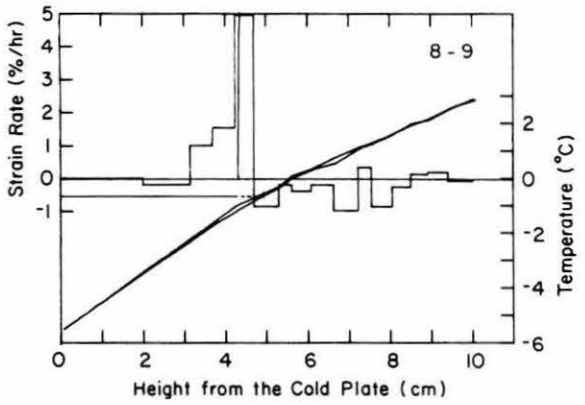
8 - 9
Strain Rate (%/hr)
Temperature (°C)
Height from the Cold Plate (cm)

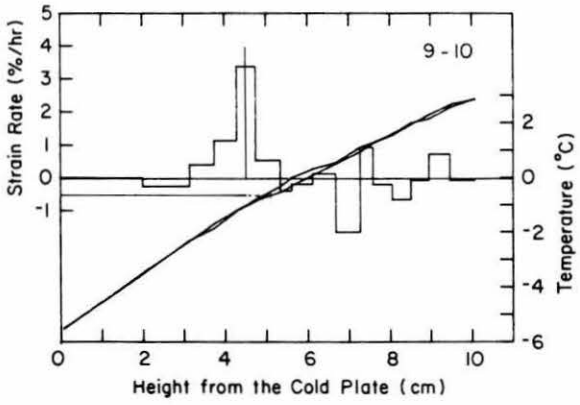
9 - 10
Strain Rate (%/hr)
Temperature (°C)
Height from the Cold Plate (cm)

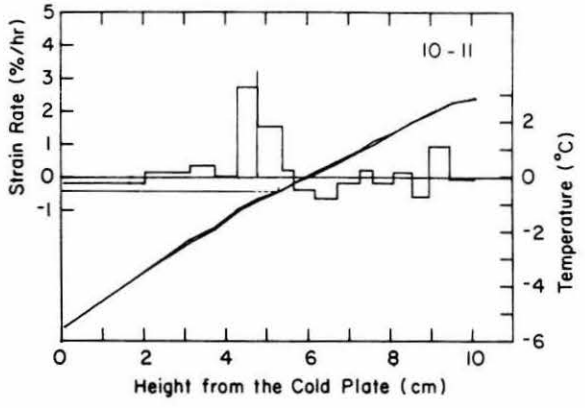
10 - 11
Strain Rate (%/hr)
Temperature (°C)
Height from the Cold Plate (cm)

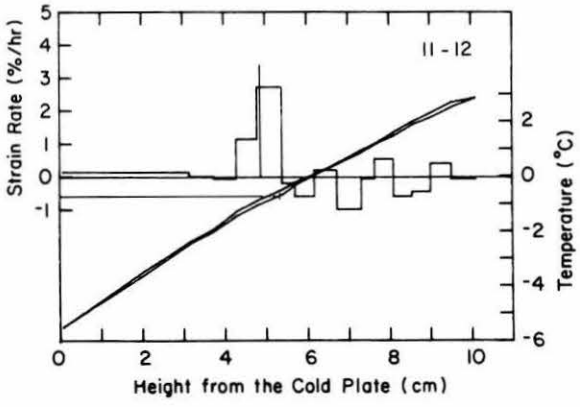
11 - 12
Strain Rate (%/hr)
Temperature (°C)
Height from the Cold Plate (cm)

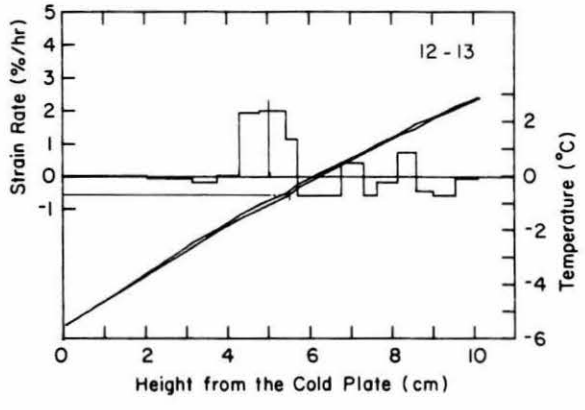
12 - 13
Strain Rate (%/hr)
Temperature (°C)
Height from the Cold Plate (cm)

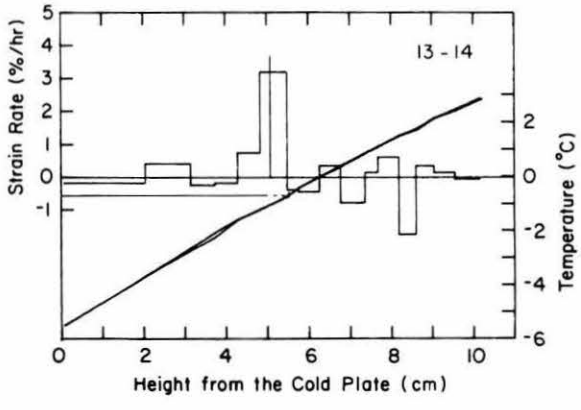
13 - 14
Strain Rate (%/hr)
Temperature (°C)
Height from the Cold Plate (cm)

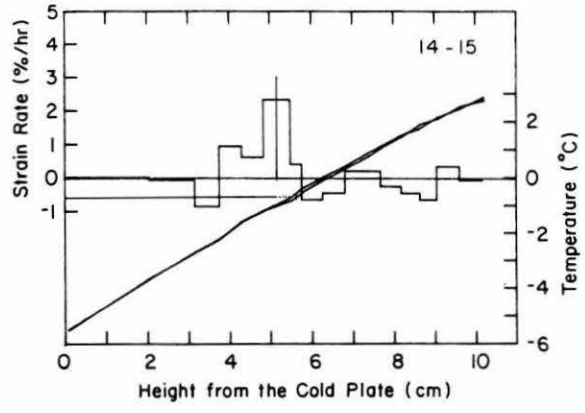
14 - 15
Strain Rate (%/hr)
Temperature (°C)
Height from the Cold Plate (cm)

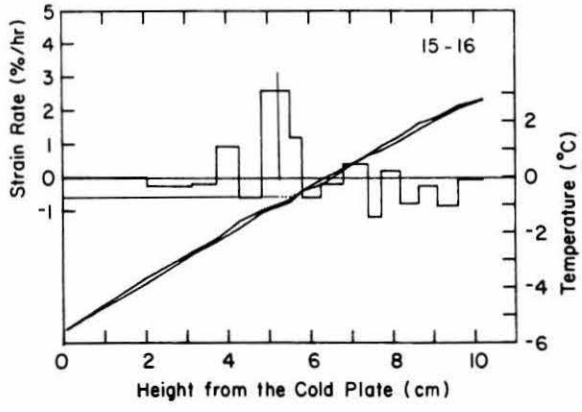
15 - 16
Strain Rate (%/hr)
Temperature (°C)
Height from the Cold Plate (cm)

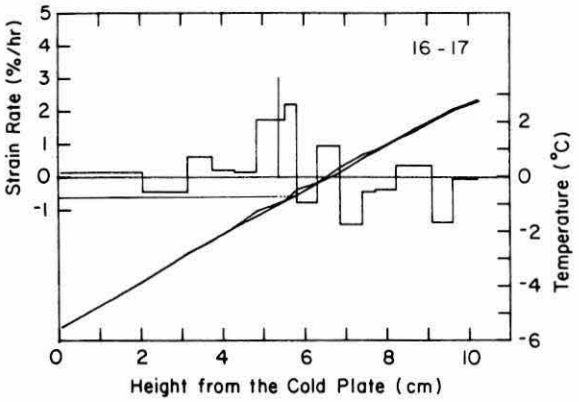
16 - 17
Strain Rate (%/hr)
Temperature (°C)
Height from the Cold Plate (cm)

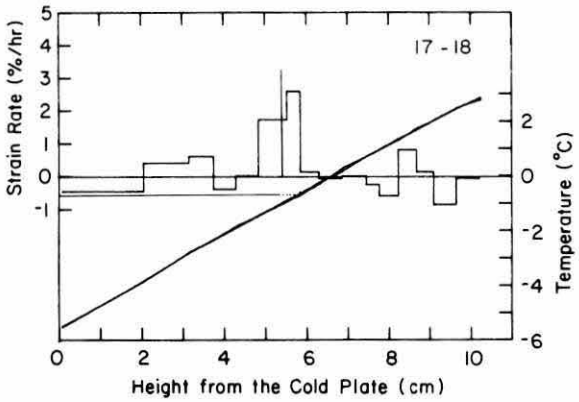
17 - 18
Strain Rate (%/hr)
Temperature (°C)
Height from the Cold Plate (cm)

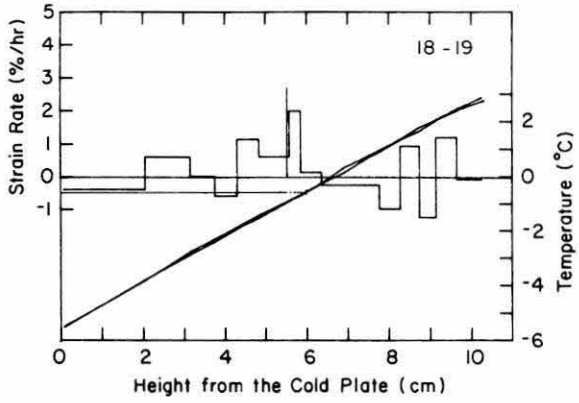
18 - 19
Strain Rate (%/hr)
Temperature (°C)
Height from the Cold Plate (cm)

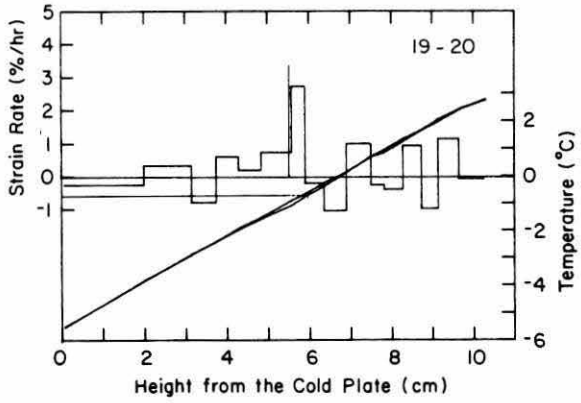
19 - 20
Strain Rate (%/hr)
Temperature (°C)
Height from the Cold Plate (cm)

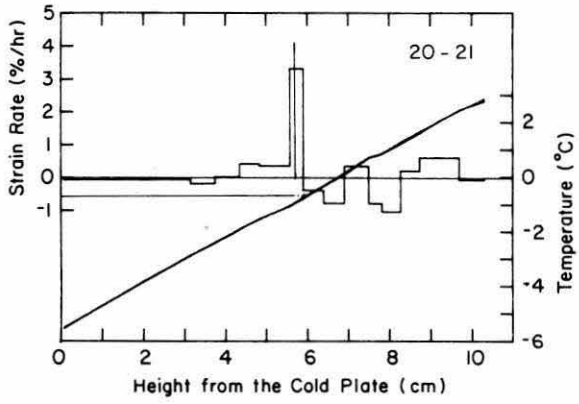
20 - 21
Strain Rate (%/hr)
Temperature (°C)
Height from the Cold Plate (cm)

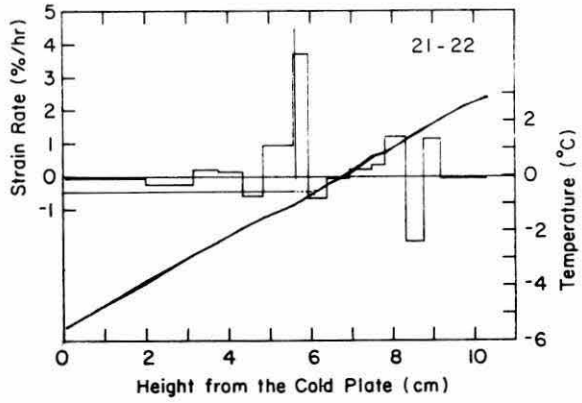
21 - 22
Strain Rate (%/hr)
Temperature (°C)
Height from the Cold Plate (cm)

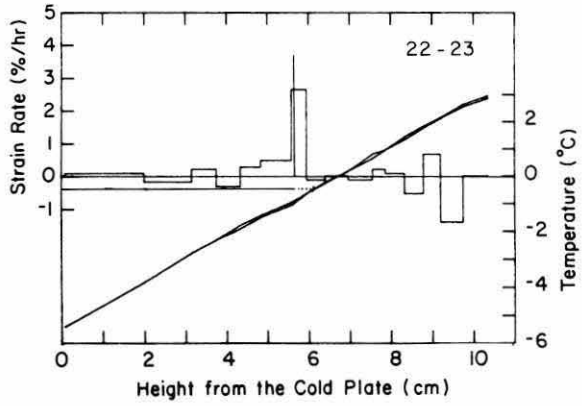
22 - 23
Strain Rate (%/hr)
Temperature (°C)
Height from the Cold Plate (cm)

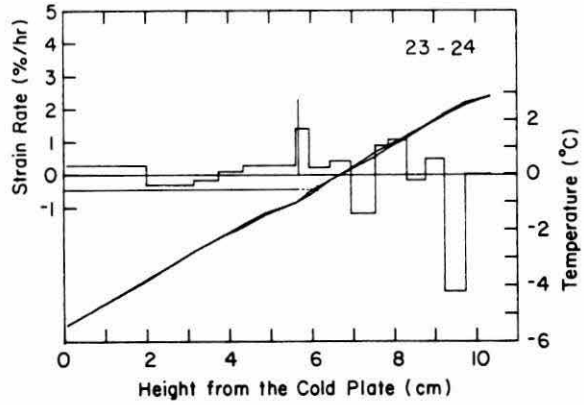
23 - 24
Strain Rate (%/hr)
Temperature (°C)
Height from the Cold Plate (cm)

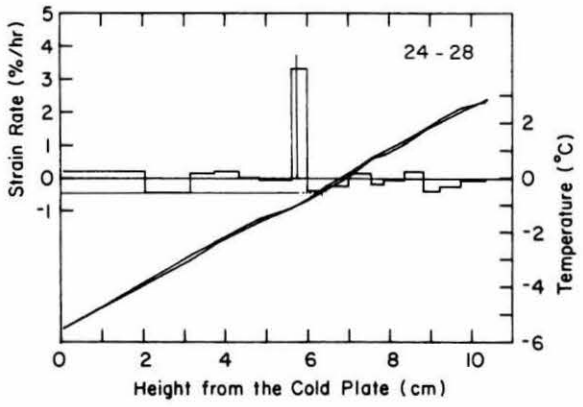
24 - 28
Strain Rate (%/hr)
Temperature (°C)
Height from the Cold Plate (cm)

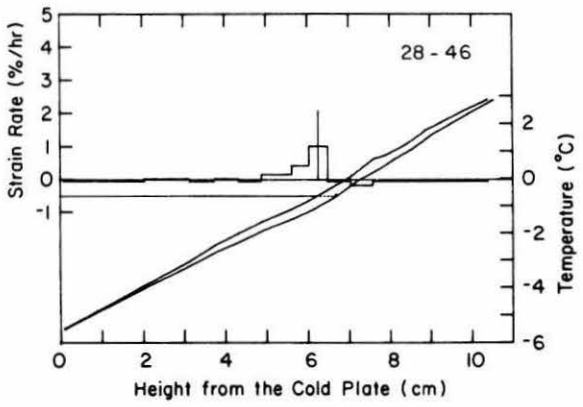
28 - 46
Strain Rate (%/hr)
Temperature (°C)
Height from the Cold Plate (cm)

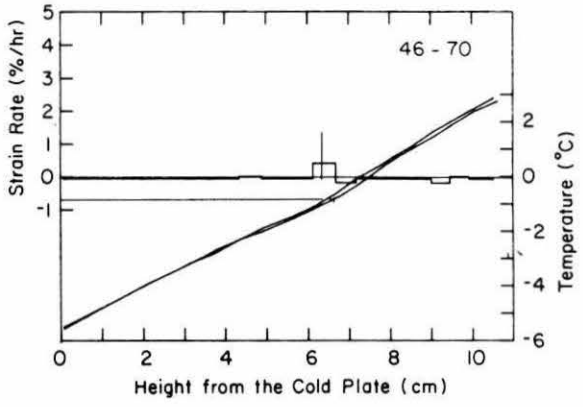
46 - 70
Strain Rate (%/hr)
Temperature (°C)
Height from the Cold Plate (cm)

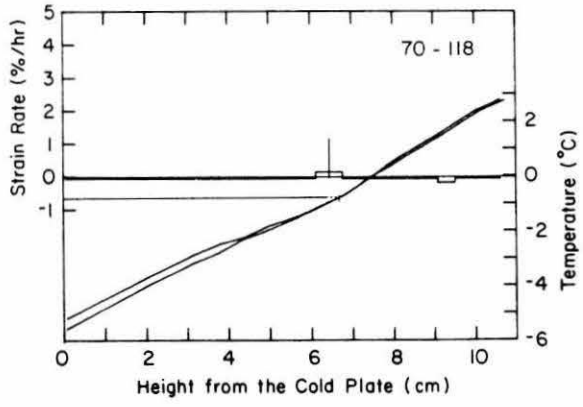
70 - 118
Strain Rate (%/hr)
Temperature (°C)
Height from the Cold Plate (cm)

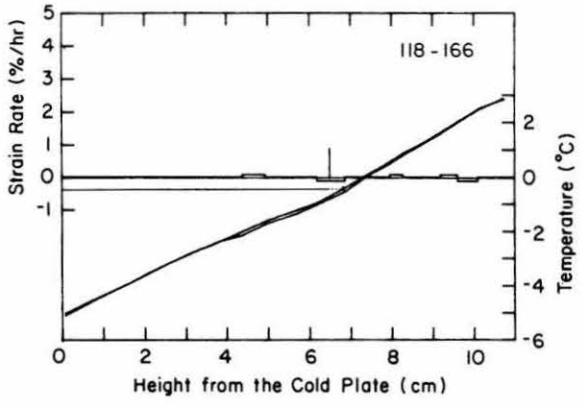
118 - 166
Strain Rate (%/hr)
Temperature (°C)
Height from the Cold Plate (cm)

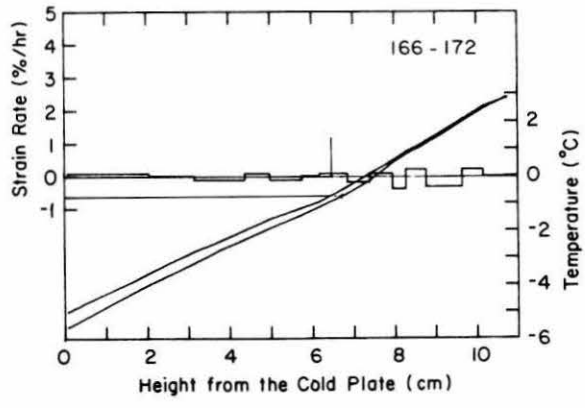
166 - 172
Strain Rate (%/hr)
Temperature (°C)
Height from the Cold Plate (cm)

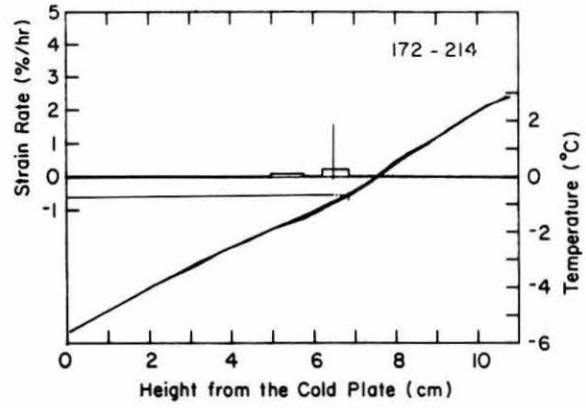
172 - 214
Strain Rate (%/hr)
Temperature (°C)
Height from the Cold Plate (cm)

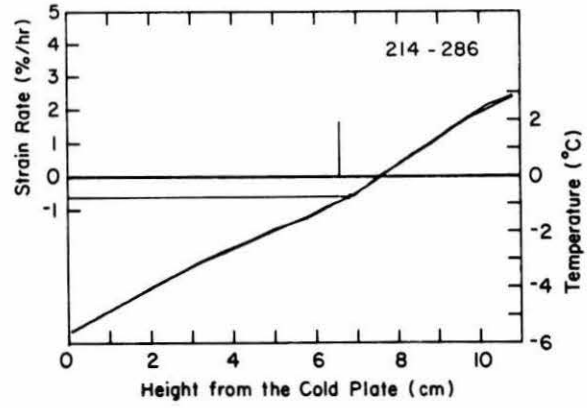
214 - 286
Strain Rate (%/hr)
Temperature (°C)
Height from the Cold Plate (cm)

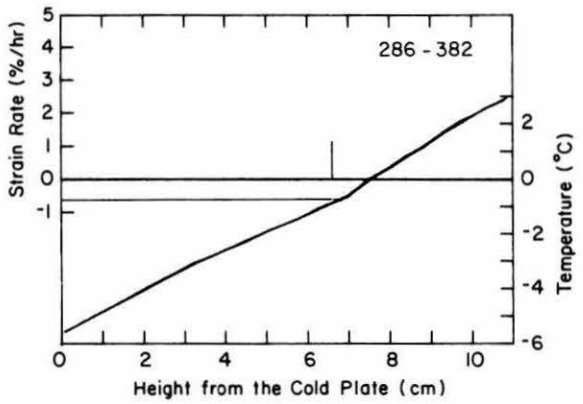
286 - 382
Strain Rate (%/hr)
Temperature (°C)
Height from the Cold Plate (cm)

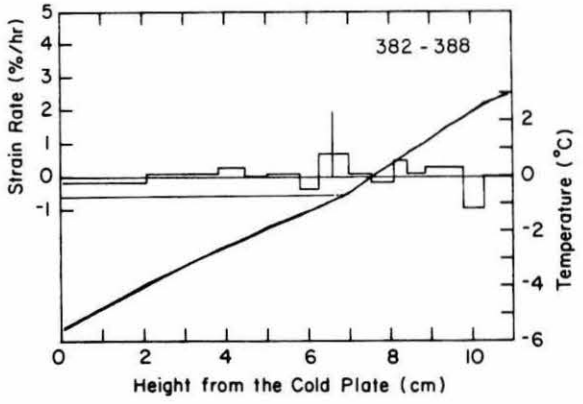
382 - 388
Strain Rate (%/hr)
Temperature (°C)
Height from the Cold Plate (cm)

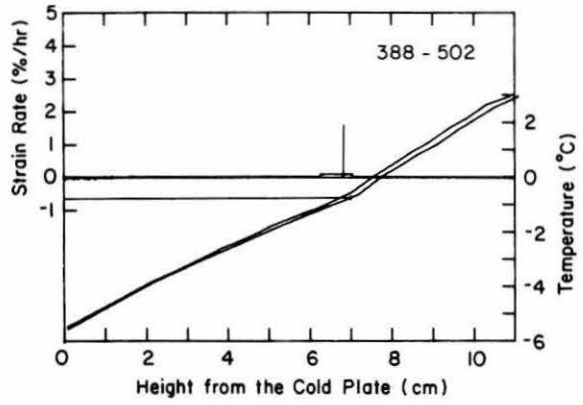
388 - 502
Strain Rate (%/hr)
Temperature (°C)
Height from the Cold Plate (cm)

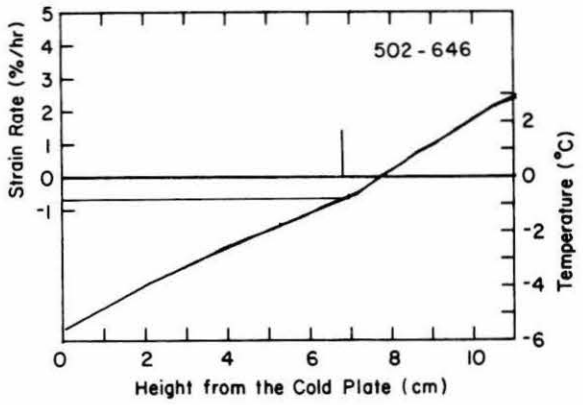
502 - 646
Strain Rate (%/hr)
Temperature (°C)
Height from the Cold Plate (cm)

APPENDIX F: LISTINGS OF T_s, L_{ff} AND LOCATION OF THE 0°C ISOTHERM.

Time (hr)	0 Iso. (cm)	Z WIL (cm)	Lff (cm)	Ts (°C)
0.5	3.29	--	--	--
1.5	3.61	--	--	--
2.5	4.15	--	--	--
3.5	4.50	--	--	--
4.5	4.88	3.47	1.41	-1.19
5.5	4.98	3.87	1.11	-0.91
6.5	5.27	4.14	1.13	-0.91
7.5	5.44	4.41	1.03	-0.76
8.5	5.65	4.50	1.15	-0.96
9.5	5.79	4.77	1.02	-0.81
10.5	5.83	4.86	0.97	-0.88
11.5	6.03	4.95	1.08	-0.87
12.5	6.01	5.04	0.97	-0.81
13.5	6.08	5.09	0.99	-0.89
14.5	6.32	5.11	1.21	-1.04
15.5	6.30	5.31	0.99	-0.77
16.5	6.37	5.36	1.01	-0.83
17.5	6.51	5.49	1.02	-0.83
18.5	6.54	5.49	1.05	-0.84
19.5	6.63	5.56	1.07	-0.86
20.5	6.58	5.58	1.00	-0.85
21.5	6.60	5.67	0.93	-0.87
22.5	6.62	5.70	0.92	-0.82
23.5	6.63	5.72	0.91	-0.75
44.5	7.06	6.20	0.86	-0.82
141.5	7.51	6.93	0.58	-0.54
304.5	7.96	7.38	0.58	-0.44
524.5	8.29	7.74	0.55	-0.38
664.5	8.26	7.74	0.52	-0.38
832.5	8.72	8.10	0.62	-0.49

Time (hr)	0 Iso. (cm)	Z WIL (cm)	Lff (cm)	Ts (°C)
1	2.24	--	--	--
2	3.07	--	--	--
3	3.84	--	--	--
4	4.26	--	--	--
5	4.73	3.46	1.27	-0.86
6	4.87	3.66	1.21	-0.88
7	5.21	4.15	1.06	-0.81
8	5.39	4.33	1.06	-0.81
9	5.47	4.41	1.06	-0.93
10	5.72	4.50	1.22	-0.87
11	5.78	4.73	1.05	-0.80
12	5.90	4.82	1.08	-0.85
13	6.05	5.01	1.04	-0.90
14	6.07	5.05	1.02	-0.88
15	6.22	5.14	1.08	-0.88
16	6.34	5.23	1.11	-0.93
17	6.39	5.37	1.02	-0.88
18	6.39	5.37	1.02	-0.89
19	6.45	5.50	0.95	-0.80
20	6.53	5.51	1.02	-0.86
21	6.55	5.60	0.95	-0.83
22	6.62	5.61	1.01	-0.83
23	6.63	5.62	1.02	-0.90
24	6.59	5.65	0.94	-0.90
28	6.75	5.71	1.04	-0.88
46	7.13	6.19	0.94	-0.86
70	7.31	6.28	1.03	-0.93
118	7.18	6.39	0.79	-0.79
166	7.22	6.42	0.80	-0.68
172	7.43	6.43	1.01	-0.88
214	7.50	6.42	1.08	-0.98
286	7.42	6.51	0.91	-0.86
382	7.47	6.51	0.96	-0.87
388	7.49	6.58	0.91	-0.79
502	7.65	6.73	0.92	-0.86
646	7.70	6.78	0.92	-0.76

0 Iso.:location of the zero isotherm from the cold plate.
Z WIL :location of warm side of the visible warmest ice lens from the cold plate.
Ts :temperature at the Z WIL.

REPORT DOCUMENTATION PAGE

Form Approved
OMB No. 0704-0188

1. AGENCY USE ONLY (Leave blank)	2. REPORT DATE	3. REPORT TYPE AND DATES COVERED
	February 1990	

4. TITLE AND SUBTITLE

X-Ray Photography Method for Experimental Studies of the Frozen Fringe Characteristics of Freezing Soil

5. FUNDING NUMBERS

PE: 6.27.30A
PR: 4A4762730AT42
TA: BS
WU: 001

6. AUTHORS

Akagawa, Satoshi

7. PERFORMING ORGANIZATION NAME(S) AND ADDRESS(ES)

U.S. Army Cold Regions Research and Engineering Laboratory
72 Lyme Road
Hanover, New Hampshire 03755-1290

8. PERFORMING ORGANIZATION REPORT NUMBER

Special Report 90-5

9. SPONSORING/MONITORING AGENCY NAME(S) AND ADDRESS(ES)

Office of the Chief of Engineers
Washington, DC 20314-1000

10. SPONSORING/MONITORING AGENCY REPORT NUMBER

11. SUPPLEMENTARY NOTES

12a. DISTRIBUTION/AVAILABILITY STATEMENT

Approved for public release; distribution is unlimited.

Available from NTIS, Springfield, Virginia 22161

12b. DISTRIBUTION CODE

13. ABSTRACT (*Maximum 200 words*)

The objectives of this report are to demonstrate a useful method for observing frost heave in freezing soil and to evaluate the method for the study of frozen fringe characteristics. X-ray photography of lead spheres containing thermocouples was tested in conjunction with frost heave tests. By applying image-processing techniques for determining the coordinates of the spheres, it is possible to obtain precise temperature profiles and determine the deformation in freezing soil. Strain and strain rate data calculated from the coordinates of the lead spheres and the temperature profiles show when, where and how much deformation (heaving and consolidation) has taken place in the freezing soil. The temperature and strain field around the frozen fringe were also observed. However, the method of determining the frozen fringe location from the location of the warmest ice lens was found to be questionable, because the active heaving zone was found to be located between the warmest visible ice lens and the 0°C isotherm. This was especially true during transient heaving, which occurs while the 0°C isotherm penetrates into the unfrozen soil. For studying the precise deformation characteristics of the frozen fringe, further precise analysis of the X-ray photo's intensity profile will be needed to convert it to a strain profile. The accuracy and spacing of the temperature sensors do not seem to be adequate for temperature measurements in the frozen fringe, and there is a need for measurement methods that are more accurate than conventional temperature sensors.

14. SUBJECT TERMS

Frost heave
Frozen soils
Soils
X-ray photography

15. NUMBER OF PAGES
76

16. PRICE CODE

17. SECURITY CLASSIFICATION OF REPORT	18. SECURITY CLASSIFICATION OF THIS PAGE	19. SECURITY CLASSIFICATION OF ABSTRACT	20. LIMITATION OF ABSTRACT
UNCLASSIFIED	UNCLASSIFIED	UNCLASSIFIED	UL

NSN 7540-01-280-5500

☆ U. S. GOVERNMENT PRINTING OFFICE: 1990--701-062

Standard Form 298 (Rev. 2-89)
Prescribed by ANSI Std. Z39-18
298-102